INSTITUTO POLITÉCNICO NACIONAL

Centro de Investigación en Computación

On Geometry-Based Statistical Channel Models for MIMO Wireless Communications

TESIS
QUE PARA OBTENER EL GRADO DE
DOCTOR EN CIENCIAS DE LA COMPUTACIÓN

PRESENTA

Marvin Rene Arias Olivas

Directores:
Dr. Adolfo Guzmán Arenas
Dr. Valeri Y. Kontorovich

México, D. F. **Noviembre de 2008**

Dedicatory

The LORD has blessed me with a wonderful family to whom this thesis is dedicated to my wife Aura, and to our two children "the twins" Mauricio and Nathaly.

Acknowledgements

I am truly indebted with many people for the work presented in this thesis. First, I would like to express my deepest thanks to my supervisors Prof. Dr. Adolfo Guzmán, Prof. Dr. Valeri Kontorovich, and my co-supervisor Assoc. Prof. Dr. Bengt Mandersson, (from LTH Lund University, Sweden), for their invaluable guidance, encouragement, support, and friendship. I would also like to thank to Dr. Hugo Coyote and Dr. Jaime Alvarez, for giving me the opportunity to join the Center for Computing Research as a PhD student.

I extend my special thanks to the remainder of my doctoral committee: Prof. Dr. Oleksiy Pogrebnyak, Prof. Dr. Alexander Guelboukh, and Prof. Dr. Hildeberto Jardón for giving me valuable comments and suggestions concerning this work. Special thanks to Lic. Emelia Velázquez, M. en C. Marta Duran, Dr. Grigori Sidorov, and Dr. Jesus Medel for helping me with all the administrative details and computer issues, during my visits here at the Center for Computing Research (CIC).

I am very grateful to the Swedish International Development Cooperation Agency for Research with Developing Countries (SIDA/SAREC) and the National University of Engineering, (UNI) for providing me with financial support my stays at CIC-IPN.

Thanks to all my friends and colleagues at CIC and CINVESTAV, at the National Polytechnic Institute, (Mexico, City), and at the Faculty of Electrical and Computer Engineering, at National University of Engineering, (Nicaragua), who have put up with me during the years as a part- time PhD student. Also I would like to thank to my colleagues Marvin Sanchez, Leonel Plazaola, Oscar Somarriba, and Enrique Silva who have contributed to my work in several ways.

I owe a great deal to my family – it would have been impossible to maintain my spirit and work habits without their continuous love and support.

Last, but by no means least, I wish to thank my mother and to my brothers and sisters who have provided me with never-ending support and encouragement during all my years in academia.

Thanks all of you!

Contents

List of Tables

List of Figures

List of Abbreviations and Acronyms

Abbreviations will be defined at their first occurrence in this thesis. For convenience, these abbreviations are listed below.

AAS	Advanced Antenna Systems = Smart Antennas
AOA	Angle of Arrival= Direction of Arrival
AOD	Angle of Departure= Direction of Departure
AP	Access Point
AS	Angle Spread = Azimuth Spread = σ_{AS}
AWGN	Additive White Gaussian Noise
BER	Bit Error Rate
BLAST	Bell Labs Layered Space-Time architecture
BS	Base Station
CDF	Cumulative Distribution Function
CIR	Channel Impulse Response
CMA	Constant Modulus Algorithm
COST	European Cooperation in the field of Scientific and Technical research
DCM	Directional Channel Model
DL	Downlink
DOA	Direction of Arrival= Angle of Arrival
DOD	Direction of Departure= Angle of Departure
DS	Delay Spread = σ_{DS}

EDF	Effective Degrees of Freedom
EM	Electromagnetic
ESPRIT	Estimation of Signal Parameters via Rotational Invariable Techniques algorithm
FDD	Frequency Division Duplex
FEC	Forward Error Correction
FFT	Fast Fourier Transform
GBSB	Geometry Based Single Bounce Channel
GBSEB	Geometry Based Single Bounce Elliptical Channel
GSCM	Geometry-Based Stochastic Channel Model
GSM	Global System for Mobile communications
HIPERLAN/2	High Performance Local Area Network type 2
IEEE	Institute of Electrical and Electronics Engineer
IFFT	Inverse Fast Fourier Transform
I.I.D	Independent and Identically Distributed
ISI	Inter Symbol Interference
LOS	Line-Of-Sight
LMS	Least Mean Squares
LS-CMA	Least Squares Constant Modulus Algorithm
LTI	Linear Time Invariant system
MIMO	Multiple Input Multiple Output
MISO	Multiple Input Single Output
MPCs	Multipath Components
MRC	Maximum Ratio Combining

MS	Mobile Station = UE = Terminal = Subscriber Unit
NLOS	Non Line-Of-Sight
OFDM	Orthogonal Frequency Division Multiplexing
OLOS	Obstructed Line-Of-Sight
PAS	Power Azimuth Spectrum
PDAPs	Power Delay Angle Profiles
PDF	Probability Density Function
PDP	Power Delay Profile
PDS	Power Delay Spectrum
PL	Path Loss
PHY	Physical Layer
RLS	Recursive Least Squares
RMS	Root Mean Square
Rx	Receiver
SAGE	Space Alternating Generalized Expectation algorithm
SCM	Spatial Channel Model
SIMO	Single-Input Multiple-Output
SISO	Single-Input Single-Output
SMI	Sample Matrix Inversion
SNR	Signal to Noise Ratio
STC	Space-Time Coding
STD	Standard Deviation
SVD	Singular Value Decomposition

TDD	Time Division Duplex
TDL	Tapped Delay Line
TF	Transfer Function
TOA	Time of Arrival
Tx	Transmitter
UE	User Equipment = Mobile Station
UL	Uplink
ULA	Uniform Linear Array
UMTS	Universal Mobile Telecommunications System
WCDMA	Wideband Code Division Multiple Access
WLAN	Wireless Local Area Network
WSS	Wide Sense Stationary
WSSUS	Wide Sense Stationary Uncorrelated Scattering
3GPP	Third Generation Partnership Project

Introduction

The development of wireless communications is one of the big engineering success stories of the last three decades, e.g. the radio systems for mobile communications sector has definitely been the fastest growing market segment in telecommunications [1–5]. This progress with exponential speed from what is commonly referred to as the first generation mobile radio systems, developed at that time were entirely based on analog technique, (analogue voice), such as the Advanced Mobile Phone System (AMPS) and Nordic Mobile Telephone (NMT), developed primarily in the 1970s and 1980s, through the second generation mobile radio systems that are characterized by digitalization of the networks (i.e., digital voice), including the widely used Global System for Mobile communications (GSM) and the cellular standard IS-95 (Interim Standard 95), developed in the 1990s, to the most recently launched in 2001/2002 third generation mobile radio systems, including the Universal Mobile Telecommunications System, (UMTS or 3GSM, also called Wideband Code Division Multiple Access (WCDMA)), the Mobile Broadband System (MBS), and the cdma2000, that includes other services, (besides voice telephony), such as the transmission of video, images, text, and data [1–7].

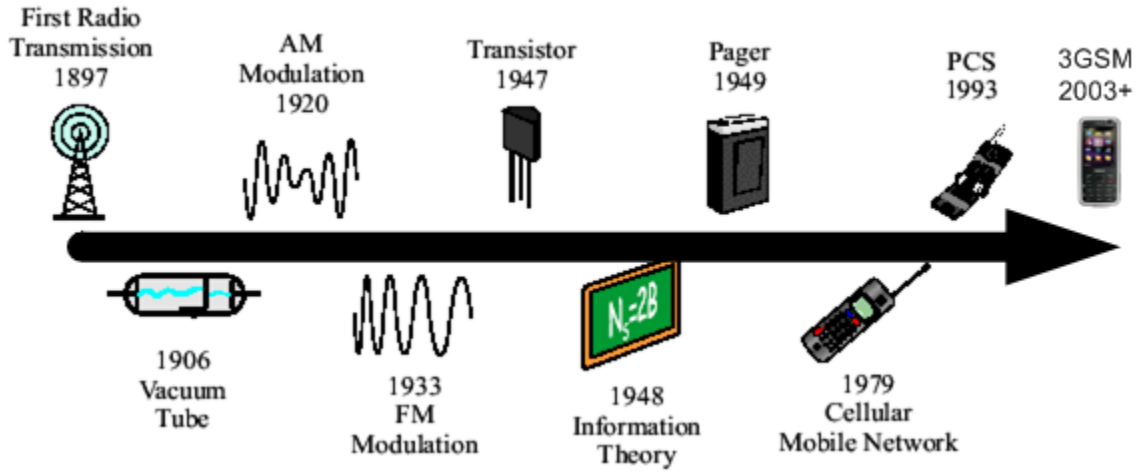

Figure 1.1 Evolutions of Wireless Communications.

Fig. 1.1 illustrates the development of wireless communications from the first radio transmission carried out by Guglielmo Marconi in 1897, until the evolution of the third generation of mobile radio systems (GSM) that up to know is in use as the evolved 3GSM and beyond.

In spite of the successful development of wireless communications industry, wireless system designers are faced with numerous challenges, including limited availability of radio-frequency spectrum and transmission problems caused by such factors as fading and multipath distortion. Meanwhile, there is increasing demand for higher data rates, better quality of service, fewer dropped calls, and higher network capacity. Meeting these needs require new techniques that improve spectral efficiency and network links' operational reliability.

Preface

There are two fundamental aspects of wireless communication that make the problem challenging and interesting. These aspects are by and large not as significant in wireline communication. First is the phenomenon of fading: the time variation of the channel strengths due to the small-scale effect of multipath fading, as well as large-scale effects such as path loss (PL) via distance attenuation and shadowing by obstacles. Second, unlike in the wired world where each transmitter-receiver pair can often be thought of as an isolated point-to-point link, wireless users communicate over the air and there is significant interference between them. The interference can be between transmitters communicating with a common receiver (e.g., uplink (UL) of a cellular system), between signals from a single transmitter to multiple receivers (e.g., downlink (DL) of a cellular system), or between different transmitter–receiver (Tx-Rx) pairs (e.g., interference between users in different cells). Recent focus has shifted more towards increasing the spectral efficiency; associated with this shift is a new point of view that fading can be viewed as an opportunity to be exploited.

This thesis is divided into six chapters that together constitute the thesis. It describes the clustering approach for channel models based on geometry that can be use for analysis and design of wireless channel modeling for third generation systems, e.g. like the Wideband Code Division Multiple Access (WCDMA). The space-time wireless channel modeling is a research area that is commonly developing and with a great deal of work and innovation left to be done. The thesis also presents an analysis of angular and time domain respectively through direction of arrival (DOA) and time of arrival (TOA) probability density functions (PDFs) for the clustering approach model. In order to evaluate the theoretical PDFs derived, we have compared them with experimental results published in the literature. The comparison with experimental results shows good agreement, however the clustering approach presented in this thesis is limited to stationary conditions of the channel, and the analysis for non-stationary conditions is outside the scope of this thesis, i.e., the model proposed does not incorporate the Doppler effect in the analysis.

The thesis is organized in the following way. Chapter 1 gives an introduction with the general background of the presented work, the purpose of the research, related works, contributions made in the research, description of the research design and some topics for future research based on our interest in multipath propagation phenomenon of the mobile radio channel. In chapter 2, we provide an overview of channel models based on geometry; this geometrical approach of the model provides analytically tractable solutions and is based on geometry

rather than measurements. In Chapter 3, we extend the Geometry Based Single Bounce Channel (GBSB) Model for Multiple Input Multiple Output (MIMO) Communication Systems and we analyze the space-time properties of the model. Then we compare the simulation results with the previous GBSB channel model operating in urban environments. Chapter 4 gives a detailed description of the clustering approach channel model proposed. In Chapter 5 we derive probability density functions (PDFs) in time and angular domain respectively, based on the clustering approach model described in the previous chapter, and we make comparisons with experimental results published in the literature in order to evaluate the theoretical PDFs obtained.

Finally chapter 6 gives a summary of the results presented in the thesis and contains some conclusions around the results presented in the earlier chapters, as well as some suggestions for future research work are also included.

The work presented in this doctoral thesis summarizes the research performed, at the National Polytechnic Institute (IPN), under the supervision of Dr. Adolfo Guzmán Arenas from the Center for Computing Research (CIC), and Dr. Valeri Kontorovich from the Center for Research and Advances Studies (CINVESTAV), at Mexico City, Mexico, in collaboration with the Department of Electroscience, Lund University, Lund, Sweden, under the co-supervision of Dr. Bengt Mandersson.

Resumen

El uso de sistemas de comunicación de banda ancha de múltiple entrada-múltiple salida (Multiple Input Multiple Output MIMO) es actualmente objeto de un interés considerable. Una razón para esto es el reciente desarrollo de sistemas de comunicación móvil de tercera generación (3G) y superiores, tales como la tecnología de banda ancha Wideband Code Division Multiple Access (WCDMA, por sus siglas en inglés), la cual proporciona canales de radio de 5 MHz de ancho de banda.

Para el diseño y la simulación de estos sistemas de radio móviles que usan propagación inalámbrica MIMO (como Wideband-CDMA por ejemplo), necesitamos modelos de canal que provean la requerida información espacial y temporal necesaria para el estudio de tales sistemas, esto es, los parámetros básicos de modelado en los dominios del espacio y el tiempo. Como ejemplo podemos mencionar, el valor cuadrático medio de la dispersión del retardo (Delay spread DS) el cual está directamente relacionado a la capacidad de un sistema de comunicación específico y nos da una idea aproximada de la complejidad del receptor.

En esta tesis, se propone un modelo basado en geometría con enfoque en grupos (clusters) y es utilizado para el análisis en los dominios del espacio y el tiempo para condiciones estacionarias, y para representar los perfiles de potencia-angulo-retardo (Power Delay Angle Profiles PDAPs) de los componentes multi-trayectoria en ambientes urbanos. Además, se han derivado soluciones en formas cerradas para las expresiones en el dominio del ángulo (espacial) y del tiempo. La investigación previa sobre el modelado de canales cubre una amplia variedad de aspectos en varios niveles de detalle, incluyendo análisis para condiciones no estacionarias. Sin embargo el trabajo presentado en la literatura no incluye las relaciones entre los grupos (cluster) físicos y los PDAPs. El modelo propuesto basado en grupos (clusters) puede ser usado para mejorar aún más el desempeño en condiciones estacionarias de los sistemas de comunicaciones móviles actuales y futuros tales como los sistemas de comunicación MIMO de banda ancha.

En la tesis también se presenta un análisis en el dominio del ángulo (espacial) y del tiempo respectivamente, a través de las funciones densidad de probabilidad (PDF) de la dirección de llegada (Direction of Arrival DOA) y el tiempo de llegada (Time of Arrival TOA) para el modelo basado en grupos. A fin de evaluar las funciones de probabilidad teóricas derivadas, éstas han sido comparadas con resultados experimentales publicados en la literatura. La comparación con estos

resultados experimentales muestran una buena concordancia, no obstante la técnica de modelado presentada en esta tesis se encuentra limitada a condiciones estacionarias del canal. La condición de no estacionariedad se ubica más allá del alcance de esta tesis, es decir, el modelo propuesto no incorpora el efecto Doppler en los análisis.

Abstract

The use of wideband Multiple Input Multiple Output (MIMO) communication systems is currently subject to considerable interest. One reason for this is the latest development of 3rd Generation mobile communication systems and beyond, such as the wideband technology: Wideband Code Division Multiple Access (WCDMA), which provides 5 MHz wide radio channels.

For the design and simulation of these mobile radio systems taking into account MIMO wireless propagation (e.g. like the wideband-CDMA), channel models are needed that provide the required spatial and temporal information necessary for studying such systems, i.e., the basic modeling parameters in the space-time domains, e.g., the root mean square (*rms*) delay spread (DS) is directly connected to the capacity of a specific communication system and gives a rough implication on the complexity of a receiver.

In this thesis a channel modeling based on the clustering approach is proposed and used for analysis in the space-time domains for stationary conditions to represent the power delay angle profiles (PDAPs) of the multipath components (MPCs) in urban environments. In the thesis, closed-form expressions are derived in angular and time domains respectively. Previous research on channel modeling covers a wide variety of aspects in varying levels of detail, including analysis for non stationary conditions. However, the work presented in the literature has not included the relationship between the physical clusters and the PDAPs. The proposed clustering approach model can be used to further performance improvement in stationary conditions of current or future mobile radio systems like the Wideband MIMO communication systems.

This thesis also presents an analysis in angular and time domain respectively through direction of arrival (DOA) and time of arrival (TOA) probability density functions (PDFs) for the clustering approach model. In order to evaluate the derived theoretical PDFs, these are compared with experimental results published in the literature. The comparison to experimental results shows good agreement, however the modeling approach proposed in this thesis is limited to stationary conditions of the channel. The non-stationary condition is outside the scope of this thesis, i.e., the clustering approach model proposed does not incorporate the Doppler effect in the analysis.

Chapter 1 Introduction

The development of wireless communications is one of the big engineering success stories of the last three decades, e.g. the radio systems for mobile communications sector has definitely been the fastest growing market segment in telecommunications [1–5]. This progress with exponential speed from what is commonly referred to as the first generation mobile radio systems, developed at that time were entirely based on analog technique, (analogue voice), such as the Advanced Mobile Phone System (AMPS) and Nordic Mobile Telephone (NMT), developed primarily in the 1970s and 1980s, through the second generation mobile radio systems that are characterized by digitalization of the networks (i.e., digital voice), including the widely used Global System for Mobile communications (GSM) and the cellular standard IS-95 (Interim Standard 95), developed in the 1990s, to the most recently launched in 2001/2002 third generation mobile radio systems, including the Universal Mobile Telecommunications System, (UMTS or 3GSM, also called Wideband Code Division Multiple Access (WCDMA)), the Mobile Broadband System (MBS), and the cdma2000, that includes other services, (besides voice telephony), such as the transmission of video, images, text, and data [1–7].

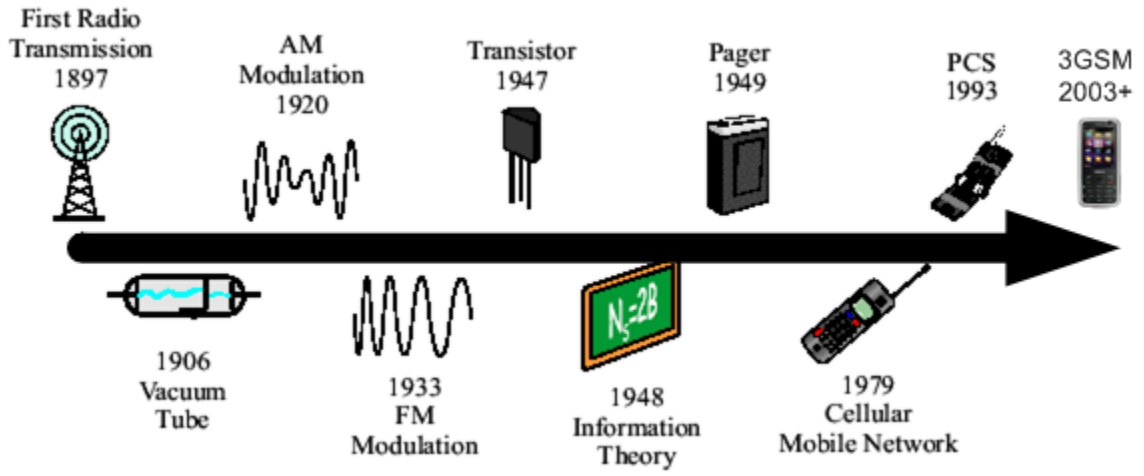

Figure 1.1 Evolutions of Wireless Communications.

Fig. 1.1 illustrates the development of wireless communications from the first radio transmission carried out by Guglielmo Marconi in 1897, until the evolution of the third generation of mobile radio systems (GSM) that up to know is in use as the evolved 3GSM and beyond.

In spite of the successful development of wireless communications industry, wireless system designers are faced with numerous challenges, including limited availability of radio-frequency spectrum and transmission problems caused by such factors as fading and multipath distortion. Meanwhile, there is increasing demand for higher data rates, better quality of service, fewer dropped calls, and higher network capacity. Meeting these needs require new techniques that improve spectral efficiency and network links' operational reliability.

1.1 General Background

Designing wireless communication systems require dedicated simulation approaches with an emphasis on the multipath propagation channel including directions of transmission and arrival. For the design and simulation of many practical mobile radio systems, (e.g., third generation systems and beyond like the wideband-CDMA), is necessary to have channel models that can be easy to implement as well as to accomplish with practical important requirements such as simplicity and adaptability [1–3]. The simulation and measurements approaches are important tools used for the design and implementation of mobile radio systems with an emphasis on the propagation modeling for mobile or wireless channel.

In a wireless mobile communication system, a signal can travel from transmitter to receiver over multiple reflective paths. This phenomenon, referred to a multipath propagation, can cause fluctuations in the received signal amplitude, phase, and angle of arrival, giving rise to the terminology multipath fading**.** In fact, the received signal is a superposition of waves coming from all directions due to reflection, diffraction, and scattering cause by buildings, trees, and other obstacles [6–9].

Due to the multipath propagation, the received signal consists of a finite sum of attenuated, delayed, and the phase of each partial wave. The superposition can be constructive or destructive. The distortions caused by multipath propagation can be modeled as linear and be compensated on the receiver side, for example by an equalizer [1–3]. Another fundamental aspect in wireless communication unlike in the wired world where each transmitter-receiver pair can often be thought of as an isolated point-to-point link, wireless users communicate over the air and there is significant interference between them. The interference can be between transmitters communicating with a common receiver (e.g., uplink (UL),

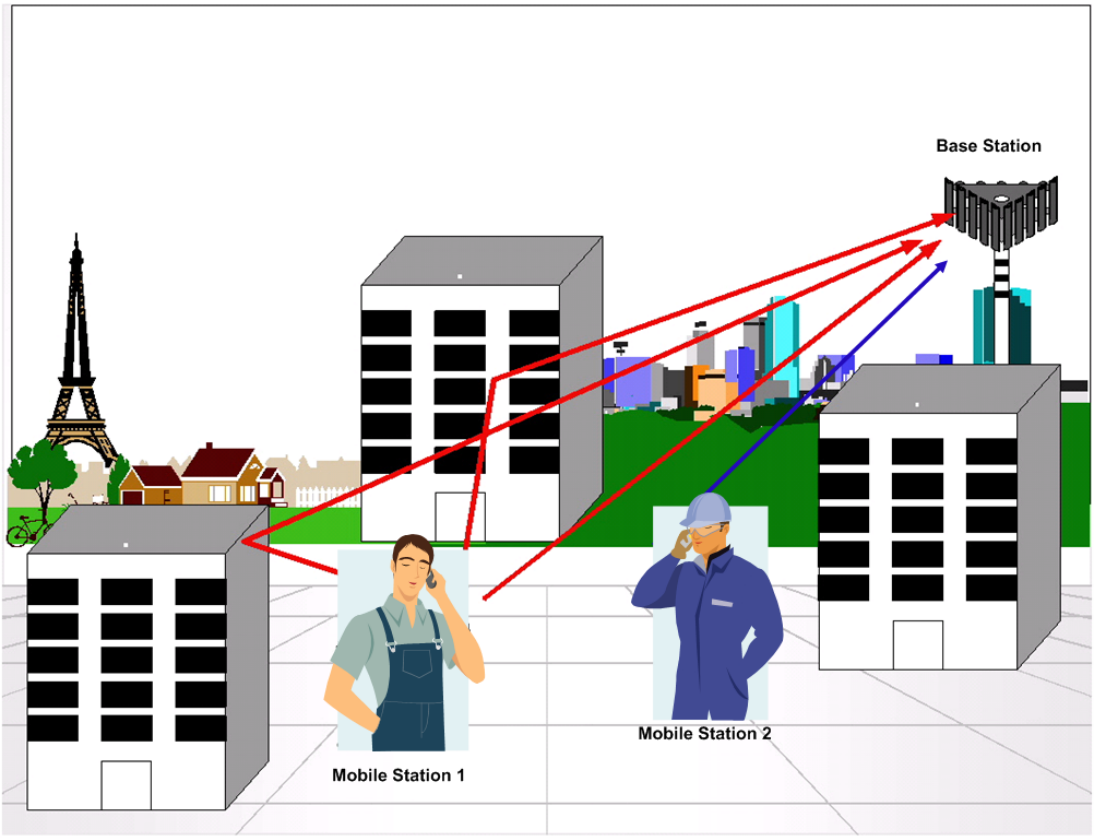

Figure 1.2 A typical example of the multipath propagation and interference phenomena.

of a cellular system), between signals from a single transmitter to multiple receivers e.g., downlink (DL), of a cellular system), or between different transmitter–receiver (Tx-Rx), pairs (e.g., interference between users in different cells) [7]. Fig. 1.2 shows an example of the multipath propagation and interference phenomena. The user number one transmits a signal which reaches the base station via Line-Of-Sight (LOS) or by reflection and scattering. Signals from other user introduce co-channel interference at the base station (BS).

1.2 Communication Channel and Models for Multiple Input Multiple Output Systems

Future wireless communication systems have the requirement of providing higher data rates and better qualities of service to nomadic users than ever before. Since the radio spectrum is known to be a limited resource, this requirement can only be fulfilled by exploiting the spatial capacities of the radio channel [9].

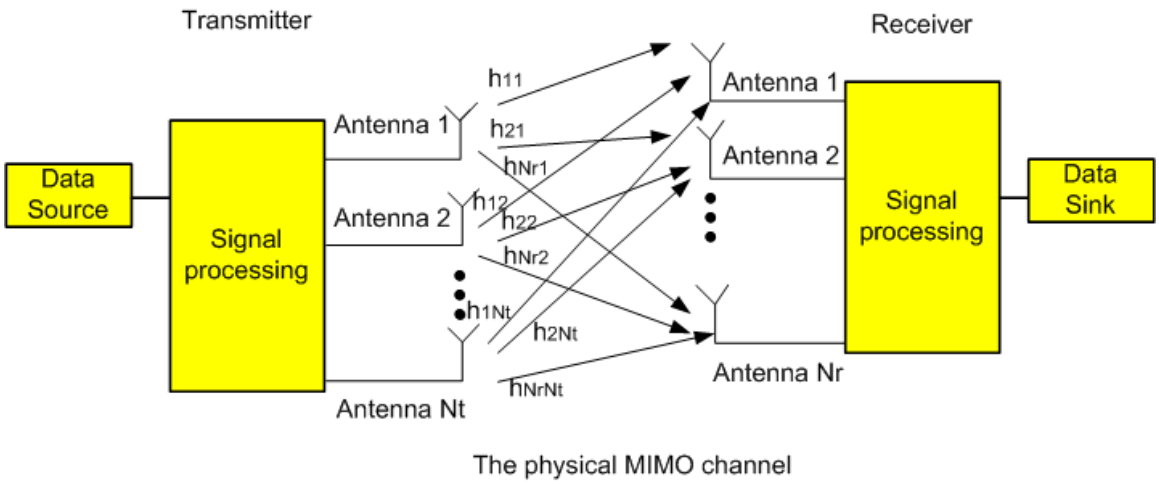

Figure 1.3 Example of a MIMO channel model. MIMO sends a transmission from multiple antennas to bounce over multiple paths to a receiver.

The highest data rates per user are expected only if multiple antennas are used at both receive and transmit sites. Such a radio propagation channel constitutes a Multiple Input Multiple Output (MIMO) system.

The increasing demand for high data rates and the limited available bandwidth motivates the investigation of wireless systems that efficiently exploit the spatial domain. Due to cost, size, and complexity limitations at the terminal, antenna arrays are usually considered only at the base stations (access points) to spatially discriminate the desired signal from interference and noise. The use of spatial diversity both on reception as well as transmission can improve throughput and coverage in addition to allowing a higher degree of spectral reuse and thereby increasing the system capacity [9–15].

A smart antenna [9] is a multi-element antenna where the signals received at each antenna element are intelligently combined by an adaptive algorithm to improve the performance of the wireless system. The reverse is performed on transmit. These antennas can increase signal range, suppress interfering signals, combat signal fading, and increase the capacity of wireless systems.

There are two basic types of smart antennas [9]. The first type is the directional antenna, which forms a narrow beam in the desired direction. This can be implemented by a switched multibeam antenna in which one of several beams (or antenna elements) is selected for reception and transmission. Generally, this is the beam with the strongest signal. Another implementation method is a linear array of half-wavelength-spaced antenna elements where the received signals are phase shifted (in linear steps across the array) and combined to form a beam in a given direction, based on direction of arrival beamforming techniques. The second type is defined here as an adaptive array in which the signals from several antenna elements (not necessarily a linear array), each with similar

antenna patterns, are weighted (both in amplitude and phase) and combined to maximize the performance of the output signal. Note that the adaptive array will form a narrow beam in a line-of-sight environment without multipath, but can also optimally suppress interference and provide fading mitigation and gain in a multipath environment. The switched multibeam antenna is less complex because it uses simple beam tracking. That is, the beam-selection technique needs only look at the signal level in each beam every few seconds to determine which beam to use. Similarly, in the linear array implementation of the directional antenna, the phase shifts only need to be slowly adjusted to track the change in angle of arrival (AOA) of the received signal. On the other hand, the beamformer weights in the adaptive array need to track the fading of the desired signal. However, although the adaptive-array processing is much more computationally complex, the requirement is well within the capability of current signal processing ICs.

Also, for transmission, the directional antenna can use the same beam for transmission as used for reception, while for the adaptive array the issue is more complicated. In time division duplex (TDD) systems the same frequency is used for transmit and receive, but at different times, and adaptive arrays can use the receive weights for transmission — although antenna calibration may be required to obtain the needed accuracy. In frequency division duplex (FDD) systems different frequencies are used for transmission and reception, and it may not be possible to determine the adaptive array transmit weights from the receive weights in a multipath environment, since the fading can be different at the two frequencies.

The adaptive array has significant advantages in performance over the directional antenna (note that the adaptive array may also be able to form a directional beam if that would provide the best performance). Although both types of smart antennas can provide an array gain, that is, increase in receive output signal to noise ratio (SNR) averaged over any fading, of M with M beams or antenna elements, with the directional antenna this gain only occurs in line of sight (LOS) or limited-scattering environments. In multipath environments, the signals can arrive from multiple directions into multiple beams, and a single beam does not contain all the signal energy, particularly when the angular spread of the environment (the range in direction of arrival (DOA) for a received signal from a single transmitter) is greater than the beamwidth of a single beam.

The adaptive algorithms are broadly classified as trained and blind algorithms. Trained algorithms use a sequence to adapt the weights of the array while blind algorithms do not require training signals to adapt their weights but attempt to restore some known property to the received channel.

The most commonly used trained algorithms is the Least Mean Squares (LMS) algorithm [7]. The main advantage of the LMS is its simplicity. It has an acceptable performance in many applications; however it converges slowly when

the eigenvalue of the covariance matrix are widely spread. One way to speed the convergence is to employ the direct Sample Matrix Inversion (SMI). Although the SMI algorithm converges more rapidly than the LMS algorithm it suffers from increased computational complexity and numerical instabilities. The recursive least squares (RLS) algorithms overcome those limitations and offer good performance provided that the SNR is high.

Many blind algorithms have been developed to derive the optimum weights vector. Examples of the blind algorithms are Constant Modulus Algorithm (CMA), Least Squares CMA (LS-CMA). A reference tutorial on adaptive beamforming algorithms can be found in [7].

MIMO was originally conceived in the early 1970s by Bell Labs engineers trying to address the bandwidth limitations that signal interference caused in large, high-capacity cables. At the time, however, the processing power necessary to handle MIMO signals was too expensive to be practical.

Advances and cost reductions in signal-processing technology, coupled with increased demands to overcome the limits of existing mobile communications approaches, have since led researchers to reconsider MIMO for wireless systems.

Signals in a wireless system frequently reflect off objects en route to the recipient and bounce along different paths. At various points, the signals become out of synch, thereby scrambling the received transmission and decreasing bandwidth, creating a problem called multipath distortion [5]. As Fig. 1.3 shows, MIMO takes advantage of this situation by sending a single transmission from two or more antennas to bounce along multiple paths to a receiver. Putting data on multiple signal paths increases the amount of information a system can carry and the number of users that can be served. In addition, this approach lets a system divide a single data set into parts that are sent over multiple paths in parallel. This lets the system handle the information faster than approaches that send data over a single path.

For example, first-generation MIMO products double IEEE 802.11's theoretical maximum data rate from 54 to 108 Mbits per second. The nature of the signals on each path is changed slightly based on the different antennas from which they are sent, the spacing of the antennas, and the type of interference the signals encounter. The recipient's system analyzes this information via matrix-manipulation signal processing technology, which cross-correlates the signals to detect their various paths and reconstitute them properly. This process also reduces the effects of interference. Moreover, by spreading a transmission signal across multiple paths, MIMO increases the chance that any given path will reach the destination, which improves link reliability. In addition, MIMO systems can

choose from the multiple antennas they work with to use those with the clearest signals. This reduces error rates and improves communication quality [4–5].

MIMO can also increase the effective transmission range of the overriding wireless technology being used. By using clearer signals and minimizing the effects of interference, MIMO signals can be resolved over longer distances than technologies whose effective ranges are reduced by noise and signal diffusion.

It is theoretically possible to continue increasing data rates and transmission ranges by adding antennas to a system. In practice, though, engineers are limited by the nature of the multipath environment, such as the number and nature of obstacles encountered, and the increased processing power required to handle the extra work generated by additional antennas.

This technology is already being deployed on mobile systems in Japan and China, with other implementations on the way. Already, MIMO has becomes part of the IEEE 802.16d wireless networking standard. In addition, the Third Generation Partnership Project, (3GPP), a collaboration of telecommunications standards organizations, is already evaluating MIMO for cellular networks [4].

Regardless of the transmission technique employed, knowledge of the wireless channel is vital to the optimal design and performance of any MIMO communication system [5–15]. It is well known that mathematical channel characterization results provide fundamental knowledge for all communication system physical layer waveform design and analysis. The use of thorough channel characterization information allows prediction and trade-off studies that affect various aspects of communication system design, such as optimal channel bandwidths and system performance (bit error rate (BER), latency, etc.) for any potential waveform used across the channel. Remedial measures (e.g. equalization, diversity) must also be design on the base of channel knowledge. Thus, a primary use of channel models is in the evaluation and comparison of different transmission schemes that can be deployed in the environment in question. In particular, these channel models are used as elements, or blocks, in a cascade of models that include the other components in a wireless communication system. Although modern channel models contain mathematical descriptions that can be used for analysis, often analysis becomes intractable, at which point evaluation and trade-off can be conducted and extended via companion computer simulations. This is also a natural way to use models that are wholly empirical: those that used stored measured channel data.

Even with a high adaptive and reconfigurable communication system, if not taken into account, the impairments caused by the channel may be severe enough to degrade performance significantly. Example outcomes of inadequately accounting for channel characteristics include a bit error probability (or bit error rate, BER) “floor”, in which error probability reaches a lower limit regardless of received power level, and a large latency, which in the case of some protocols

would translate to link outage. The large latency could be caused, for example, by severe channel fading, which causes packet errors and forces the system to employ retransmissions. Retransmissions also reduce the achievable throughput, and this can significantly degrade both objective and subjective performance for many applications. Hence, channel characteristics also affect protocol design. Clearly the undesirable outcomes noted here should occur with very low probability, particularly for MIMO channel applications related to safety.

There are well-known ways to mitigate such detrimental channel effects, some of which are prudently incorporated into the above mentioned transmission schemes. Mitigation techniques at the physical layer (PHY) include antenna diversity, strong Forward Error Correction (FEC) coding and interleaving, rapid power control, and equalization [9]. At higher layers one may incorporate network coding and cooperative transmissions. However, the efficient and effective design of these channel impairment mitigation techniques relies on good models for the wireless channel over which transmission take place. This is the primary focus of this thesis.

In the following Section, first briefly, it describes some of the main parameters needed to characterize a wireless channel; both analytical and empirical models are reviewed and highlight key differences between MIMO channels and more conventional channels. It is also described very briefly some existing models for the MIMO channel.

1.3 Research Overview and Related Work

The study and modeling of wireless channels has many decades of history behind it, and for reasons of brevity, this Section provides only a cursory overview here. Wireless channels can be modeled either deterministically or statistically [6–9]. For most applications, deterministic modeling is site-specific and computationally intensive; hence, statistical models are often more attractive in that they do not attempt to provide exact estimation of a channel's small scale fading characteristics at points in space at any particular time; rather, they attempt to faithfully emulate the variation in these channel effects. Henceforth this thesis is focused on geometry-based statistical models. It is also concerns only with small scale fading, which most often arises due to the destructive interference from multiple replicas of the transmitted signal arriving at the receiver with different delays. This results from multipath propagation and such fading is observed on spatial scales on the order of one half wavelength ($\lambda/2$). In contrast, for frequency bands of current interest (VHF and higher), large-scale fading (often termed shadowing, obstruction, or blockage) occurs on scales of many (e.g., 20 or more [6–9] wavelengths). First, it is provided a very brief review of some important parameters used to characterize wireless channels. (See [1–3], and [6–9] for a much more comprehensive review.)

The term channel characterization is used to describe the models, theory, and experimental data that constitute one's knowledge of a wireless channel in a specific type of environment, typically a function of channel bandwidth and center frequency. One can define the channel as the complete set of parameters for all paths that transmitted electromagnetic (EM) waves in the frequency band of interest take from transmitter to receiver over the spatial region of interest. For engineering purposes, the characterization must be quantitative and as thorough as possible. Conversely, the thorough quantitative description must not be so complex as to limit its usefulness; thus, a balance is sought. The final characterization must also be in a form convenient for use in analysis, computer simulations, and experiment if it is to be widely employed. Most often, a mathematical (statistical) model for the time-varying channel impulse response (CIR) and its components constitutes the most useful characterization.

Broadly speaking, wireless channels can be either dispersive or nondispersive. A dispersive channel is strictly defined as one in which phase velocity is a function of frequency; hence, wideband signals are more likely to encounter dispersion than narrowband signals. This dispersion can also yield time spreading, or time dispersion of a signal. In the multipath propagation case, the effect of time dispersion arises from the different path lengths the multiple replicas of the transmitted signal travel. This could include a direct or Line-Of-Sight (LOS) path, but also often includes multiple reflected paths. The multipath channel is said to be time-dispersive when the spread of these multiple received replicas in delay is on the order of a digital symbol duration (T_s) or longer. The spread of the replicas is termed the delay spread (DS), and in a statistical characterization, the root mean square (*RMS*) value is the most often used. The *RMS-DS*, or $\sigma_{\tau,}$ is used to denote the measurement of channel dispersion. Since the wireless channel is well modeled as linear, it can be characterized completely in terms of its channel impulse response (CIR) or, equivalently, the Fourier transform of this, the channel transfer function (TF). The *RMS-DS* is the *RMS* value of the spread in delay of the power-weighted delayed multipath components (MPCs) when an impulse is input to the channel (strictly, $\sigma_{\tau,}$ is the RMS value of the autocorrelation of the CIR at any instant of time, but in practice, the CIR can only be sampled via measurements, and $\sigma_{\tau,}$ can be computed for each sample CIR or power delay profile (PDP). The CIR is often given as a function of two variables, $h(\tau, t)$, where, roughly, τ is short-term delay, and t is the independent variable that allows for time variation: more precisely, $h(\tau, t)$ is the output of the channel at time t due to an impulse input at time t-τ. For causal channels $h(\tau, t)=0$ for $\tau < 0$, and so often $h(\tau, t)$ *vs.* τ is plotted for various instants of time, yielding sets of CIR samples or, roughly equivalently, PDP samples. If the channel is time-invariant, $h(\tau,t)$ is $h(\tau)$, the usual impulse response for a linear time invariant (LTI) system. Real channels also have an impulse response that is finite.

In mobile channels time variation is commonly present, and this variation is typically characterized by correlation functions that measure the rate of change of CIR or PDP components or transfer function frequency components with respect

to time. The scattering function $S(t,\upsilon)$ measures the average power output of the channel as a function of the time delay (τ) and the resulting Doppler frequency (υ) due to motion. The approximate width of the scattering function in the Doppler variable is called the Doppler spread $f_{D,}$ measures the amount the channel spreads a transmitted tone in frequency; this is sometimes also called frequency dispersion.

Thus, for a first order characterization of the channel, it is sufficient to have σ_τ or its approximate reciprocal, the coherence bandwidth B_c, and f_D or its approximate reciprocal, the coherence time t_c. The coherence bandwidth is a measure of frequency selectivity of the channel, and the coherence time is a measure of time selectivity of the channel; hence, both are important to consider when designing and evaluating any communication system to be used on the channel.

Finally, on these general channel characteristics, channels are often assumed to be wide sense stationary (WSS) in time, which implies uncorrelated Doppler shifts at different frequencies within the channel band. Similarly, scattering that occurs at different delays is often assumed to be uncorrelated scattering (US), which implies that the channel's frequency response is WSS. These conditions are commonly combined to yield widely used WSSUS channel models.

Many models exist for the cellular channel, and some models are even incorporated into cellular radio standards. In many of these models the channel characteristics (e.g. $\sigma_{\tau,} f_D$) have been determined empirically from comprehensive measurement campaigns. Analytical models are also used. For most cases, the tapped delay line (TDL) structure is used for the channel model. This is a linear, finite impulse response, filter model for the CIR, and for statistical modeling the filter coefficients, or tap weights, are random processes.

The most common statistical model for the random tap amplitudes (α_s) is the Rayleigh fading model. The Rayleigh model arises from the Central Limit Theorem, in which both the in-phase and quadrature components of each tap are modeled as Gaussian. This Gaussianity requires that the multiple subcomponents which sum to create each tap be approximately equal on energy and large in number, although good approximations are often obtained when the number of multipath components (MPCs) in each tap is as small as 6-10 [5]. These subcomponents that make up each tap are received with approximately the same delay and rare said to be unresolvable by the receiver, which occurs when their separation in delay is much smaller than the reciprocal of the signal bandwidth. Other common statistical models for random tap amplitude distributions include Ricean, Nakagami, log-normal, and Weibull distributions [5].

Thus, to completely specify the TDL model for the channel, it needs the number of taps (obtainable from σ_τ), their rate of change in time (obtainable from f_D), and a statistical model for the tap amplitudes. (Unless there is a dominant, often LOS component, the tap phases are typically modeled as uniformly distributed on

$[0,2\pi)$.) Finally, the relative energy of each tap is also required. Typically the longer the delay, the weaker the multipath component (MPC), so an exponentially decaying power vs. delay characteristic is often employed [1, 3, and 9].

Even within a specific application area, channel models are often subdivided into classes, where each class aims to represent a particular type of physical situation. For the cellular channel, the rural, suburban, and urban classes are commonly used. For indoor channels, office and factory classes may be used. Some models also explicitly identify the presence of a LOS component, and divide into LOS and Non-LOS (NLOS) cases, see [1, 3, and 9].

There are two generic modeling approaches for spatial channels, (see Fig. 1.4 for illustration, the shaded blocks is the main focus of this thesis). So-called "nonphysical models" [5] model the correlation of the fading of the signals at the antenna elements. "Physical models", on the other hand, model the location of scatterers/reflectors, or the direction of multipath components (MPCs) at the transmitter and receiver. Physical models have become more and more popular recently, and are used in such standard models as the European Cooperation in the field of Scientific and Technical research (COST) 259 Directional Channel Model (DCM) [4, 5, and 59] as well as the model developed by the "Spatial Channel Modeling Ad-hoc group " formed by the third-generation standardization organizations 3GPP and 3GPP2 [5].

For physical models, it is a well-established fact that the scatterer locations (or equivalently, the angles and delays of MPCs) are not distributed uniformly over space, but tend to be concentrated in certain regions. Previous indoor and outdoor measurements report that multipath components (MPCs) arrive in clusters, where each cluster consists of a group of MPCs with similar AOAs, AODs, and TOA, and corresponds to a dominant path to the receiver (Rx) [24, 29, 36, 41, 47 and 93–96]. The model introduced by [8], which is still widely used today, assumes that all scatterers are located near the mobile station (MS). A more general model, called "multiple cluster" model takes into account not only the scatterers around the MS, but also clusters of "far scatterers" that correspond to high-rise buildings (in urban environments) or mountains (in rural environments) [27 and 29].

On the other hand from the applications point of view, there are two main channel models approach [9]:

For the design, testing, and type approval of wireless system, it needs simple channel models that reflect the important properties of propagation channel – i.e., properties that have an impact on system performance. This is usually achieved by simplified channel models that describe the statistics of the impulse response in parametric form. The number of parameters is small and independent on specific locations. Such models sometimes lead to insights due to closed-form

relationships between channel parameters and system performance. Furthermore, they can be easily implemented by system designers for testing purposes.

The designers of wireless networks are interested in optimizing a given system in a certain geographical region. Location of base stations (BSs) and other network design parameters should be optimized by the computer, and not by field tests and trial error. For such applications, location-specific channel models that make good use of available geographical and morphological information are desirable. However, the models should be robust with respect to small errors in geographical databases.

The following two modeling methods are in use for these applications; [1, 3, and 9]:

Deterministic channel models: These models use the geographical and morphological information from a database for a deterministic solution of Maxwell's equation or some approximation thereof. The basic philosophy is determining the impulse response in a certain geographic location. This method is therefore often known as site-specific models. The drawbacks of deterministic channel models are (i) the large computational effort, and (ii) the fact that the

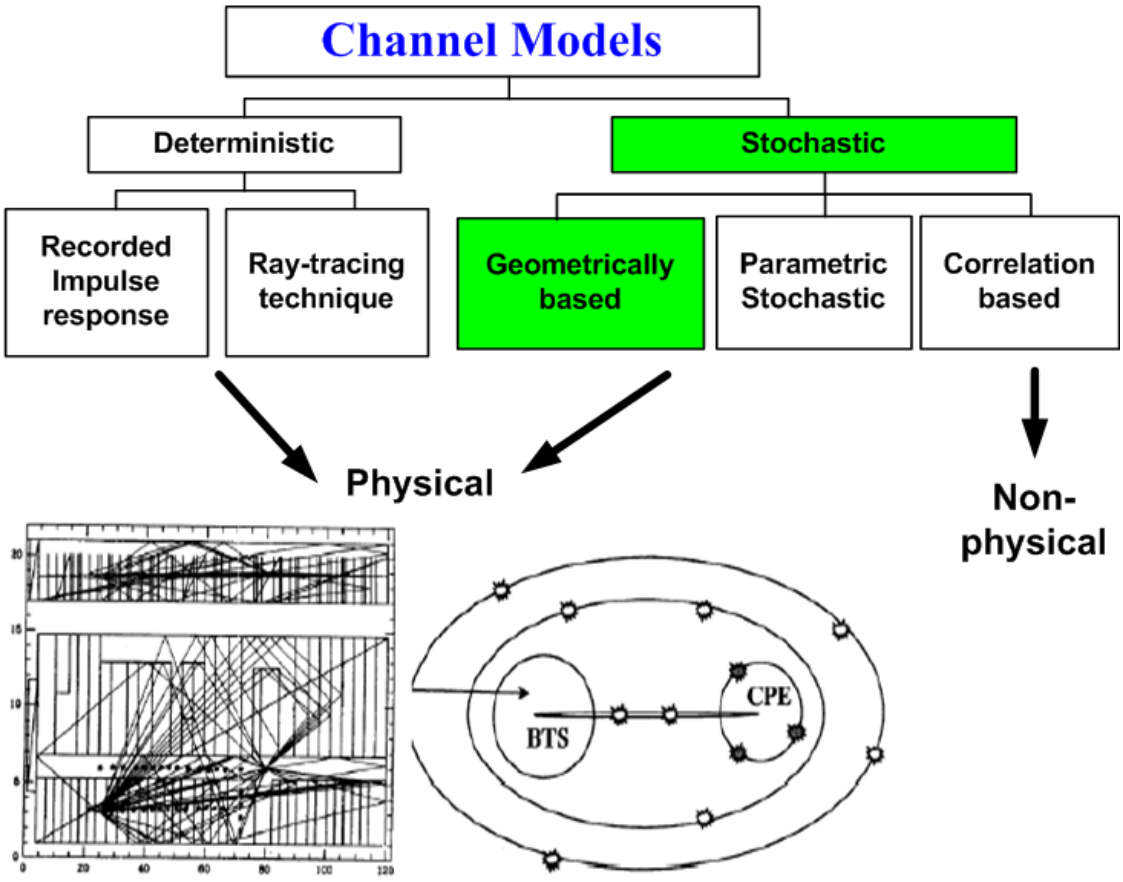

Figure 1.4 General classification of channel models.

results are inherently less accurate, due to inaccuracies in the underlying databases and the approximate nature of numerical computation methods. The main advantage is that the computer simulations are easier to perform than measurement campaigns. Furthermore, certain types of computation methods (e.g., ray tracing) allow the effects of different propagation mechanisms to be isolated.

Stochastic channel models model the probability density function (PDF) of the channel model impulse response (CIR). These methods do not attempt to correctly predict the impulse response in one specific location, but rather to predict the probability density function over a large area. The simplest example of this approach is the Rayleigh fading model: it does not attempt to correctly predict the field strength over a large area. Stochastic wideband models can be created in the same way. The average power delay angle profiles (PDAPs) and its statistical distributions are specified by the model. For the simulation, instantaneous PDAPs are then selected, where the probability of a specific realization is determined by the statistical distributions. Fig. 1.5 shows an example of the stochastic wideband model based on geometry.

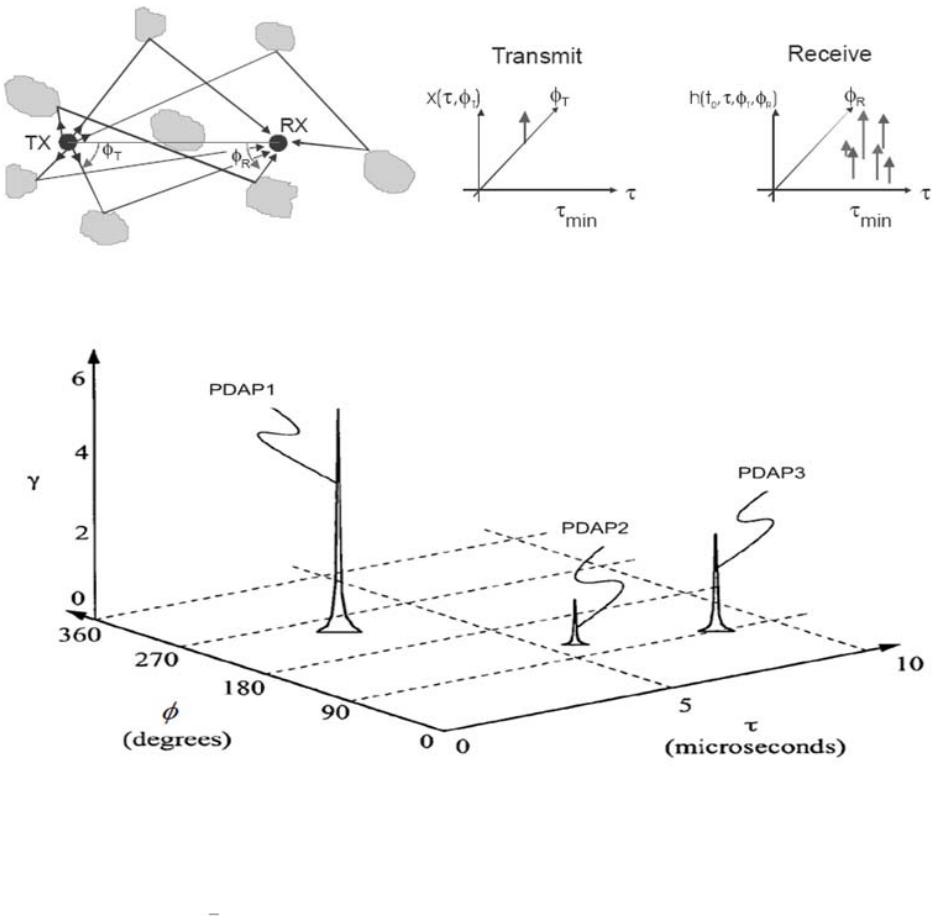

Figure 1.5 Example of Geometry-based stochastic channel model with its corresponding Power Delay Angle Profiles (PDAPs).

Generally speaking, stochastic models are used more for the design comparison of systems, while site-specific models are preferable for network planning and system deployment. Furthermore, deterministic and stochastic approaches can be combined to enhance the efficiency of a model: for example, large–scale averaged power can be obtained from deterministic models, while the variations within an averaging area are modeled stochastically.

In this Section, the work dealing with the statistical channel models is reviewed. Because of the rapidly intensifying efforts in channel modeling research, a complete and accurate survey is not possible. As mentioned earlier, for the design, simulation, and planning of wireless systems it need models for the propagation channels. A good overview of different spatial channel models can be found in [3, 6, 9, 13, 30, 85, and 86]. However, extending these models to the MIMO case is not straightforward, since the spatial characteristics must now be considered at both ends either directly or indirectly.

As reported in [10, 14–20, 57, 64, and 89–91] channel capacity can be greatly increased by using antenna arrays at both the transmitter and receiver, so-called Multiple Input Multiple Output (MIMO) systems, as long as the environment provides sufficient scattering. Conceptually, a MIMO channel can be seen as parallel spatial sub-channels which allow the transmission of parallel symbol streams. Therefore, the MIMO channel capacity can potentially increase linearly with the number of spatial sub-channels (minimum number of receive or transmit antenna elements). This has been demonstrated in [11], where architecture, called Bell Labs Layered Space-Time (BLAST), was proposed along with a coding and decoding scheme. Some field measurements investigating MIMO channel capacity have been reported in [47–51, 56, 62, 77–79, and 91]. Several of the reported results are encouraging in that the scattering has been sufficiently rich to provide capacities close to the ideal situation.

Several techniques have been proposed to utilize the spatial diversity of MIMO communication channels. These techniques can be divided into two groups, i.e. space-time coding and spatial multiplexing. The space-time coding, in general, assumes no knowledge on the propagation channel at the transmitter. At the receiver, the structure of space-time codes is exploited to correct the errors. Examples on space-time block coding can be found in [20], the space-time trellis codes have been discussed. In [13], the space-time block codes have been improved using imperfect channel information at the transmitter. The spatial multiplexing, on the other hand, attempts to utilize parallel spatial sub-channels by exploiting channel information at the receiver. It is well known [15] that when the transmitter has full knowledge about the channel, by using waterfilling technology [9], maximum channel capacity can be achieved. The propagation conditions determine the channel capacity that can be expected for a MIMO system. It is of great interest to characterize and model the MIMO radio channel for different conditions in order to predict, simulate, and design high performance communication systems.

Among other advantages, the simulation of MIMO propagation channel can assist in the choice of efficient modulation schemes under different scenarios and system performance can be accurately predicted. Much work has been reported regarding single-input single-output (SISO) channel modeling area. Models on SISO channel were reported in the literature, references for indoor radio channel models and also examples of outdoor channel models can be found in [1–3]. The single-input multiple output (SIMO) and multiple-input single-output (MISO) channels have also been studied and different models were proposed, see [7, and 16–17] and references there in.

1.4 Problem Statement

The purpose of this thesis is to analyze the clustering approach based on simulations of Geometry-based mobile radio channel models for urban environments and how these can be used to further improve the performance of current or future mobile radio systems. Furthermore, it is extended the GBSB channel model for MIMO modeling approach and derived some statistical characteristics of the extended model and compared it with the model based on geometry for conventional technique with a single antenna, at the transmitter (Tx) and the Receiver (Rx), better known as single-input single-output (SISO) system in different environments and a comparison between the channel models based on theoretical data against measured data.

1.5 Method

For the investigation of the MIMO channel models, the article contribution already done and the web research articles using the Internet were a major source.

For the analysis and simulation of the MIMO channel models, two different tools were considered, simulation tool and programming in Matlab®.

For the comparison of the MIMO channel models based on the theoretical data and measured data, the simulations using Matlab® was performed.

1.6 Thesis Contribution

Essentially, the main objective of this thesis is to propose a generic statistical channel model that would be useful in simulating high-speed transmission systems operating in a stationary environment or low mobility scenarios. First, the departure and arrival rays are grouped into a few scattering clusters. Each cluster can generates a set of angles of arrival (AOAs), angles of departure (AODs), and time of arrival (TOA) for each frequency interval. Some of the main characteristics of the urban channels like angular/delay spreads (ASs/DSs) are incorporated in the model.

This thesis presents analysis and design of geometry-based statistical channel models for MIMO wireless communications with applications in urban areas. Taking into account the clustering approach, it describes the spatio-temporal properties of the channel. The clustering approach analysis is performed over the prescribed bandwidth of 5 MHz for the 3GPP-3GPP2 channel model with the carrier frequency, f_c = 2 GHz. The scenario is focused on the Urban Microcell

scenario with one stationary MS and one BS. It is also assumed that the MS is at a fixed distance from the BS, but its orientation with respect to the BS is randomly generated from U(0,360°). The antenna spacing at the BS and MS are set at $d = 0.5\lambda$ respectively. Finally, it is also assumed that the receive antennas are in the far field of the transmit antennas, i.e., the BS is assumed to be 500 m away from the MS. So far urban areas have been attractive to private investors due to high population density, large coverage areas, in perhaps no difficult terrain together with the high income of potential users.

Furthermore, it is proposed a new channel model that unlike the previous geometrical models based only on single bounce reflection, it is also described a model to represent the PDAPs by clusters plus background single bounce scatter components, i.e. the waves arrive at the receiver by double scattering at least.

The PDAP is known to be constant over small variations in location and to be stable in time (absent any significant changes in environmental structures). Thus, the PDAP is a gradually varying function of location, and may be used at either or both Tx-Rx to improve reception and/or transmission of signals propagating over the wireless channel.

The main contributions proposed in this thesis are summarized as follows:

- A new methodology for evaluating the performance of MIMO communications systems is proposed through the geometry-based channel models. The quantification of such approach is mainly performed, evaluated and analized for urban scenarios in stationary or low mobility conditions.

- Through comparisons to measurements results available in the literature the performance gain of the MIMO system are evaluated utilizing different physical urban scenarios that comprise the wireless channel model.

- The probability density functions (PDFs) in the angular and time domain respectively are derived through direction of arival (DOA) and time of arrival (TOA) for the clustering approach model. The derved theoretical PDFs are compared with experimental results published in the literature. The comparison results between the channel model based on theoretical data and parameter setup to the channel models based on statistical characteristics obtained from measured data shows good agreement.

1.7 Thesis Organization

This thesis is written in the form of a monograph and is divided into six chapters and one appendix that together constitute the thesis. It is organized in the following way. Chapter 1 gives an introduction with the general background of the presented work, the purpose of the research, and description of the research design, research overview and related works, and contributions made in the research.

This thesis gives an analysis of the clustering approach based on simulations of Geometry-based mobile radio channel models for urban environments and how these can be used to further improve the performance of current or future mobile radio systems. It is also presented an analysis of angular and time domain respectively through direction of arrival (DOA) and time of arrival (TOA) probability density functions (PDFs) for the clustering approach model. Besides, the thesis gives a brief overview of the recent development in modeling of MIMO radio propagation channels. The Clustering approach for geometry-based channel model is described in detail and verified from the data collected in a 2 GHz outdoor MIMO channel measurement campaign available in the literature. Finally, this thesis gives some suggestions for future research. In the following an outline of the thesis and a summary of the contributions, listed chapter by chapter, are given. After the introduction in Chapter 1 the following chapters are treated:

Chapter 2. This chapter reviews some published research on spatial channel modeling. First, these models are categorized into two main groups, i.e. non-physically and physically based models. The non-physical models are derived from the statistical characteristics of the channels, while the physical models use some important physical parameters to provide a reasonable description of the spatial channel characteristics and the surrounding scattering environment. The spatial channel models will be reviewed based on this classification in the chapter with emphasis on physical channel models based on geometry. Part of this chapter has been published in

- M.R. Arias and B. Mandersson, “An approach of the Geometrical-based single bounce elliptical channel model for mobile environments,” Proceedings of The 8th International Conference on Communication Systems, (ICCS 2002), vol.1, pp 11–16, Singapore, Nov. 2002.

Chapter 3. This chapter extends the Geometrically Based Single Bounce channel model developed by Liberty and Rappaport [8] to narrowband MIMO Channel model. The propagation environment is composed of scatterers that are uniformly distributed in space and have equal scattering cross sections. However in this extended MIMO channel model the scatterers are grouped into clusters. Clusters are distributed inside the environment and the scatterers inside the

cluster follow a uniform distribution.The chapter focuses on statistical description of the first and second order moments of the narrowband MIMO channel. Part of this chapter has been published in

- M.R. Arias and B. Mandersson, “Clusters PDF in Angle and Time Domain for Geometrically Based Channel Model”, Proceedings of International Symposium on Intelligent Signal Processing and Communication Systems (ISPACS 2004), pp 433-438, Seoul, Korea, Dec. 2004.

- M. R. Arias, “Derivación Analítica del Tiempo de Llegada en Modelos de Canal Basados en Geometría para Sistemas Inalámbricos”, “Revista Científica de la Universidad Nacional de Ingeniería, Nexo Vol. 20, No. 02, pp. 69-77/Noviembre 2007. Available in the Directory of Open Access Journals, (DOAJ).

Chapter 4. This chapter proposes the double bounce approach of the geometry-based elliptical channel model, where it describes and analyzes the model to represent the power delay angle profiles (PDAPs) by clusters plus background single bounce scatter components, i.e. the waves arrive at the receiver by double bounce at least. Instead of analyzing the number of scatterers as uniformly distributed in the whole coverage area, the scatterers are grouped into “clusters”, to obtain a cluster of scatterers from which is obtained the parameters of interest, e.g., delay spread (DS), angle of arrival (AOA) and also known as direction of arrival (DOA), angle spread (AS), and the power delay angle profiles (PDAPs). Part of this chapter has been published in

- M.R. Arias and B. Mandersson, “Clustering approach for geometrically based channel model in urban environments”, IEEE Antennas and Wireless Propagation Letters, Vol. 5 pp 290-293, Dec. 2006. Available in the Institute for Scientific Information database (ISI Thomson).

Chapter 5. Here, it analyzes the clustering approach for geometry-based channel model proposed in the previous chapter, and employ it to derive analytical expressions for the angle of arrival (AOA) PDF and time of arrival (TOA) PDF (expressed in terms of distance) respectively of the multipath signal components. To evaluate the theoretical clusters PDFs in angular and time domain proposed, computer simulations are carried out from the geometry-based channel model proposed in Chapter 4. Then it makes comparisons to experimental results published in the literature showing good agreement. The cluster PDF in angular and time domain derived can be used to simulate temporal dispersion of the multipath signal group into clusters in a variety of urban propagation conditions to quantify second order statistics, i.e., delay and angle spread respectively for a given elliptical shape of the cluster. Part of this chapter has been published in

- M.R. Arias and B. Mandersson, “A Generalized Angle Domain Clusters PDF and Its Application in Geometrically Based Channel Models”, Proceedings of International Conference. on Information, Communications and Signal Processing (ICICS 2005), pp 1339-1343, Bangkok, Thailand, Dec. 2005.

- M.R. Arias and B. Mandersson, “Time Domain Cluster PDF and Its Application in Geometry-Based Statistical Channel Models”, Proceedings of The 18th Annual IEEE International Symposium on Personal, Indoor and Mobile Radio Communications (PIMRC 2007), pp 1-5, Athens, Greece, Sept. 2007.

Chapter 6. This chapter summarizes the thesis and gives some concluding remarks. Some suggestions for future research are also included.

Chapter 2 Geometry-Based Channel Models

Radio propagation is an important aspect of any radio design or radio network planning. Channel models try to give a realistic representation of the radio propagation between two or more points, and can widely be divided into two groups as mentioned in the previous chapter: the non-physical and physical models [24–26]. The non-physical models are based on the channel statistical characteristics using non-physical parameters. In general, the non-physical models are easy to simulate and provide accurate channel characterization for the situations under which they were identified. On the other hand they give limited insight to the propagation characteristics of the spatial channels and depend on the measurement equipment, e.g. the bandwidth, the configuration and aperture of the arrays, the heights and response of transmit and receive antennas in the measurements. The influence of the channel and measurement equipment on the model can not be separated. Another category is the physical models. In general, these models choose some crucial physical parameters to describe the spatio-temporal propagation channels. Some typical parameters include angle of arrival (AOA), angle of departure (AOD) and time of arrival (TOA).

This chapter introduces the topics of the spatial channel models for mobile radio communications, with emphasis on physical channel models based on geometry. As mentioned in [7], a basic understanding of the channel is important for finding modulation and coding schemes that improve the channel, for designing equalizers or, if this is not possible, for deploying base station antennas in such a way that the detrimental effects are less likely to occur. This chapter presents also a modeling approach with simulations results obtained by a Geometrically Based Single Bounce Elliptical Channel model (GBSBEM), defined in [8] that it is implemented for two urban scenarios: a) Scenario I, City-Street-Scenario and b) Scenario II, Cross-Street-Scenario, respectively, in both cases the height of the buildings as part of the modeling approach is taken into account. Part of this chapter has been published in [34].

2.1 Background

Over the past two decades, radio communication systems have undergone extensive developments. The demands that a radio system must fulfill are greater by the day. The propagation of radio signals on both forward or downlink (base station to mobile) and reverse or uplink (mobile to base station) links is affected by the physical channel in several ways. These physical objects and structures are: buildings, hills, streets, and trees, among others. The collection of objects in any given physical region describes the propagation environment [1].

A signal propagating through a wireless channel usually arrives at the destination along a number of different paths, referred to as multipath components (MPCs). These paths arise from scattering, reflection, refraction or diffraction of the radiated energy off objects that lie in the environment. Fig. 2.1 illustrates an example of multipath propagation. For analyzing the performance of wireless communication systems, a statistical channel model (which provides the direction of arrival (DOA) and time of arrival (TOA) of the MPCs) is required.

In a typical mobile-radio application, the base station is fixed in position, while the mobile unit is moving. This is usually subject to a condition such that the propagation between them is largely through scattering, either by reflection or diffraction from buildings and terrain or objects within buildings, because of obstruction of the Line-Of-Sight (LOS) path. Radio waves therefore arrive at the mobile receiver from different directions with different amplitudes, phases, and time delays, resulting in multipath propagation. The radio channel is then obtained as the sum of the contributions from all the paths. If the input signal is a unit impulse, $\delta(t)$, the output will be the channel impulse response, which can be written as [6–10]:

$$h(t,\tau) = \sum_{n=1}^{N} A_n \delta(t-\tau_n) \exp(-j\varphi_n). \tag{2.1}$$

The channel impulse response can thus be characterized by N time-delayed impulses, each represented by an attenuated and phase-shifted version of the original transmitted impulse. Here, A_n, τ_n, and, φ_n are the attenuation, delay in time of arrival, and phase, corresponding to path n, respectively.

Although multipath interference seriously degrades the performance of communication systems, little can be done to eliminate it. However, if the multipaths medium are characterized well, and having some knowledge of the propagation mechanisms and their influence on the system, the best design for

the system can be selected to achieve good propagation performance and hence, to achieve a better quality of service. Furthermore, as mentioned before, wireless systems of the future like Multiple Input Multiple Output (MIMO) systems, exploit the presence of multipath to enhance the transmission of data through a wireless link.

Besides, as a result of the *Doppler effect*, the motion of the receiver leads to a frequency shift (*Doppler shift*) of the partial waves impinging the antenna. Depending on the direction of arrival of these partial waves, different Doppler shifts occur, so that for the sum of all scattered (and reflected) components, finally a continuous spectrum of Doppler frequencies is obtained, which is called the Doppler power spectral density.

If the propagation delay differences among the scattered signal components at the receiver are negligible compared to the symbol interval, then the channel is said to be *frequency-nonselective* (*flat fading*) [1]. In this case, the fluctuations of the received signal can be modeled by multiplying the transmitted signal with an appropriate stochastic model process. After extensive measurements of the envelope of the received signal in urban and suburban areas, i.e., in regions where the Line-Of-Sight (LOS) component is often blocked by obstacles, the Rayleigh process was suggested as suitable stochastic model process. In rural regions, however, the LOS component is often a part of the received signal, so that the Rice process is the more suitable stochastic model for these channels [6].

However, the validity of these models is limited to relatively small areas with dimensions in the order of about some few tens of wavelengths (λ), where the local mean of the envelope is approximately constant. In larger areas, however, the local mean fluctuates due to shadowing effects and is approximately lognormally distributed, as shown in [1–3].

The knowledge of the statistical properties of the received signal envelope is necessary for the development of digital communication systems and for planning mobile radio networks. Usually, Rayleigh and Rice processes are preferred for modeling fast-term fading, whereas slow-term fading is modeled with a lognormal process [4]. Slow-term fading not only has a strong influence on channel availability, selection of the carrier frequency, handover, etc., but also is important in the planning of mobile radio networks [7]. For the choice of the transmission technique and the design of digital receivers, however, the properties of the fast-term statistics, on which is concentrated the focus of this thesis, are of vital importance.

Excess delay, root mean square (*rms*) delay spread (DS) , angle of arrival (AOA), and *rms* angle spread (AS) are the basic modeling parameters, e.g., the *rms* delay spread is directly connected to the capacity of a specific communication system and gives a rough implication on the complexity of a receiver. In fact, the

directions from which the signals arrive, the direction of arrival (DOA) is an important property when characterizing the channel as well as designing receiver algorithms [14]. The angle spread (AS), among others, essentially determines the diversity gain by using an antenna array [8].

Models for mobile radio channels must fulfill conflicting requirements. On one hand, they should be detailed enough to reflect all relevant properties of propagation channels; they should also not be misleading, and relevant limitations should be explained to prevent misapplication. On the other hand, they should be simple enough to allow rapid implementation and short simulation times [18–25].

A common channel modeling strategy is the statistical description of time variant fading effects of the physical channel due to moving terminals, moving obstacles and the transmission environment, including directional information [21–32]. This information has to be obtained from practical measurements.

Geometrically Based Single Bounce (GBSB) Statistical Channel Models are defined by a spatial scatterer density function. These models are useful for both simulation and analysis purposes. Use of the models for simulation involves randomly placing scatterers in the scatterer region according to the form of the spatial scatterer density function. From the location of each of the scatterers, the DOA, TOA, and signal amplitude are determined.

Liberti and Rappaport [8] developed a Geometrical Based Single Bounce model (GBSB) for microcells. The GBSB model assumes that scatterers are uniformly distributed in space and have equal scattering cross sections. This model provides a structure in which short delay multipath components (MPCs) are more likely to arrive with direction of arrival near the direct path, while MPCs with longer delays are more uniformly distributed in DOA.

From the spatial scatterer density function, it is possible to derive the joint and marginal TOA and DOA probability density functions (PDFs). Knowledge of these statistics can be used to predict the performance of an adaptive array. Furthermore, knowledge of the underlying structure of the resulting array response vector may be exploited by beamforming and position location algorithms [7].

The shape and size of the spatial scatterer density function required to provide an accurate model of the channel is subject to debate. Validation of these models through extensive measurements remains an active area of research.

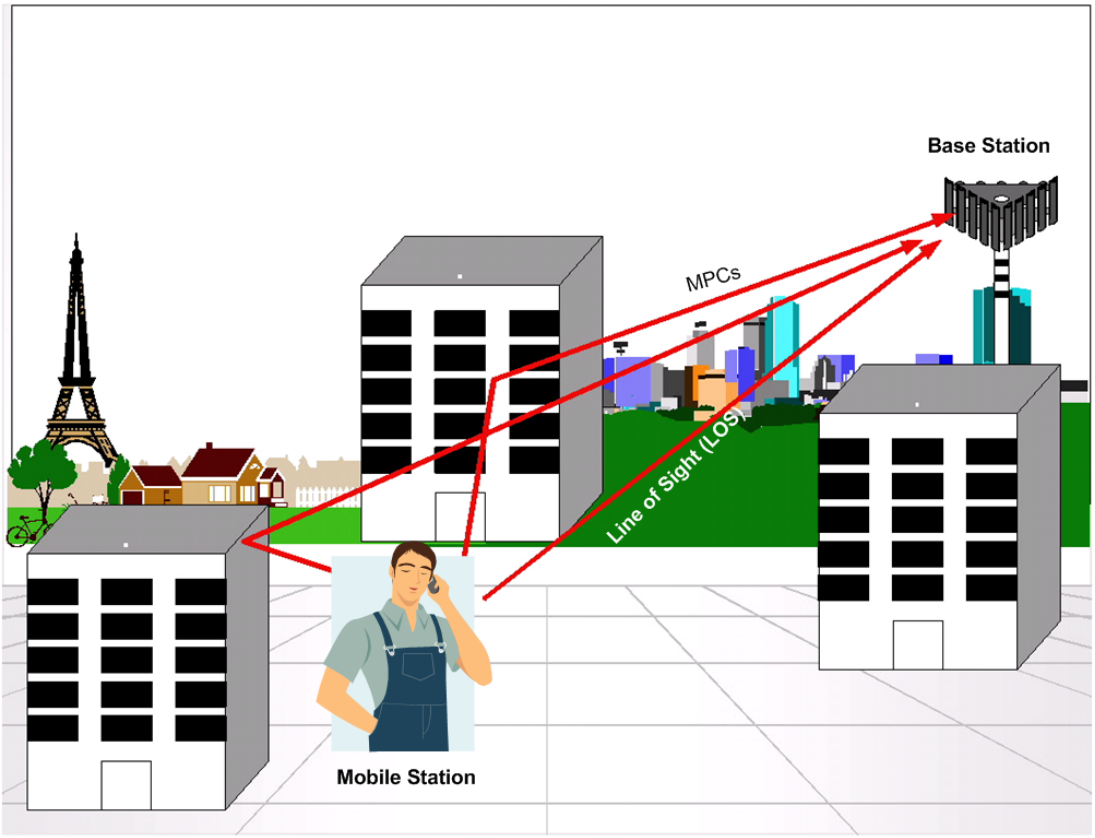

Figure 2.1 Example of multipath propagation.

2.2 Overview of Space-Time Geometrical Channel Models

The propagation models, which have been developed to date in order to simulate the radio channels, have evolved according to the needs of the mobile communications industry. Consequently, there is a demand for new models that will provide the required spatial and temporal information needed to study many practical mobile radio systems (e.g. third generation systems and beyond like the wideband-CDMA) of communication systems.

The recent literature on communication systems contains a vast quantity of articles dealing with the modeling and analysis of spatial channel models, particularly indoor wireless and outdoor mobile channels, see e.g. [21–41] and references there in. While a complete review of the literature is outside the scope of this chapter, however it provides a brief review of the modeling of spatial channel models to the development of simulations techniques.

Multiple Input Multiple Output (MIMO) channels are commonly called vectorial or matrix channels as for each transmitter-receiver (Tx-Rx) antenna pairs, there is

established a channel. In this context, for every single channel is trying to model the spatio-temporal channel statistics with the help of a geometrical model.

Most of the existing geometrical channel models take into account only the local scattering cluster [4], which is always located around the mobile unit with few available models defining the shape and distribution of far clusters. The geometrical channel models are well suited for simulations that require a complete model of the wireless channel, due to its ray-tracing nature. However, the shape and size of the spatial scatterers' density function required to achieve a reliable simulation of the propagation phenomenon is subject to debate.

The most important requirements for channel models are [6–9]:

1) Correct reproduction of measured joint angular delay power spectrum (PDAPs)

2) Compatibility with previously used stochastic wideband channel models, in order to facilitate comparisons with previous simulation results.

3) The model should clearly reflect essential physical propagation mechanisms. This makes the model easy to understand and enables realistic parameter selection by means of straightforward geometrical and environmental considerations.

4) A further practically important requirement is simplicity, which should allow extensive simulations in short time. Unfortunately, this is usually in contradiction to requirement (1), i.e. faithful reproduction of measured results. Furthermore, for different applications, the balance between these two requirements may have to shift.

5) This leads to a new model requirement, namely adaptivity, i.e. the model should allow the user to define a set of functionalities included in the current simulation. This flexibility is especially important because future systems can have different requirements for the channel models.

2.3 Geometrically Based Single Bounce Channel Models (GBSB)

The spatial properties of wireless communication channels are extremely important in determining the performance of smart antennas systems. Modern Spatial channel models build upon the classical understanding of multipath fading and Doppler spread by incorporating additional concepts such as time delay spread (DS), direction of arrival (DOA), time of arrival (TOA), and adaptive

array antenna geometries [7]. Spatial channel models find use in the design and pretest evaluation of wireless systems in general and of mitigation technique in particular. They are generic, but their formation can be quite labor-intensive and they are not well suited to specific deployments.

The importance of spatial channel models can be summarized as follows:

- They are useful to analyze and design by simulation both wideband and narrowband systems.
- Explore different ways that the model can be applied:
- Applications of adaptive antenna array systems for capacity improvements and range extension of the system.
- MIMO system design for: diversity, spatial multiplexing, and beamforming.
- The spatio-temporal correlation properties can be analyzed.

2.3.1 Geometry-Based Stochastic Channel Model (GSCM)

In this approach, described in more details in [19], the statistical distribution of the scatterers (and not their exact location, as in a deterministic approach) is prescribed by the model. For the actual simulation a specific realization of scatterers is selected at random, and a simple ray-tracing algorithm computes the angularly resolved impulse response. Of course, the scatterer distributions have to be chosen in such a way that the resulting power delay profiles (PDPs), power angle profiles (PAPs), etc. agree reasonably well with typical measured values.

In the geometrically-based stochastic channel model (GSCM) [21], first, it compute the location of the scatterers, then , in a semi-analytic way it compute the average power delay angle profiles (PDAPs), then the MS moves over a small area, i.e. averaging over Rayleigh fading. In this case it does not need to compute instantaneous realizations in order to obtain the average PDAPs.

As long as the MS move less than about 10 wavelengths, the average PDAPs stays constant, so it is possible to compute the instantaneous realizations of the PDAPs by using the stochastic model. When the MS has moved a large distance, it computes a new average PDAPs from the GSCM, and so on.

First results indicate that the single- scattering assumption is often correct in macrocells, but breaks down in micro- and picocells. Waves guided in a street canyon, for example, suffer multiple reflections, as waves in indoors environments, where multiple reflections from walls, floors, and ceilings are

common. However, a correct implementation of the multiple scattering leads to a significant increase in computational complexity, and is thus not advisable.

The question of single-scattering can also be considered from a slightly different point of view. Under the assumption of single scattering, the PDAPs and the scatterer location are related by a bijective mathematical transformation. Thus, for a given PDAPs (e.g. from a measurement), it can be assigned a scatterer distribution that is not necessarily the true physical distribution, but allows reproducing the correct PDAPs by ray-tracing under the assumption of single-scattering. More interesting is the question whether the scatterer distribution produced that way can e.g., extrapolate the PDAPs correctly when the MS is moved.

The Geometrical based single bounce macrocell channel model (GBSBM) is an extension of the circular disk of scatterers model described earlier and in more details in [21]. Fig. 2.2 shows the geometry used to derive this model [3 and 9]. The next Section will describe in detail the GBSM channel model.

2.3.2 Geometrically Based Model for Line-Of-Sight Multipath Radio Channels (GBSBEM)

This model, as mentioned before was developed by J. C Liberti and T.S. Rappaport, (see [8] for more details), and was designed for microcell and picocell environments where antenna heights are low, so that multipath scattering is just as likely near the base station as it is near the mobile. An essential feature of the Geometrical Based Single Bounce Elliptical Model (GBSBEM), is the physical interpretation that only multipath signals that arrive with an absolute delay of less than or equal to τ_m (maximum delay) are considered.

The model is used to simulate power delay angle profiles (PDAPs), power delay profiles (PDPs), power angle profiles (PAPs), joint time-angle statistics, marginal characteristics of the direction of arrival (DOA), and narrowband fading envelopes. However, their model is limited to a LOS condition and does not allow for an accurate evaluation of direction-sensitive wireless systems due to the lack of spatial information for NonLOS conditions.

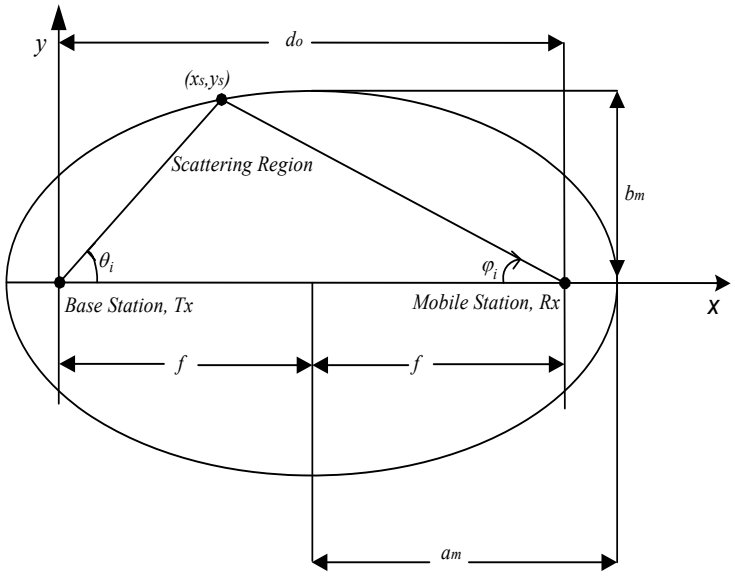

Figure 2.2 Elliptical scatterer density geometry.

The GBSBEM model is appropriate for low-tier systems, including microcell and picocell systems, where base station antennas are surrounded by clutter and scatterers are distributed between and around both the transmitter and receiver [7]. The scatterer resulting in a single bounce multipath component (MPC) arriving at time τ_i lie at coordinates (x_s, y_s) such that x_s, y_s satisfy:

$$\frac{x_s^2}{a^2} + \frac{y_s^2}{b^2} = 1. \tag{2.1}$$

This elliptical model assumes that each MPC of the propagating signal undergoes only one bounce traveling from the transmitter to the receiver and that scattering objects are uniformly distributed in space with equal scattering cross section within an elliptical region between and around both the mobile and the base station, as shown in Fig. 2.2, where the base station (transmitter, Tx) and mobile (receiver, Rx) are the foci of the ellipse.

Assuming that the distance from the scatterer at (x_S, y_S) to the base station (BS) is ($-f$, 0), and the distance from the scatterer to the mobile station (MS) is (f, 0), then, this sum to $2a=c\tau_i$, (where c, is speed of light and τ, time delay).

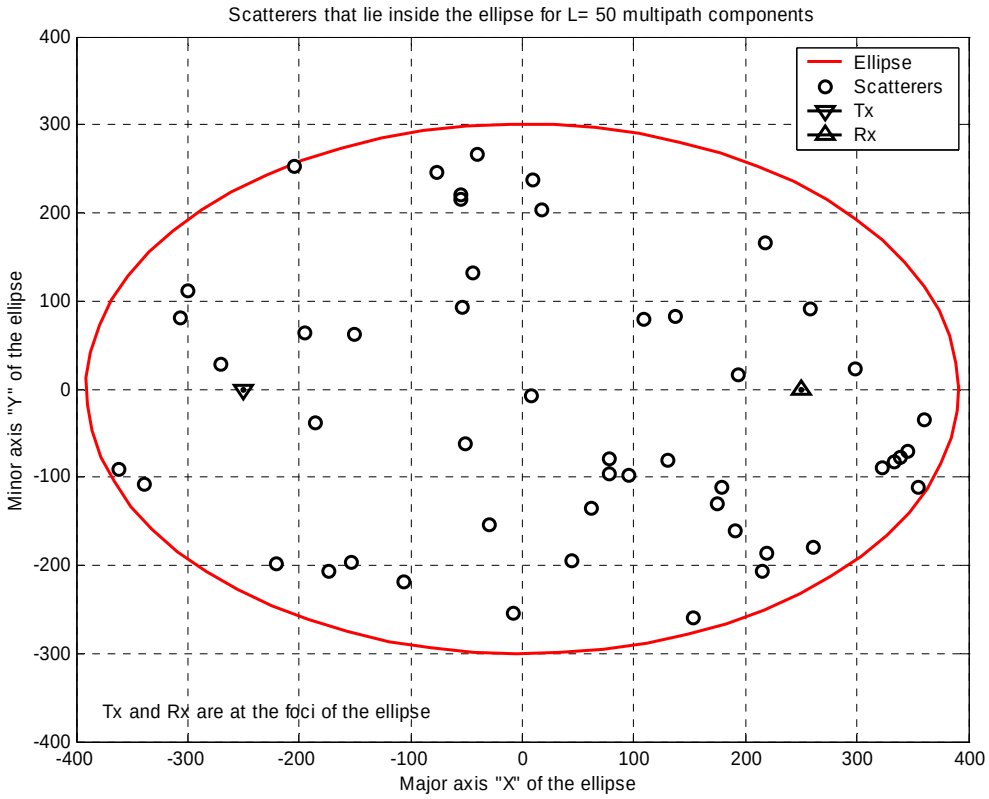

Figure 2.3 Example of scattering region that lies inside the ellipse for L=50 multipath components (MPCs). Based on GBSBEM channel model.

This is because the distance from the scatterer at (x_s,y_s) to the transmitter at $(-f,0)$, and the distance from the scatterer to the receiver at $(f,0)$ sum to $2a = c\tau_i$ provided that the scatterer lies on the ellipse $\{a,b\}$.

$$x_\phi = a\left(\frac{f - a\cos\phi}{a - f\cos\phi}\right), \tag{2.2}$$

$$y_\phi = \frac{b^2 \sin\phi}{\left(a - f\cos\phi\right)}, \tag{2.3}$$

where, f is the foci of the ellipse given by $f = \sqrt{a^2 - b^2}$. Similar analysis results can be found in [6, and 21–23].

A good thing with this elliptical model is the physical interpretation that only multipath signals that arrive with an absolute delay $\leq \tau_m$ are accounted for by the model; where τ_m is the maximum time of arrival (TOA) to be considered.

Ignoring components with larger delays is possible since signals with longer delays will experience greater path loss, and hence have relatively low power compared to those with shorter delays. Therefore, provided that τ_m is chosen sufficiently large, the model will account for nearly all the power and DOA of the multipath signals [6]. Fig. 2.2 shows that the parameters a_m and b_m are the semimajor axis and semiminor axis values respectively, which are given by [6]:

$$\begin{aligned} a_m &= \frac{c\tau_m}{2}, \\ b_m &= \frac{1}{2}\sqrt{c^2\tau_m^2 - d_0^2}, \end{aligned} \tag{2.4}$$

where c is the speed of light. The choice of τ_m will determine the delay spread (DS) and angle spread (AS) of the channel. Methods for selecting an appropriate value of τ_m are given in [7]. In simulating the DOA, TOA, and power levels for MPCs, it is necessary to generate samples of random variables from specified distributions. Using the GBSB elliptical model approach, the simplest way to create sample spatio-temporal channels is to generate a set of L scatterers which are uniformly distributed in x and y and fall within the ellipse described by equation (2.1).

Fig. 2.3 shows an example of the scattering region described by the ellipse illustrated in Fig. 2.2, using the Geometrically Based Single Bounce Elliptical Channel Model (GBSBEM), for L= 50 MPCs. From Fig. 2.3 note that all the scatterers lie inside the ellipse.

In summary, the following assumptions are applyied [8]:

- All scatterers lie in the same plane as the transmitter and receiver and this plane is roughly parallel with the ground. Scatterers are uniformly distributed in this plane and have equal scattering cross section.

- Each scatterer is an omnidirectional re-radiating element with equal scattering coefficients and uniform random phases.

- A Line-Of-Sight (LOS) path exists between the transmitter and the receiver.
- The receive signal at the antenna undergoes no more than one reflection by scatterers when traveling from transmitter to receiver, i.e., single bounce multipath is the dominant mode of propagation.

- The model includes ground reflections, based on the assumption that the Tx-Rx separation d_0, is much larger than the transmitter antenna height and the receiver antenna height.

The joint TOA/DOA PDF at the base station is given by [2 and 5]

$$f(\tau_k,\theta_{bk})=\begin{cases}\dfrac{l(\tau_k,\theta_{bk})}{4\pi a_m b_m} & :\dfrac{D}{c}\le\tau_k\le\tau_m,\ \theta_{bk}\neq 0\\ \dfrac{c(D+\tau_k c)}{4\pi a_m b_m} & :\dfrac{D}{c}\le\tau_k\le\tau_m,\ \theta_{bk}=0\\ 0 & :\text{elsewhere}\end{cases} \tag{2.5}$$

Where

$$l(\tau_k,\theta_{bk})=\frac{\left(D^2-\tau_k^2c^2\right)\left(D^2c+\tau_k^2c^3-2\tau_kc^2D\cos(\theta_{bk})\right)}{\left(D\cos(\theta_{bk})-\tau_kc\right)^3} \tag{2.6}$$

While the joint TOA/DOA PDF at the mobile station is similar to the joint TOA/DOA PDF at the base station except the angle of arrival is replace by the angle at the mobile station, θ_{mk} [2 and 5]. Fig. 2.4 shows the joint TOA/DOA PDF for the elliptical channel model GBSEM).

In the above equations (2.5) and (2.6) D is the distance between the base station and the mobile, τ_k is the delay of the k^{th} path, θ_{bk} is the DOA at the base station, θ_{mk} is the DOA at the mobile station, and c is the speed of light.

The values of the path delay (τ_i), DOA (φ_i), and power (P_i), are generated for MPCs using the statistics above described. This procedure is useful in performing Monte Carlo simulations of the multipath channel [6]. In simulating the DOA, TOA, and power levels for MPCs, it is necessary to generate samples of random variables from specified distributions. Using the GBSB elliptical model approach, the simplest way to create sample spatio-temporal channels is to generate a set of L scatterers which are uniformly distributed in x and y and fall within the ellipse described by [7].

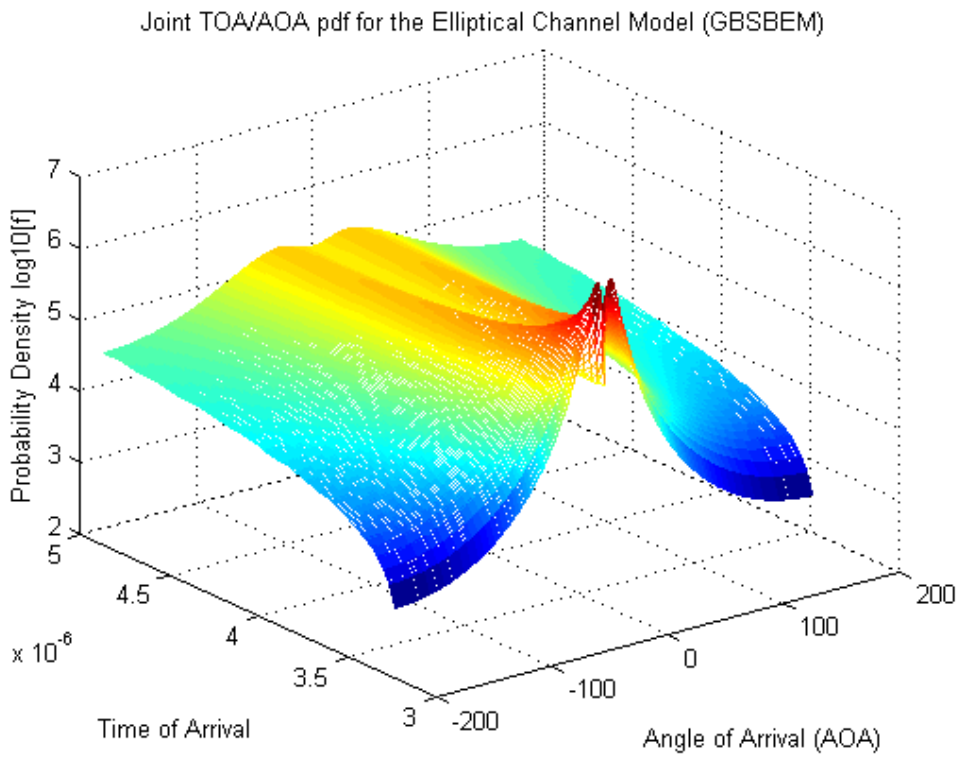

Figure 2.4 A sample of the joint TOA/AOA PDF for the geometrically based single bounce elliptical channel model (GBSBEM).

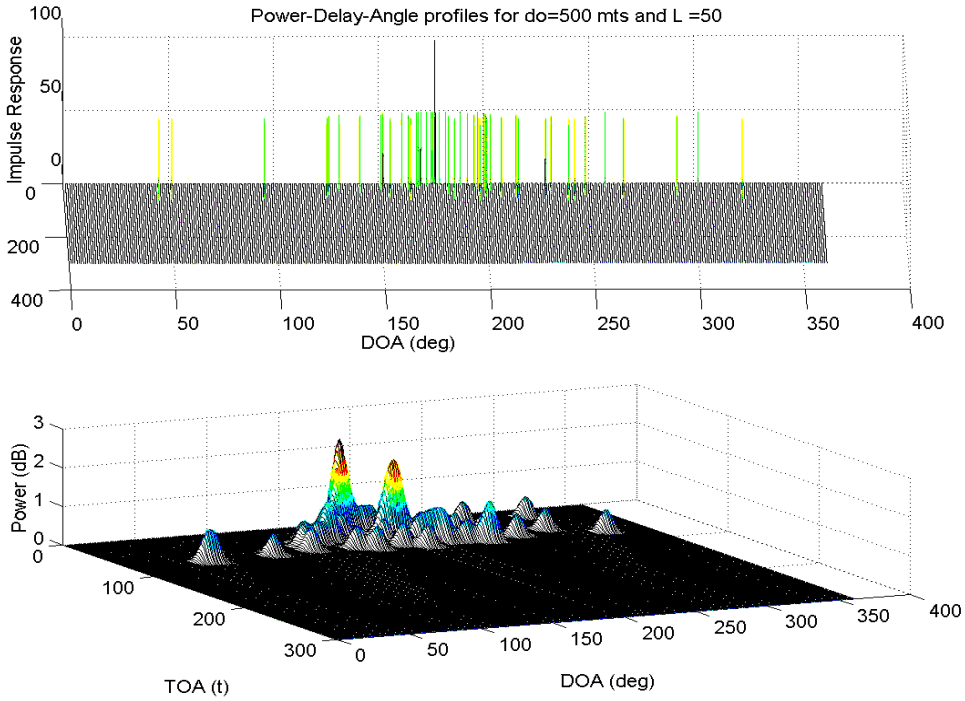

Figure 2.5 A sample of PDAPs generated for L=50 multipath components (MPCs).

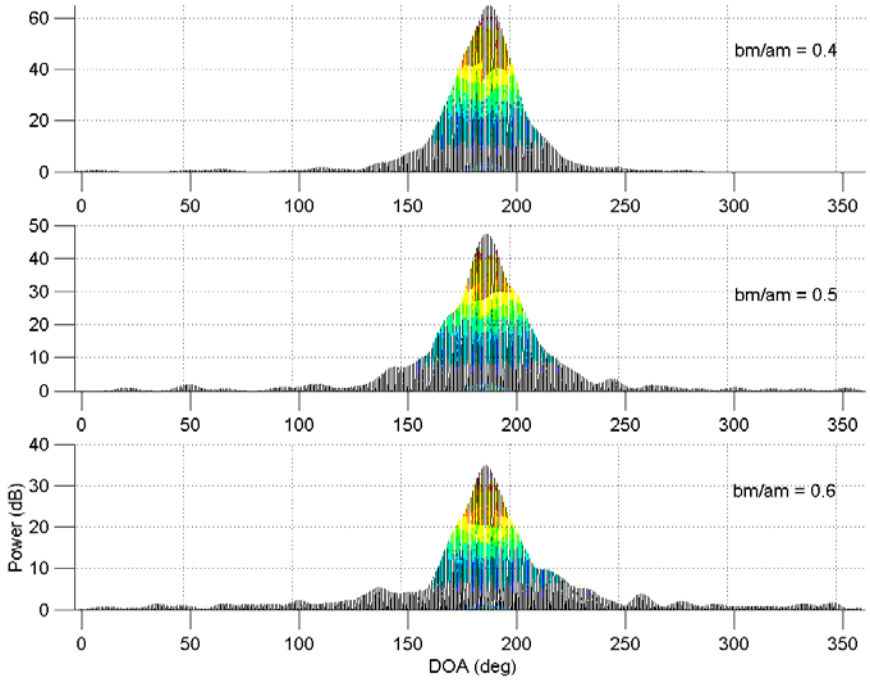

Figure 2.6 PAPs generated for L=500 multipath components (MPCs) for three different elliptical ratios b_m/a_m=0.4,0.5, and 0.6 respectively, Tx-Rx=500 mts.

Table 2.1 Simulation Parameters.

Parameter	Value
Tx-Rx separation (d0)	500 (mts)
Path loss exponent (n)	3
Reference Power (Pref) (calculated using free space link eq.)	-38 dBm
Reflection loss (Lr)	6 dB
Maximum normalized multipath delay rm	2
Elliptical Ratio (bm/am)	0.4, 0.5 and 0.6
Receiver Antenna Gain Gr(ϕ) (as a function of DOA)	7.8 dBi
Transmitter Antenna Gain Gt(θ) (as a function of DOD)	16 dBi
Multipath components (L)	L = 5000

The DOA, DOD and delay can then be computed from the coordinates of the transmitter, receiver and scatterer [33]. Using the algorithm presented in [8] multipath profiles are generated, as an example of the simulation result of the PDAPs is illustrated in Fig. 2.5, for a path loss exponent of n=3, the loss in dB, due to reflection from the scatterers, Lr is equal to 6 dB, and a Tx-Rx separation distance = 500 mts.

For these simulations it was assumed that omnidirectional antennas were used at both the transmitter (Tx) and receiver (Rx). The direct connection between MS and BS (LOS) corresponds to $\varphi \approx 180^{\circ}$. From Fig. 2.5 can be noted that the principal portion of the received energy hits from a range of directions between $\varphi \approx 150^{\circ}$ *and* $\varphi \approx 210^{\circ}$. Note also that the MPCs are tightly clustered in angle about the LOS. This is due to the fact that the GBSB model predicts that paths with low excess delays, and therefore higher power levels, tend to be clustered about the direct path, this is also illustrated in the following simulation results shown in Fig. 2.6, where it use three different time excess delay for the elliptical ratios b_m/a_m: 0.4, 0.5, and 0.6, respectively, and increasing the number of MPCs L, from 50 to 500. Table 2.1 summarizes the parameters used for the simulations.

From Fig. 2.6 note that as the b_m/a_m ratio of the ellipse increase the range of directions φ of the principal portion of the received energy increase, but the paths with low excess delay are always clustered about the direct path. Based on the previous simulation results, the general idea consists in uses the GBSB elliptical model for more realistic urban environments for stationary case, i.e., for simplicity, it does not take into account the *Doppler effect* caused by the relative velocity of the mobile with respect to various components of the signal.

2.3.3 GBSB Modelling Approach

Based on the assumptions required to apply the GBSB elliptical channel model, described in the previous sub-section, it uses the GBSB elliptical model for more realistic urban environments for stationary case, i.e., for simplicity, as before, it does not take into account the *Doppler effect* caused by the relative velocity of the mobile with respect to various components of the signal [27].

Simulations are carried out for different street positions of the Rx, (mobile station), using two different street position scenarios, as might be appropriate for microcellular applications and mobile-to-mobile communication.

Scenario I: MS lie on street with Line-Of-Sight (LOS) as illustrated in Fig. 2.7, with Tx-Rx separation distance of 500 meters, the number of MPCs $L=5000$, and using three different time excess delay for the elliptical ratios $b_m/a_m = 0.4, 0.5,$ *and* $0.6,$ respectively. This intuitively, it assumes that the three different elliptical ratios can be related to the height of the buildings in urban environments, (high, medium, and low buildings areas, for $0.4, 0.5,$ and 0.6,respectively), i.e. as the elliptical ratio increases the height of the building areas decreases, due to the elliptical coverage area is increased. It also assumes that the height of the buildings areas is uniformly distributed.

Scenario II: Here it uses the approach of elliptical model with scatterers uniformly distributed inside the ellipse to get a model of the reflection paths from a mobile station that lie on a cross street, using the same parameters as in scenario I, but keeping the same position of the transmitter. The center of the ellipse is the main scatterer with coordinates (x_s,ys), and then the TOA and DOA from the transmitter to the receiver of these scatterers are calculated. This scenario is illustrated in Fig. 2.8.

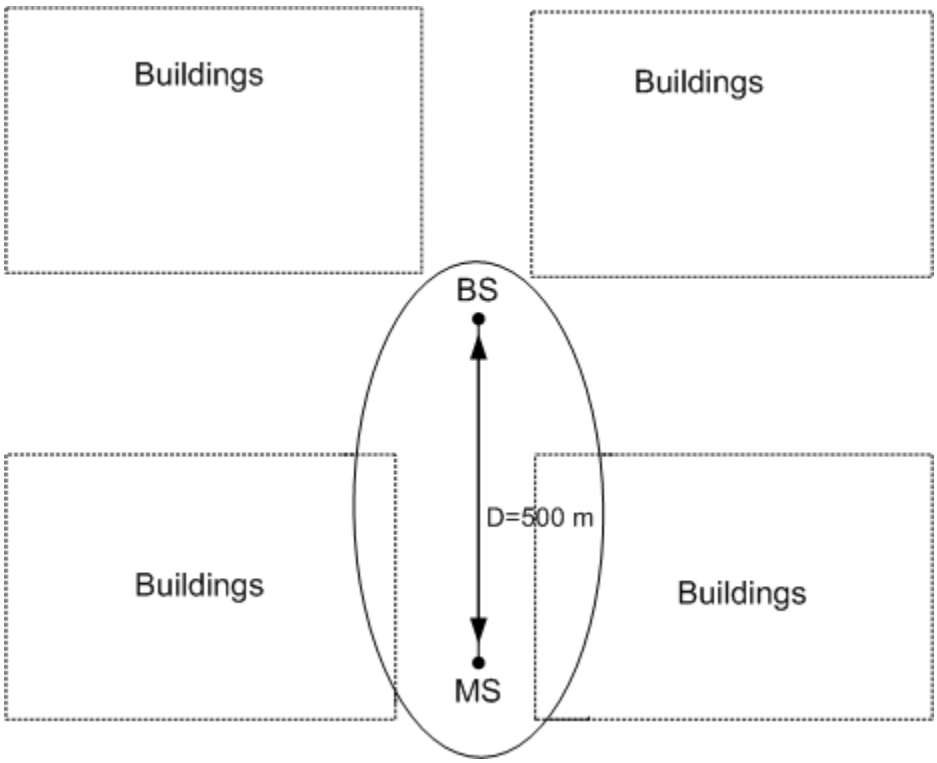

Figure 2.7 The regions in the city-street scenario I.

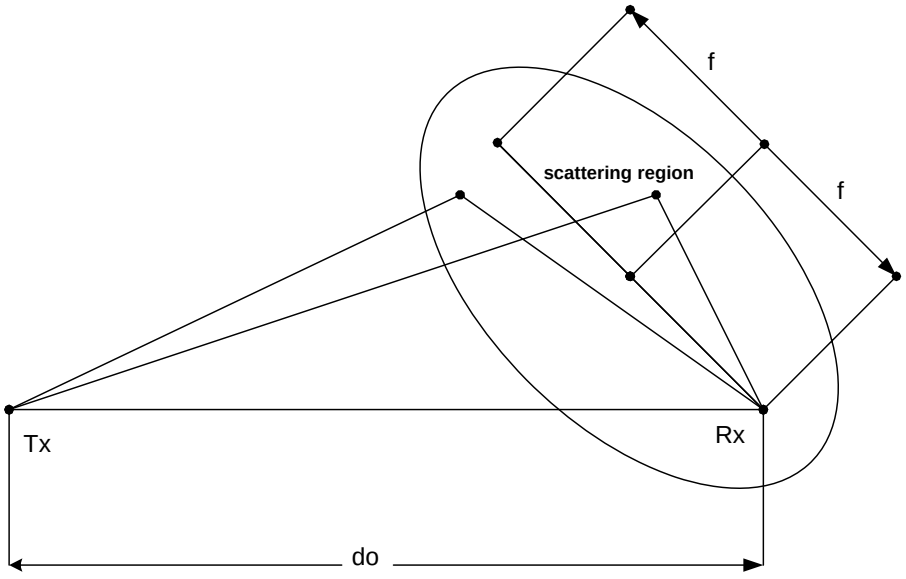

Figure 2.8 Different approach of the GBSBEM Model for Scenario II. (Single bounce).

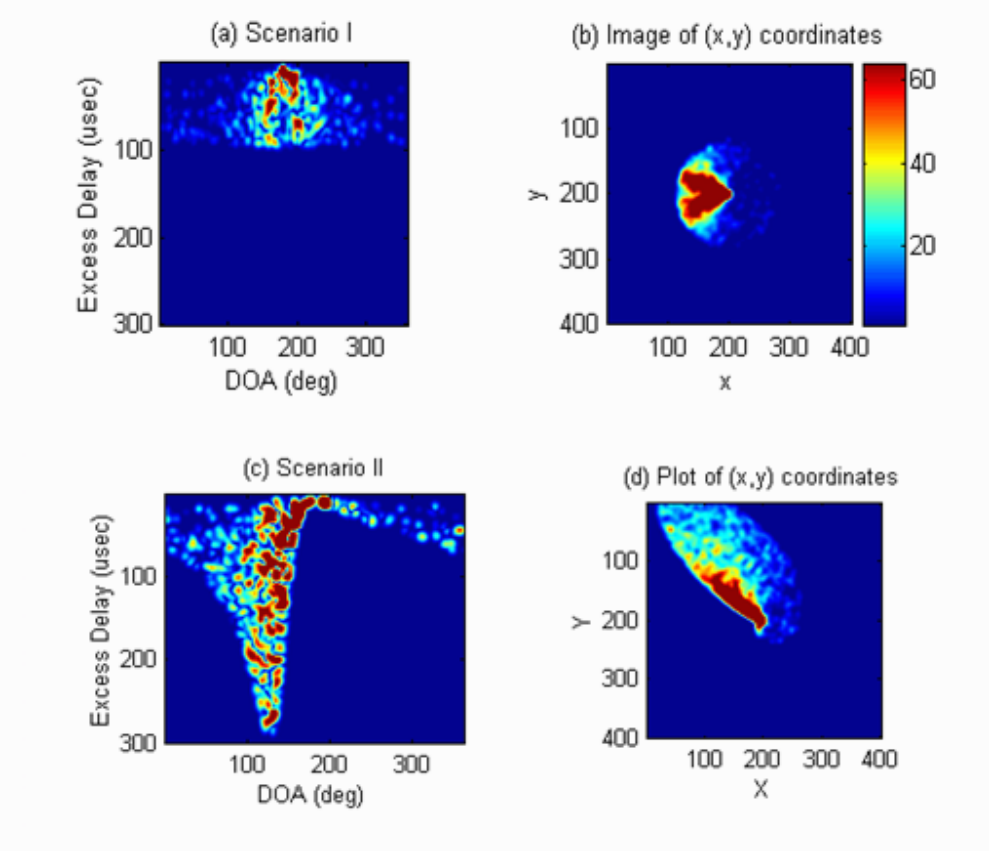

Figure 2.9 Images of the PDAPs for the scenarios described. (a) and (b) PDAPs for scenario I, (c) and (d) for scenario II, for all cases the elliptical ratio b_m/a_m=0.5.

Fig. 2.9 shows the image of the power delay angle profiles (PDAPs) simulated for the two different scenarios described earlier, for both scenarios I, and II respectively. The darker colors of the plots indicate higher received power. The color scale is normalized to the maximum power in each graph. It has used an elliptical ratio of 0.5. In both cases it uses Tx-Rx separation distance of 500 meters, with the Tx-Rx positions for the scenario I as shown in Fig. 2.7 and for scenario II, as shown in Fig. 2.8 respectively.

2.3.4 Simulation Results

Using the previous simulation results of the scenarios I and II respectively, the average statistics can be computed, i.e., mean of the MPCs from the power delay angle profiles as a function of the DOA (integrating over angle), by summing up the PDAPs (Fig. 2.9) with respect to the angle to obtain the power delay profile (PDP), using equation (2.8), and the TOA, (integrating over delay), by summing up the PDAPs with respect to the delay time to obtain the power angle profile PAP), using equation (2.9) as follows:

$$\hat{\mu}_{\tau}(\varphi) = \sum_{i=0}^{L-1} \tau_i P_i(\tau, \varphi) \frac{1}{\sum_{i}^{\varphi} \sum_{j}^{\tau} P(\tau_i, \varphi_j)}, \tag{2.7}$$

$$\hat{\mu}_{\varphi}(\tau) = \sum_{i=0}^{L-1} \varphi_i P_i(\tau, \varphi) \frac{1}{\sum_{i}^{\varphi} \sum_{j}^{\tau} P(\tau_i, \varphi_j)}, \tag{2.8}$$

where $P(\tau, \varphi)$ is the power delay angle profile, τ_i is the TOA and φ_i is the DOA of the ith multipath component (MPC). Note that in both cases are normalized with respect to PDAPs. Figures 2.10(a) and 2.11(a) show the power angle profiles obtained from the simulations for the scenarios I and II, respectively, while Figures 2.10(b) and 2.11(b), show the power delay profiles for the scenarios I and II, respectively.

In Figures 2.10 and 2.11 respectively, note that the TOA exhibits an exponential decay for both scenarios, and for the case of scenario I, this presents the shortest delay due to LOS. The scenario II has a similar delay; due to the effects of cross streets. Comparing the DOA for the two scenarios it can be noted that the angle of arrival for the two cases are different in each scenario, e.g., in scenario I (LOS between Tx-Rx). Besides, Figures 2.10 and 2.11 also show that the variation of angle increases as the elliptical ratio decreases.

Besides, this variation is wider compared to scenario II, where it has less variations, and clearly define the influence of the cross street effects, due to the DOA is concentrated basically on the elliptical regions for this scenario. It can also be noted in the same figures that for scenario I the peak of energy in angle is around $\varphi = 180$ degrees (LOS), and for scenario II the peak of energy in angle is around $\varphi = 140$ degrees (cross street).

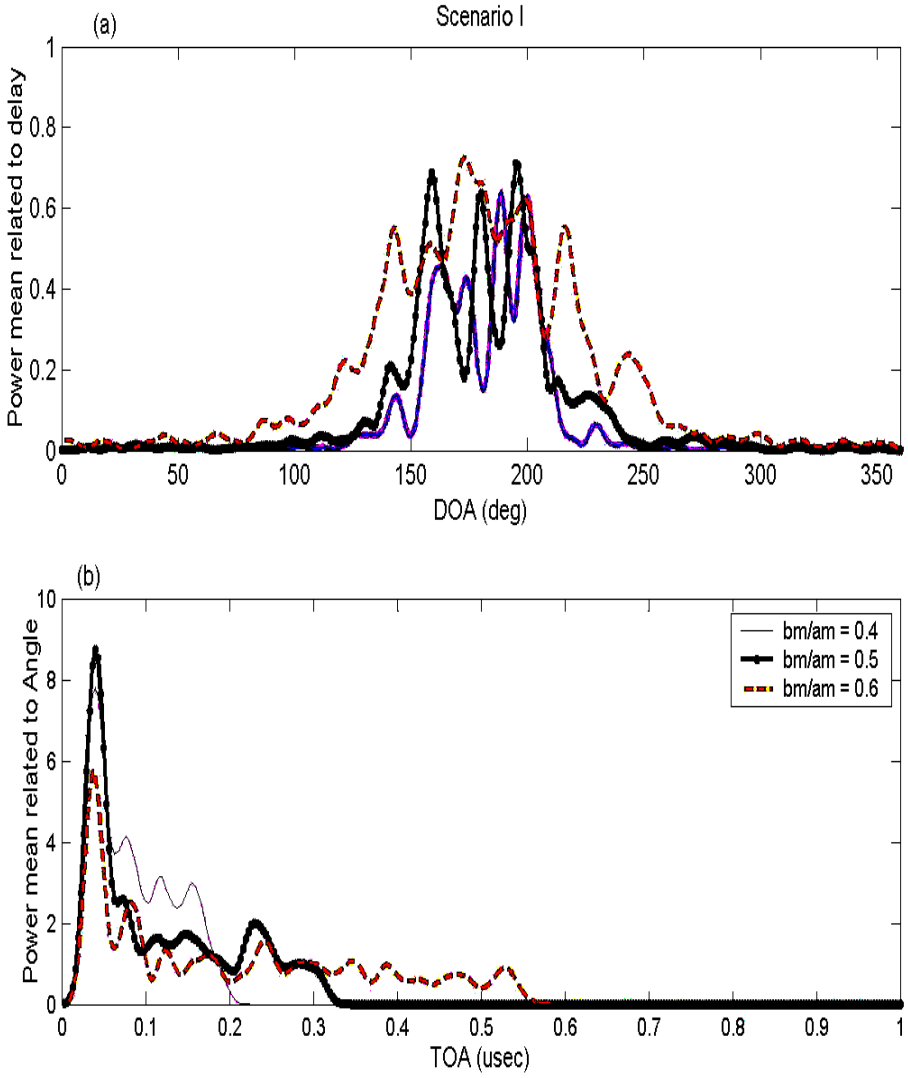

Figure 2.10 Resolution of multipath components (MPCs) for scenario I in (a) angle domain (angular profiles), and (b) delay domain (delay profiles).

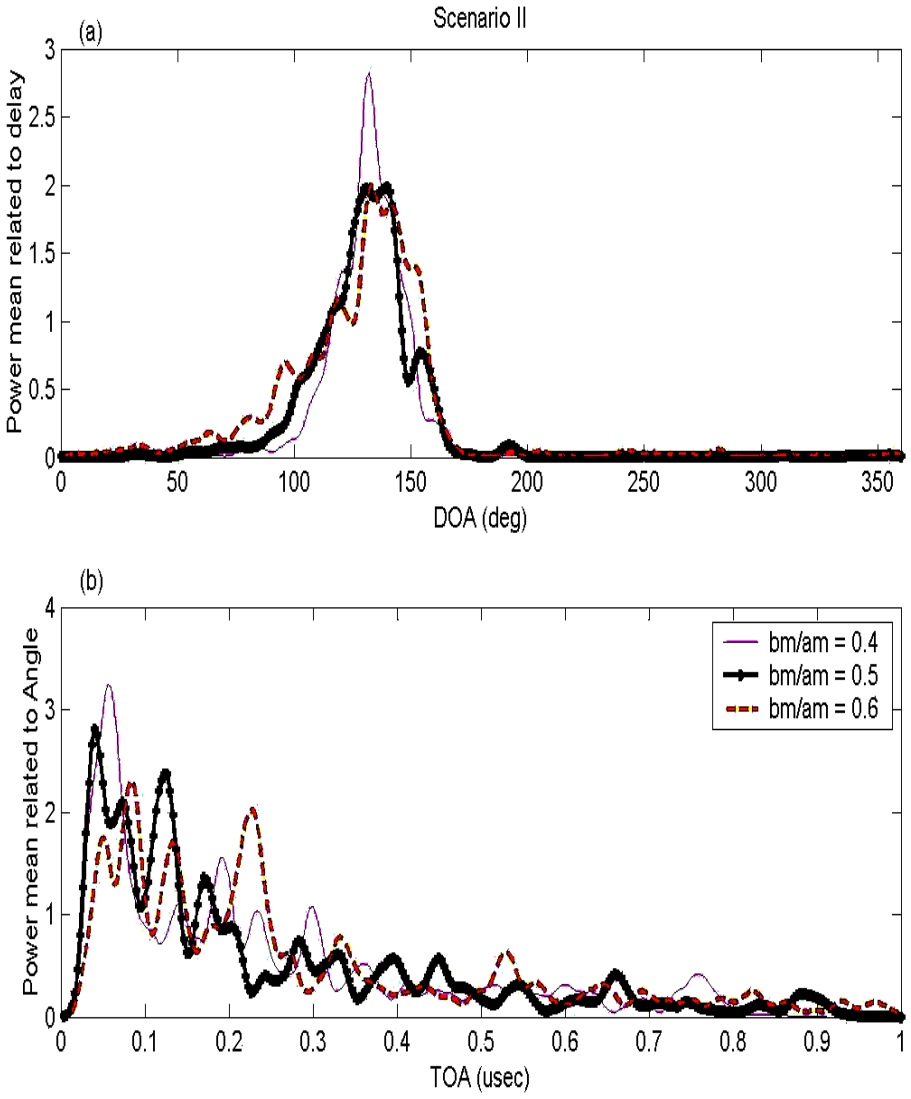

Figure 2.11 Resolution of multipath components (MPCs) for scenario II (a) angle domain (angular profiles), and (b) delay domain (delay profiles).

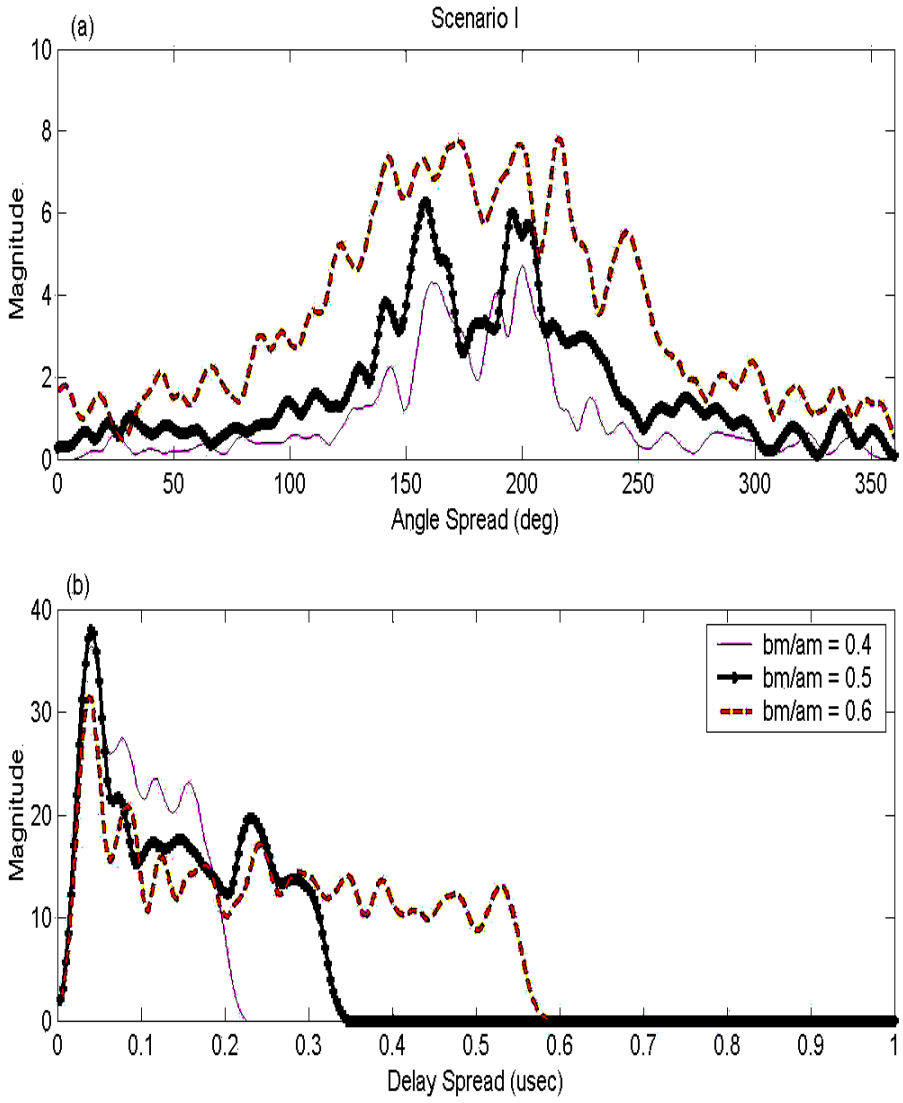

Figure 2.12 (a) Angle spread and (b) delay spread for mobile station located at LOS for the three different elliptical ratios.

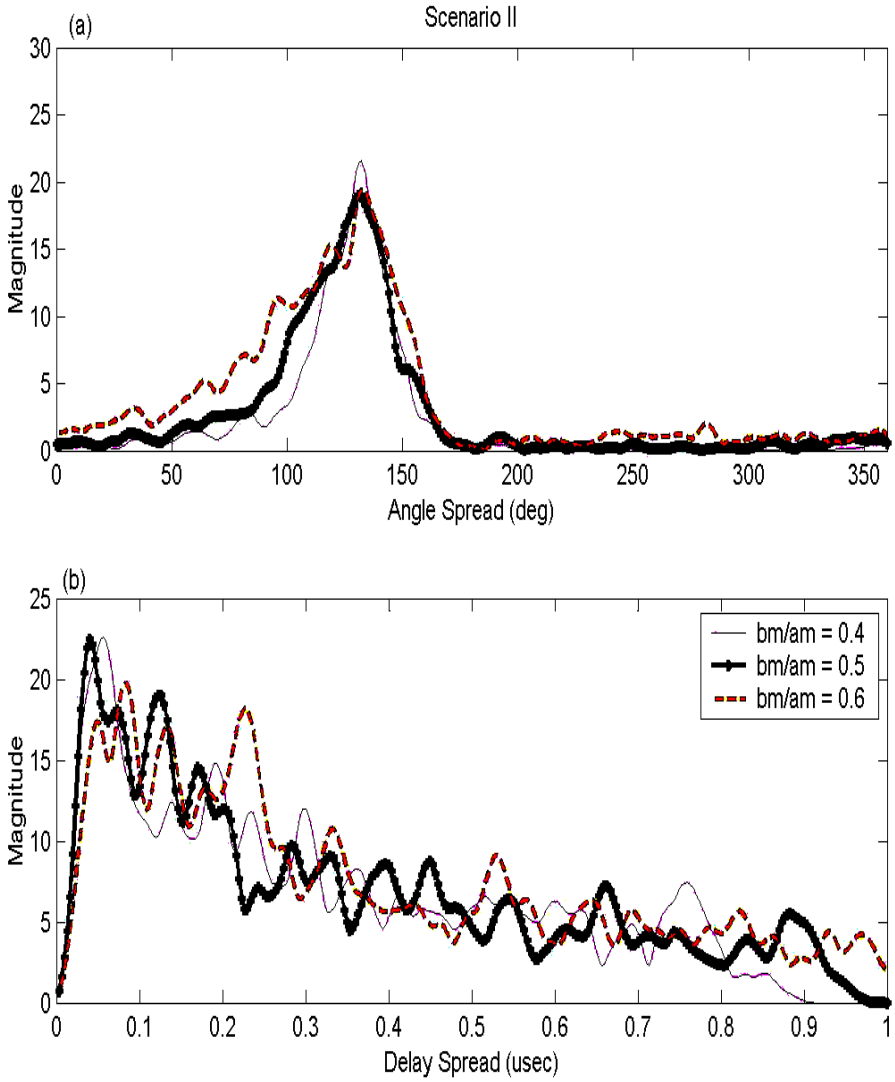

Figure 2.13 (a) Angle spread and (b) delay spread for mobile station located at cross street scenario for the three different elliptical ratios.

Due to scattering, MPCs arrive at angles different from the direct component, the angle spread is a measure used to determine the angular dispersion of the channel. A measure for angle spread, $\sigma_{\varphi}(\tau)$, (by definition), [1] is the square root of the second central moment and can be calculated using equation (2.9) as in [27]. From Fig. 2.12(a) and Fig. 2.13(a) respectively, note that the angle spread is wider for scenario I (LOS) than the Scenario II (Cross Street).

The angle spread is a measure of the spread of the MPCs, and it gives a measure to which multipaths can be reduced using directional antennas, due to; it determines the correlation between spatially separated antennas, and consequently the ability to mitigate fast fading by means of antenna diversity techniques.

In a similar way like in [27], the delay spread is a measure based on the second central moment and is defined as the square root of the second central moment of the power delay profile, and can be calculated using equation (2.8), the delay spread is a measure of the time dispersion of the channel. The Fig. 2.12(b) and Fig. 2.13(b), show that the delay spread increases as the elliptical ratio b_m/a_m increases, by intuition that means, as the height of the building areas increases the delay spread decreases, as also shown in Table 2.2 and Table 2.3 for both scenarios I and II respectively.

Table 2.2 Mean and standard deviation of the delay spread (σ_d) and angle spread (σ_a) for each elliptical ratio with LOS scenario.

Elliptical Ratio b_m/a_m (Scenario I)	**Mean delay (ns)**	**Delay spread (ns)**	**Mean Angle (deg)**	**Angle spread (deg)**
0.4/High*	60	50	180	24
0.5/Medium*	90	80	180	29
0.6/Low*	180	150	180	37

Table 2.3 Mean and standard deviation of the delay spread (σ_d) and angle spread (σ_a) for each elliptical ratio with cross street scenario.

Elliptical Ratio b_m/a_m (Scenario I)	**Mean delay (ns)**	**Delay spread (ns)**	**Mean Angle (deg)**	**Angle spread (deg)**
0.4/High*	60	50	180	24
0.5/Medium*	90	80	180	29
0.6/Low*	180	150	180	37

* It has assumed by intuition, a relationship of the elliptical ratio with the height of the building areas.

The simulations show that the delay profiles exhibits an exponential decay, for the two different scenarios analyzed, independent of the scenarios while, the shape of the angle profiles is defined by the type of scenario. These results show also that the delay spread (DS) and the angle spread (AS), they increase as the elliptical ratio b_m/a_m increases for scenarios I and II. In conclusion, the delay spread is small on LOS streets (Scenario I), and it is increases for mobile station on cross streets (Scenario II).

2.4 Conclusions

This chapter has presented the topics of the spatial channel models for mobile radio communications, with emphasis on physical channel models based on geometry. This chapter has also presented a modeling approach with simulations results obtained by a Geometrically Based Single Bounce Elliptical Channel model (GBSBEM), defined in [8] that it was implemented for two urban scenarios: a) Scenario I, City-Street-Scenario and b) Scenario II, Cross-Street-Scenario, respectively, in both cases taking into account the height of the buildings as a part of the modeling an overview of the Geometry-Based channel models as well as the different ways that the model can be applied, (modeling approach). From the GBSB model (geometrical considerations), it was obtained statistics for the path delay (τ), DOA (φ) and power P(dB) of MPCs. The simulation results have shown that the MPCs are tightly clustered in angle about the direct path component. This is typically found in urban environments. In the next chapter, the GBSB channel model is extended using the Multiple Input Multiple Output (MIMO) modeling approach and it will derive some statical characteristics of the extended GBSB channel model, and then compare it to the GBSB for SISO system in terms of capacity for a 2x2 MIMO system and investigate the useful limiting results in terms of the number of antennas or SNR.

Chapter 3 GBSB MIMO Modeling Approach

The increasing demand for high data rates and the limited available bandwidth motivates the investigation of wireless systems that efficiently exploit the spatial domain and improved spectral efficiency. The so-called Multiple Input Multiple Output technology promises a cost-effective way to provide these capabilities. MIMO uses antenna arrays at both the transmitter (Tx) and receiver (Rx). Algorithms in a radio chipset send information out over the antennas. The radio signals reflect off objects, creating multiple paths that in conventional radios cause interference and fading. But MIMO sends data over these multiple paths, thereby increasing the amount of information the system carries. The data is received by multiple antennas and recombined properly by other MIMO algorithms. This chapter extends the GBSB channel model for MIMO modeling approach and derives some statistical characteristics of the extended model and compares it to the model based on geometry described in the previous chapter. The focus is on the capacity of single-user MIMO channels.

The model used in this work is a semi-stochastic one, as it uses some information from the environment to give more realistic results. For example, for microcells, when modeling a scenario (as previously presented in Chapter 2), where the transmitter (Tx) and the receiver (Rx) are located in a street, the width of the street is used as a parameter. In contrast with deterministic models, the model shown here does not require detailed building information or street-layouts.

The idea behind MIMO is that the signals on the transmit (TX) antennas at one end and the receive (RX) antennas at the other end are “combined” in such a way that the quality (bit-error rate or BER) or the data rate (bits/sec) of the communication for each MIMO user will be improved. Such an advantage can be used to increase both the network’s quality of service and the operator’s revenues significantly. Part of this chapter has been published in [65 and 66].

3.1 Introduction

MIMO wireless systems are those that have multiple antenna elements at both transmitter and receiver [13]. They were first investigated by computer simulations in the 1980s [14], and later papers explored them analytically [10 and 15]. Since that time, interest in MIMO systems has been a hot topic of research. They are now being used for third-generation cellular systems (WCDMA), and are discussed for future high-performance mode of the highly successful IEEE 802.11 standard for wireless local area networks.

The multiple antennas in MIMO systems can be exploited in two different ways. One is the creation of a highly effective antenna diversity system; the other is the use of the multiple antennas for the transmission of several parallel data streams to increase the capacity of the system.

Antenna diversity is used in wireless systems to combat the effects of fading. If multiple independent copies of the same signal are available, it can combine them to a total signal with high quality even if some of the copies exhibit low quality. Antenna diversity at the receiver is well-known, and has been studied for more than 50 years. The different signal copies are linearly combined, i.e., weighted and added. The resulting signal at the combiner output can then be demodulated and decoded in the usual way. The optimum weights for this combining are matched to the wireless channel (maximum ratio combining MRC) [7]. If it has N receive antenna elements, the diversity order, which describes the effectiveness of diversity in avoiding deep fades, is N; in other words, the diversity order is related to the slope of the SNR distribution at the combiner output [9]. The multiple antennas also increase the average SNR seen at the combiner output. The study of transmit diversity is much more recent, starting in the 1990s. When the channel is known to the transmitter, it can again be "matched" the multiple transmitted signal copies to the channel, resulting in the same gains as for receiver diversity. If the channel is unknown at the transmitter, other strategies, like delay diversity or space-time coding, have to be used [9]. In that case is possible to gain high diversity order, but not improvement of average SNR. The logical next step is the combination of transmit and receive diversity. It has been demonstrated that with Nt transmit and Nr receive antennas, a diversity order of $NtNr$ can be achieved [16]. A MIMO system can thus be used for a high-quality transmission of a single data stream even in challenging environments. The principle of this approach is sketched in Fig. 3.1.

An alternative way of exploiting the multiple antenna elements is the so-called "spatial multiplexing" [17] or "BLAST" [18] approach. Different data streams are transmitted (in parallel) from the different transmit antennas. If the channel is well-behaved, so that the Nr received signals represent linearly independent combinations, then the transmit signals can be recovered as long as $Nt \leq Nr$.

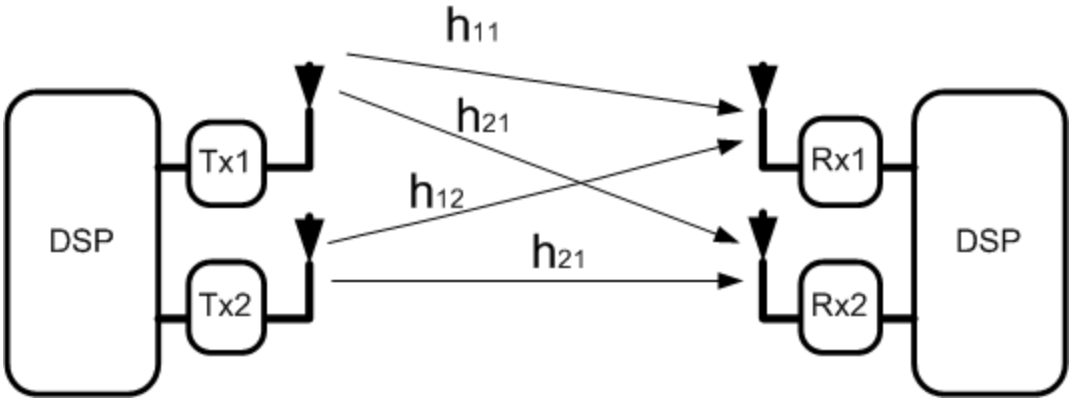

Figure 3.1 Scheme of a 2x2 MIMO system.

The advantage of this method is that the data rate can be increased by a factor Nt without requiring more spectrum. In this chapter, it will mostly discuss the information-theoretic capacity, i.e., the data rate that can be transmitted over a channel without errors if ideal coding is used. Practical schemes, like layered space-time (ST) receiver structures [11, 18, and 19] combined with space-time codes [20] allow to approach these capacity limits.

Regardless of the use as diversity or spatial multiplexing system, the main drawback of any MIMO system is the increased complexity, and thus cost. While additional antenna elements (patch or dipole antennas) are usually inexpensive, and the additional digital signal processing becomes ever cheaper, the RF elements are expensive. MIMO systems with Nt transmit and Nr receive antennas require Nt (Nr) complete RF chains at the transmitter, and the receiver, respectively, including low-noise amplifiers, downconverters, and analog-to-digital converters [9].

3.2 Capacity of MIMO systems

This Section explores the absolute gains offered by MIMO in terms of capacity bounds. These results are summarized in selected key system scenarios. It begins with fundamental results which compare single-input–single-output (SISO), single-input–multiple-output (SIMO), and MIMO capacities, then it moves on to more general cases that take possible a priori channel knowledge into account. Finally, it makes computer simulations for a 2x2 MIMO system and investigates useful limiting results in terms of the number of antennas or SNR.

The capacity of a MIMO system is largely dependent on the correlation between the CIRs of the different antenna pairs. The capacity of a SISO system is given for reference, which is obtained by using Shannon's formula for the capacity of a band-limited system:

$$C_{SISO} = \log_2(1+\rho|h|^2) \quad \text{b/s/Hz} \tag{3.1}$$

where h is the normalized complex gain of a fixed wireless channel or that of a particular realization of a random channel. In equation (3.1) and subsequently, ρ is the SNR at any RX antenna. As it deploys more Rx antennas the statistics of capacity improve and with M antennas, it has a SIMO system with capacity given by

$$C = \log_2\left(1+\rho\sum_{i=1}^{M}|h_i|^2\right) \quad \text{b/s/Hz} \tag{3.2}$$

where h_i is the gain for RX antenna i. Note in equation (3.2) that increasing the value of M only results in a logarithmic increase in average capacity. Similarly, if it uses transmit diversity, in the common case, where the transmitter does not have channel knowledge, it has a multiple-input–single-output (MISO) system with N Tx antennas and the capacity is given by [10]

$$C = \log_2\left(1+\frac{\rho}{N}\sum_{i=1}^{N}|h_i|^2\right) \quad \text{b/s/Hz} \tag{3.3}$$

where the normalization by ensures a fixed total transmitter power and shows the absence of array gain in that case (compared to the case in equation (3.2), where the channel energy can be combined coherently). Again, note that capacity has a logarithmic relationship with N. Now, the use of diversity at both transmitter and receiver is considered giving rise to a MIMO system. For N Tx and M Rx antennas. Thus, the ergodic capacity equation is given by the now very well known capacity equation [10, and 15]

$$C_{MIMO} = E\left[\log_2\left[\det\left(\mathbf{I}_M+\frac{\rho}{N}\mathbf{H}\mathbf{H}^{*T}\right)\right]\right] \quad \text{b/s/Hz} \tag{3.4}$$

where ($*^T$) means transpose-conjugate and **H** is the MxN channel matrix. Note that both equations (3.3) and (3.4) are based on N equal power uncorrelated sources. In [10 and 15] both demonstrated that the capacity in equation (3.4) grows linearly with $m = \min(M, N)$ rather than logarithmically as in equation (3.3). This result can be intuited as follows: the determinant operator yields a product of

min(M, N) nonzero eigenvalues of its (channel-dependent) matrix argument, each eigenvalue characterizing the SNR over a so-called channel eigenmode. An eigenmode corresponds to the transmission using a pair of right and left singular vectors of the channel matrix as transmit antenna and receive antenna weights, respectively. Thanks to the properties of the logarithm, the overall capacity is the sum of capacities of each of these modes, hence the effect of capacity multiplication. Clearly, this growth is dependent on properties of the eigenvalues. If they decayed away rapidly then linear growth would not occur. However (for simple channels), the eigenvalues have a known limiting distribution and tend to be spaced out along the range of this distribution. Hence, it is unlikely that most eigenvalues are very small and the linear growth is indeed achieved. With the capacity defined by equation (3.4) as a random variable, the issue arises as to how best to characterize it. The upper bound is obtained when the CIRs between different antenna pairs are uncorrelated, while the lower bound is obtained when the CIRs of the antenna pairs are completely correlated. The upper and lower bound for an MxN system are given by [49]

$$C_{upper} = \min(M, N)\log_2(1+\rho) \quad \text{b/s/Hz} \tag{3.5}$$

and

$$C_{lower} = \log_2\left[1+\rho\min(M, N)\right] \quad \text{b/s/Hz} \tag{3.6}$$

Two simple summaries are commonly used: the mean (or ergodic) capacity [15], and capacity outage [10]. Capacity outage measures (usually based on simulation) are often denoted or, i.e., those capacity values supported 90% or 99% of the time, and indicate the system reliability. A full description of the capacity would require the probability density function (PDF).

Some caution is necessary in interpreting the above equations. Capacity, as discussed here and in most MIMO work [10 and 15], is based on a “quasi-static” analysis where the channel varies randomly from burst to burst. Within a burst the channel is assumed fixed and it is also assumed that sufficient bits are transmitted for the standard infinite time horizon of information theory to be meaningful. A second note is that our discussion will concentrate on single user MIMO systems but many results also apply to multiuser systems with receive diversity. Finally, the linear capacity growth is only valid under certain channel conditions. It was originally derived for the independent and identically distributed (i.i.d.) flat Rayleigh fading channel and does not hold true for all cases. For example, if large numbers of antennas are packed into small volumes, then the gains in H may become highly correlated and the linear relationship will plateau out due to the effects of antenna correlation [13]. In contrast, other propagation

effects not captured in equation (3.4) may serve to reinforce the capacity gains of MIMO such as multipath delay spread.

More generally, the effect of the channel model is critical. Environments can easily be chosen which give channels where the MIMO capacities do not increase linearly with the numbers of antennas. However, most measurements and models available to date do give rise to channel capacities which are of the same order of magnitude as the promised theory. Also the linear growth is usually a reasonable model for moderate numbers of antennas which are not extremely close-packed [13].

3.3 Extended GBSB Modeling Approach

In the GBSB developed by Liberty and Rappaport [8], the propagation environment is composed of scatterers that are uniformly distributed in space and have equal scattering cross sections. However in this extended model the scatterers are grouped into clusters. Clusters are distributed inside the environment and the scatterers inside the cluster follow a uniform distribution. Among others, the number of clusters and the average number of scatterers within a cluster can be set with a parameter. The reflection coefficient of each scatterer can be described by its complex value, where the magnitude of the reflection coefficient is the attenuation, due to reflection losses, uniformly distributed in $[0,1]$. The phase of the reflection coefficient is an extra phase change, which is uniformly distributed in $[0,2\pi]$. For pico and microcell environments it considers a Line Of Sight (LOS) signal only. LOS modeling is not defined for the suburban or urban macrocell scenarios due to the low probability of occurrence [9]. LOS modeling is based on the Ricean K factor defined as the ratio of power in the LOS component to the total power in the diffused Non Line Of Sight (NLOS) component. As in the SISO case, analyzed in the previous chapter, the microcell environment is modeled by an ellipse, i.e., the Base station (BS) and the Mobile station (MS) are located inside the area at the foci of the ellipse. Fig. 3.2 depicts the microcell scattering model.

The previously described model is simulated in Matlab®, for a 2x2 MIMO channel where a Channel Impulse Response (CIR) is calculated for each channel between MS-BS pairs. For each pair, a scatterer region is defined, common clusters of scatterers for two or more regions having the same reflection coefficient. In the case of MIMO, the CIR is also calculated between all Tx and Rx antenna pairs of each region. In this case, the exact location of the antennas is used to calculate the direction of departure (DOD) and direction of arrival (DOA), and the distances between transmitter and cluster, and cluster and receiver. However, time differences between the paths from a reflector to the receiver antennas are neglected. The mutual coupling between antennas is not considered, which holds true in some cases [10]. This configuration includes L

scatterers within an elliptical area in which the MIMO system operates. The transmitting and receiving arrays, separated by a distance D, include n_T and n_R elements respectively.

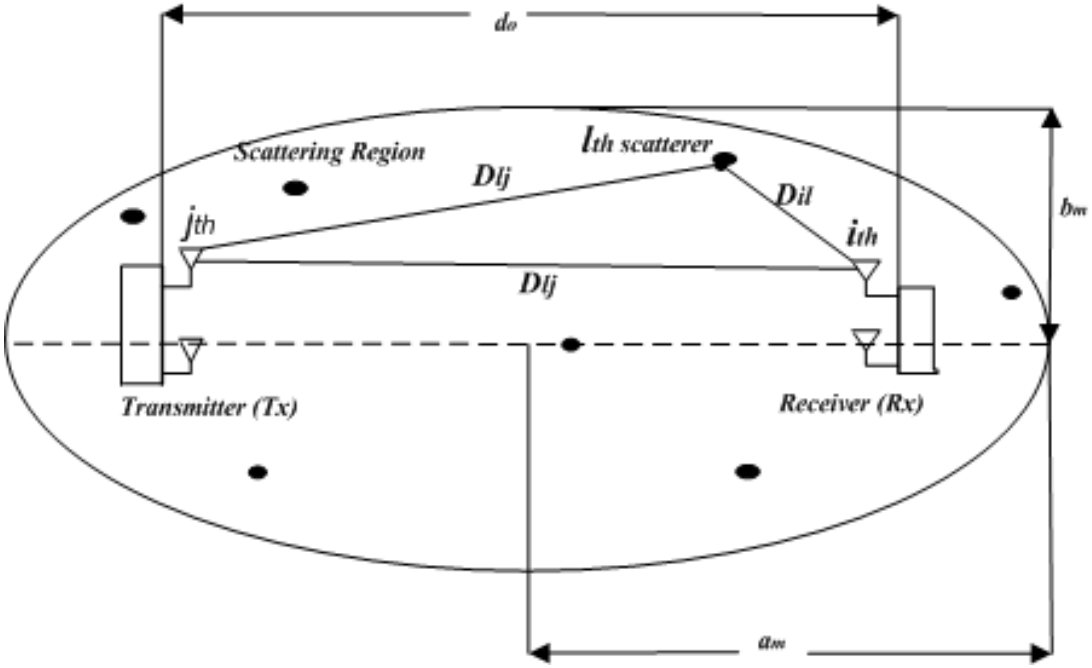

Figure 3.2 The configuration showing a single bounce scattering model of a 2x2 MIMO system.

In order to obtain results relevant to contemporary indoor wireless communications standards, the following parameters are selected. The operating frequency and root mean square delay spread are assumed to be $f = 5\ GHz$ and τ_{RMS}=100 ns respectively, which are typical values for Wireless Local Area Network (WLAN) standards such IEEE 802.11a and the High Performance Local Area Network type 2 (HIPERLAN/2) [67]. Following this initial assumption, the distance between transmitter and receiver D is set equal to 300λ (or 18 $mts.$). Using τ_{RMS} and f, the ellipse major axis parameter is found to be $a = 250\lambda$ (or 15 $mts.$) [67]. Finally, the ellipse minor axis is calculated as $b = \sqrt{a^2 - (D/2)^2} = 200\lambda$ (or 12 m). The chosen dimensions are relevant for indoor scenarios such as an exhibition hall or a large office building.
D_{il} is the distance between the i^{th} receiving element and the l^{th} scatterer and D_{lj} is the distance between the l^{th} scatterer and the jth transmitting element and D_{ij} is the distance between j^{th} transmitting element and ith receiving element, as shown in Fig. 3.2.

The next Section presents some statistical characterization of the extended GBSB multipath channel model using the clustering approach definition, and then it presents the simulation results for a 2x2 MIMO system.

3.4 Cluster Modeling Approach

The cluster model was introduced first by Saleh and Valenzuela [42] and later verified, extended, and elaborated upon by many other researchers in [32, 44–46]. The received signal amplitude β_{kl} is a Rayleigh-distributed random variable with a mean-square value that obeys a double exponential decay law

$$\overline{\beta_{kl}^{\,2}} = \overline{\beta^2(0,0)} e^{-T_l/\Gamma} e^{-\tau_{kl}/\gamma} \tag{3.7}$$

where $\overline{\beta^2(0,0)}$ represents the average power of the first arrival of the first cluster, T_l represents the arrival time of the l^{th} cluster, and τ_{kl} is the arrival time of the k^{th} arrival within the l^{th} cluster, relative to T_l. The parameters Γ and γ determine the inter-cluster signal level rate of decay and the intra-cluster rate of decay, respectively. The rates of the cluster and ray arrivals can be determined using exponential rate laws

$$p(T_l \mid T_{l-1}) = \Lambda e^{-\Lambda(T_l - T_{l-1})} \tag{3.8}$$

$$p(\tau_{kl} \mid \tau_{k-1,l}) = \lambda e^{-\lambda(T_l - T_{l-1})} \tag{3.9}$$

where Λ is the cluster arrival rate and λ is the ray arrival rate.

A set of WLAN channel models was developed by Medbo et al. [50, 51, and 54]. In [50], five delay profile models were proposed for different environments (Models A-E):

- Model A for a typical office environment, non-line-of-sight (NLOS) conditions, and 50 ns rms delay spread.
- Model B for a typical large open space and office environments, NLOS conditions, and 100 ns rms delay spread.
- Model C for a large open space (indoor and outdoor), NLOS conditions, and 150 ns rms delay spread.
- Model D, same as model C, line-of-sight (LOS) conditions, and 140 ns rms delay spread (10 dB Ricean K-factor at the first delay).
- Model E for a typical large open space (indoor and outdoor), NLOS conditions, and 250 ns rms delay spread.

The models A-C together are used with three additional models more representative of smaller environments, such as residential homes and small offices, for the modeling purposes. The resulting models are as follows:

- Model A (optional, should not be used for system performance comparisons), flat fading model with 0 ns rms delay spread (one tap at 0 ns delay model). This model can be used for stressing system performance, occurs small percentage of time (locations).
- Model B with 15 ns rms delay spread.
- Model C with 30 ns rms delay spread.
- Model D with 50 ns rms delay spread.
- Model E with 100 ns rms delay spread.
- Model F with 150 ns rms delay spread.

The Tables with channel coefficients (tap delays and corresponding powers) can be found in Appendix A.

For modeling purposes it is not using the equations (3.7) through (3.9) since the delay profile characteristics are already predetermined by the model B-F delay profiles.

3.4.1 Number of clusters

The number of clusters found in different indoor environments varies between 1 and 7. In [32], the average number of clusters was found to be 3 for one building, and 7 for another building. In [44] the number of clusters reported was found to be 2 for Line-Of-Sight (LOS) and 5 for Non-LOS (NLOS) conditions. In Fig. 3.3, the scatterers are represented with arrival times. It can be seen that the scatterers which are closer to Rx have faster arrival time compared to those that are placed far away. Fig. 3.4 shows Model D delay profile with clusters outlined by exponential decay (straight line on a log-scale).

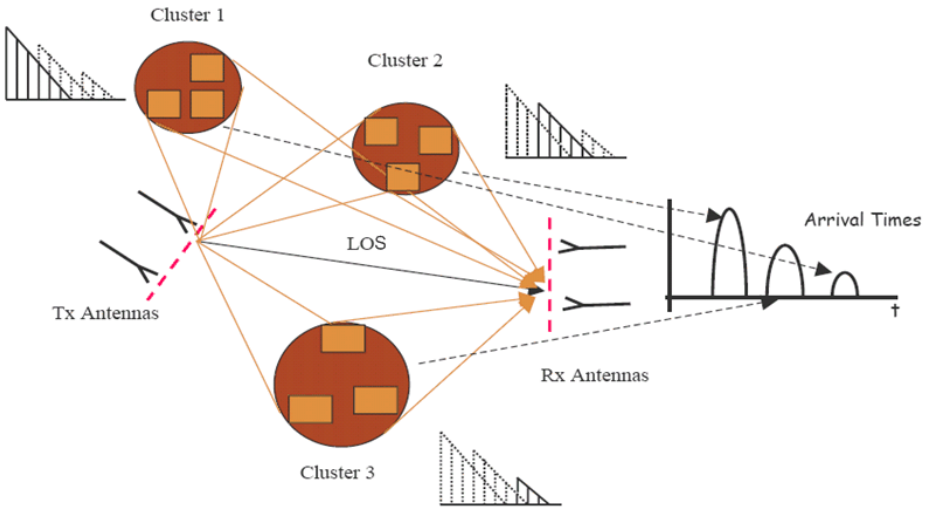

Figure 3.3 Scatter cluster example.

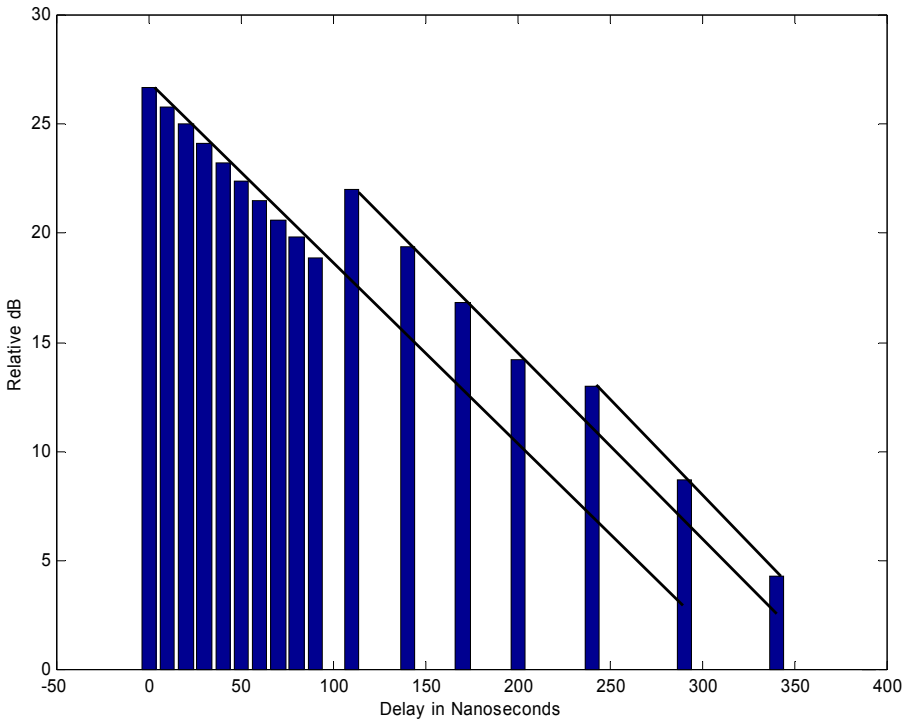

Figure 3.4 Model D delay profile with cluster extension (overlapping clusters).

From Fig. 3.4 three clusters are clearly identified. For Models B, C, D, E, and F are identified (assigned) 2, 2, 3, 4 and 6 clusters, respectively. The number of clusters in each of the models B-F agrees well with the results reported in the literature. See for references [32, 44–46, and 93–94]. The model A consists of only one tap.

Next, it extends each cluster in B-F models so that they overlap (see Fig.3.4). It uses a straight-line extrapolation function (in dB) on the first few visible taps of each cluster. The powers of overlapping taps were calculated so that the total sum of the powers of overlapping taps corresponding to different clusters equals to the powers of the original B-F power delay profiles. Table 3.1 summarizes the channel model parameters for both Line-Of-Sight (LOS) and Non Line-Of-Sight (NLOS) conditions.

Table 3.1 Summary of model parameters for LOS/NLOS conditions. K-factor for LOS conditions applies only to the first tap, for all other taps K=∞ dB [50].

Model	**Type**	**K-factor**	**Time Delay Nanoseconds**	**No. Clusters**
A (optional)	LOS/NLOS	0/-∞	0	1 tap
B	LOS/NLOS	0/-∞	15	2
C	LOS/NLOS	0/-∞	30	2
D	LOS/NLOS	3/∞-	50	3
E	LOS/NLOS	6/-∞	100	4
F	LOS/NLOS	6/-∞	150	6

K-factor values for LOS conditions are based on the results presented in [93 and 50] where it was found that for LOS condition, open (larger) environments have higher K-factors than smaller environments with close-in reflecting objects (more scattering). The LOS K-factor is applicable only to the first tap while all the other taps K-factor remain at -∞ dB. LOS conditions are assumed only up to the breakpoint distance. In [39], it was also found that, for the LOS conditions, the power of the first tap relative to the other taps is larger than for the NLOS conditions.

The LOS component of the first tap is added on top of the NLOS component so that the total energy of the first tap for the LOS channels becomes higher than the value defined in the power delay profiles (PDP). The procedure can be described as follows: (see appendix A for details)

- Start with delay profiles (NLOS) as defined in Table in appendix A.
- Add LOS component to the first tap with power according to the specified K-factor and 45^{o} DOA (DOD).

- The resulting power of the first tap increases due to the added LOS component (the power of the first tap should not be scaled back to match the original NLOS PDPs).

Note that the above procedure reduces (slightly) the *rms* delay spread for the LOS channels when compared to the NLOS channels.

3.4.2 PAS Shape

The angle of arrival statistics within a cluster were found to closely match the Laplacian distribution [32, 43–44]

$$p(\theta) = \frac{1}{\sqrt{2}\sigma} e^{-\left|\sqrt{2}\theta/\sigma\right|} \tag{3.10}$$

where σ is the standard deviation (STD) of the power azimuth spectrum (PAS) (which corresponds to the numerical value of AS). The Laplacian distribution is shown in Fig. 3.5 (a typical simulated distribution within a cluster, with AS = 30° (degrees).

The Laplacian distribution and the Uniform distribution are used to model the per-path power azimuth spectrum (PAS) at the mobile station (MS). The PAS of a path arriving at the MS is modeled as either a Laplacian distribution or a uniform over 360 degree distribution. Since an omnidirectional MS antenna gain is assumed, the received per-path PAS will remain either Laplacian or uniform. For an incoming AOA $\bar{\theta}$ and RMS angle spread σ, the MS per-path Laplacian PAS value at an angle θ is given by:

$$P(\theta, \sigma, \bar{\theta}) = N_o \exp\left[\frac{-\sqrt{2}\left|\theta - \bar{\theta}\right|}{\sigma}\right] \tag{3.11}$$

where both angles $\bar{\theta}$ and θ are given with respect to the boresight of the antenna elements. It is assumed that all antenna elements' orientations are aligned. Also, P is the average received power and No is the normalization constant:

$$N_o^{-1} = \int_{-\pi+\bar{\theta}}^{\pi+\bar{\theta}} \exp\left[\frac{-\sqrt{2}\left|\theta-\bar{\theta}\right|}{\sigma}\right] d\theta \qquad (3.12)$$

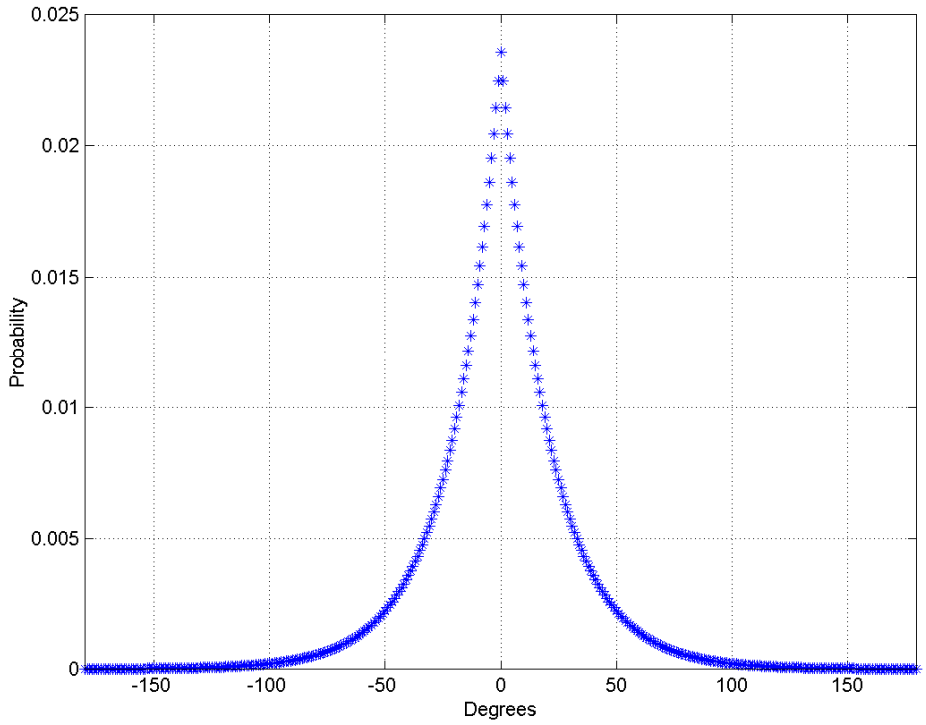

Figure 3.5 Example of a Laplacian distribution, AS=30°.

In the above equation, θ represents path components (sub-rays) of the path power arriving at an incoming AOA $\bar{\theta}$

3.4.3 Mean DOA (DOD) of Each Cluster

It was found in [43 and 44] that the relative clusters mean DOA has a random uniform distribution over all angles.

In the model, it assumes that the relative cluster mean AOD also has a random uniform distribution over all angles. Since for indoor WLANs, the multipath reflectors tend to be similar for both the access point (AP) and the client (user). Note, this is usually not the case for mobile phone communications where the base station (BS) is mounted high on a tower, while the mobile station (MS) is

often surrounded by local scatterers, or in the case of indoor WLAN communication when AP and the user's antenna heights and surrounding environments are significantly different [41].

3.4.4 Doppler Spectrum

The fading characteristics of the indoor wireless channels are very different from the one known from the mobile case. In indoor wireless systems transmitter and receiver are stationary and people are moving in between, while in outdoor mobile systems the user terminal is often moving through an environment. As a result, a new function $S(f)$ has to be defined for indoor environments in order to fit the Doppler power spectrum measurements. $S(f)$ can be expressed as (in linear values, not dB values) [1]:

$$S(f) = \frac{1}{1 + A\left(\frac{f}{f_d}\right)^2} \tag{3.13}$$

where A is a constant, used to define the $0.1S(f)$, at a given frequency f_d, being the Doppler spread.

$$\left(S(f)\right)\Big|_{f=f_d} = 0.1, \quad \text{so, } A = 9 \tag{3.14}$$

The Doppler spread f_d is defined as [1]

$$f_d = \frac{v_o}{\lambda} \tag{3.15}$$

where υ_0 is the environmental speed determined from measurements that satisfy equation (3.15) and λ is the wavelength defined by [1]

$$\lambda = \frac{c}{f_c} \tag{3.16}$$

where c is the speed of light and f_c is the carrier frequency. The value for v_0 is proposed equal to $1.2\ km/h$. In fact f_d values, experimentally determined in indoor

environments, were found to be up to approximately $6\ Hz\ at\ 5.25\ GHz$ center frequency and up to approximately $3\ Hz\ at\ 2.4\ GHz$ center frequency. Represented in dB values, $S(f)$ is similar to the "Bell" shape spectrum, as shown on Fig. 3.6:

f_{max} is the maximum frequency component of the Doppler power spectrum. It limits the range of frequencies to an upper bound, and can be arbitrarily set to 5 times f_d. Fig. 3.7 shows a typical experimental data Doppler spectrum at 5.25 GHz of a single tap (10 ns measurement system resolution) together with the fitting function of equation (3.14). Note that the measured $S(f)$ component at $f = 0$ Hz is related to the K-factor (DC-component) and is not included in the fitting function.

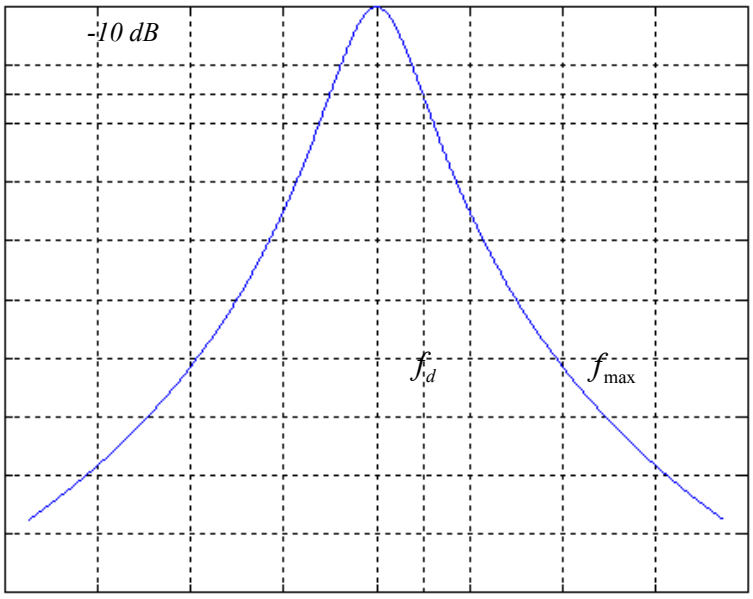

Figure 3.6 "Bell" shape Doppler power spectrum.

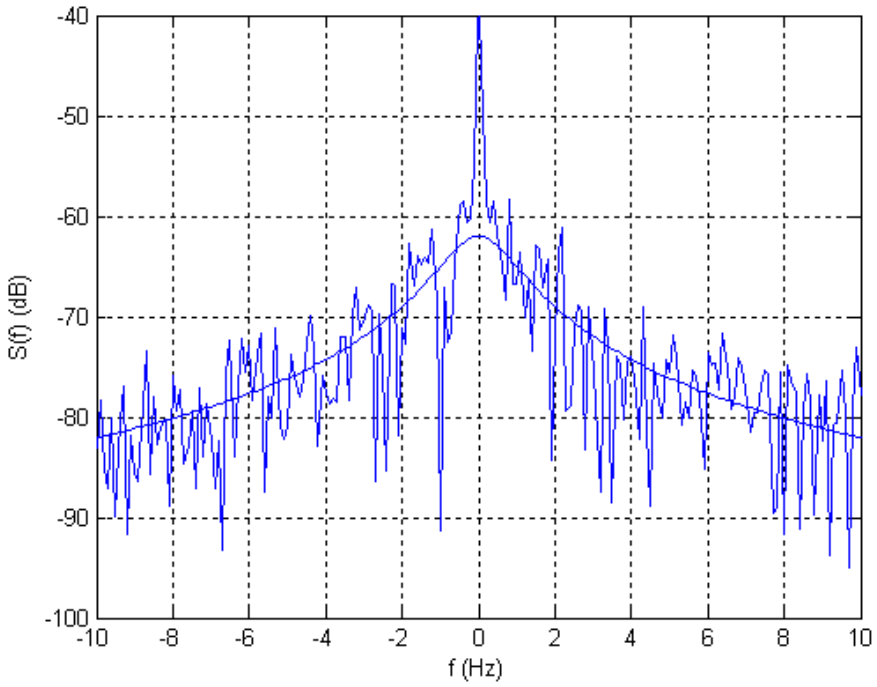

Figure 3.7 Measured Doppler power spectrum for a single delay tap together with the "Bell" shape fitting function.

In mobile radio channels, the Doppler power spectrum, $S(f)$, of the received signal can be found in [1 and 3], and is known as the "horn spectrum", quite different that the one in Figures 3.6 and 3.7.

The autocorrelation function of the Bell shape spectrum is given by

$$R = \frac{\pi f_d}{\sqrt{A}} \cdot \exp\left(-\frac{2\pi f_d}{\sqrt{A}} \cdot \Delta t \right) \tag{3.17}$$

and the coherence time is given by

$$T = \frac{\sqrt{A}}{2\pi f_d} \ln(2) \tag{3.18}$$

For the channel model F, a Doppler component was included for the 3rd tap that represents a reflection from a moving vehicle. The proposed Doppler power spectrum, $S(f)$, can be expressed as (in linear values, not dB values):

$$S(f) = \frac{1}{1 + A\left(\frac{f}{f_d}\right)^2} + \frac{B}{1 + C\left(\frac{f - f_{spike}}{f_{spike}}\right)^2} \tag{3.19}$$

where f_{spike} is defined as

$$f_{spike} = \frac{v_1}{\lambda} \tag{3.20}$$

where v_1 is the speed of a vehicle in a factory or outdoor hot-spot environment. The proposed value for v_1 *is* 40 *km/h*. The spike is present at positive frequencies only. Parameter A is set equal to 9, same as the for the "Bell" shape Doppler spectrum equation (3.15). B represents the ratio between the spike peak and the maximum of the Bell Shape. B has been determined such that the ripple on the narrowband channel responses using Model F is equal to 2-4 dB. The proposed value for B is 0.5. The reader should note that such ripple depends on the relative power between the 3rd tap and the other taps of Model F for which simple Bell shapes apply. C determines the spike bandwidth. The bandwidth is set equal to αf_{spike} where the amplitude is 10 dB below the spike peak. In this way α represents the relative bandwidth of the spike. The proposed value for α is 0.02. Since $f_{spike} >> f_d$ and $\alpha << 1$ only the second term of equation (3.20) can be adopted to determine C under this assumption.

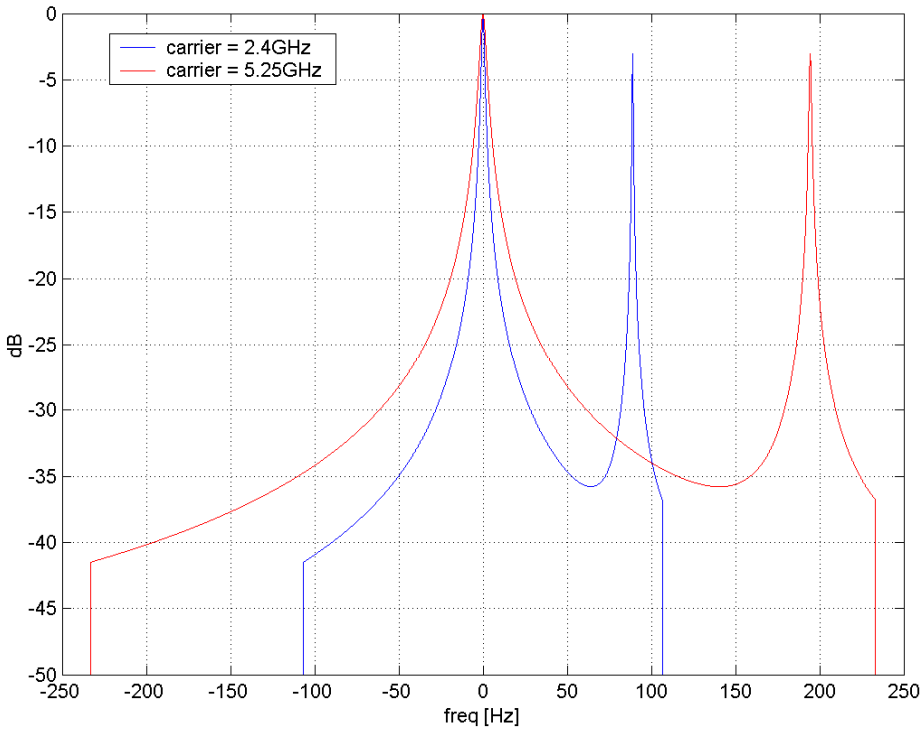

Figure 3.8 Example “Bell” shape Doppler spectrum with a Doppler component due to a moving vehicle.

$$\frac{S\left(f_{spike}\left(1\pm\frac{\alpha}{2}\right)\right)}{S\left(f_{spike}\right)}=0.1,\quad \text{so,}\ \ C=\frac{36}{\alpha^2}=90000 \tag{3.21}$$

The resulting Doppler power spectrum is illustrated in Fig. 3.8.

Note that the Doppler spectrum can be truncated similarly to the truncation in the previous case, (5 times f_d).

3.5 Simulation Results

Unless otherwise stated, it assumes in the following that

- The fading at the different antenna elements is assumed to be independent identically distributed (i.i.d.) Rayleigh fading. This is fulfilled if the directions of the MPCs at the transmitter and receiver are approximately uniform, and/or the antenna elements are spaced far apart from each other [9].

- The fading is assumed to be frequency flat. This is fulfilled if the coherence bandwidth of the channel is significantly larger than the transmission bandwidth.

- The receiver has perfect knowledge of the channel. For the transmitter, it will analyze both cases where the transmitter has no channel knowledge, and where it has perfect channel knowledge.

- When talking about capacity, it also assumes that the channel is quasi-static. By quasi-static, it means that the coherence time of the channel is so long that “almost infinitely” many bits can be transmitted within this time. Thus, each channel realization is associated with a (Shannon-AWGN) capacity value. The capacity thus becomes a random variable, described by its cumulative distribution function (CDF).

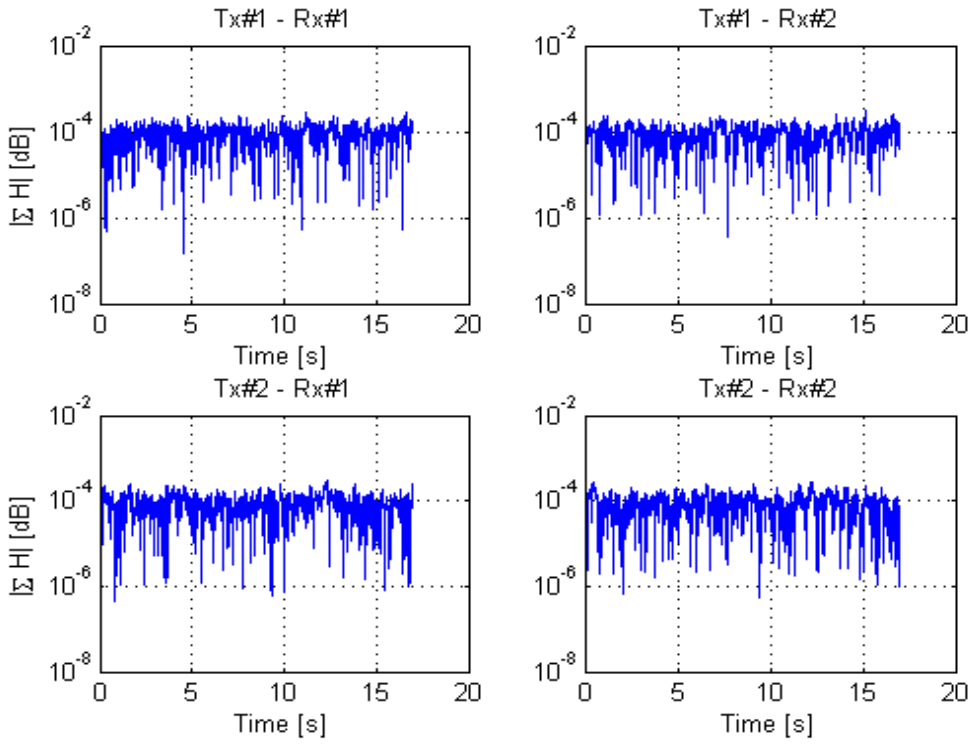

Figure 3.9 Narrowband impulse responses of a 2x2 MIMO channel using model F.

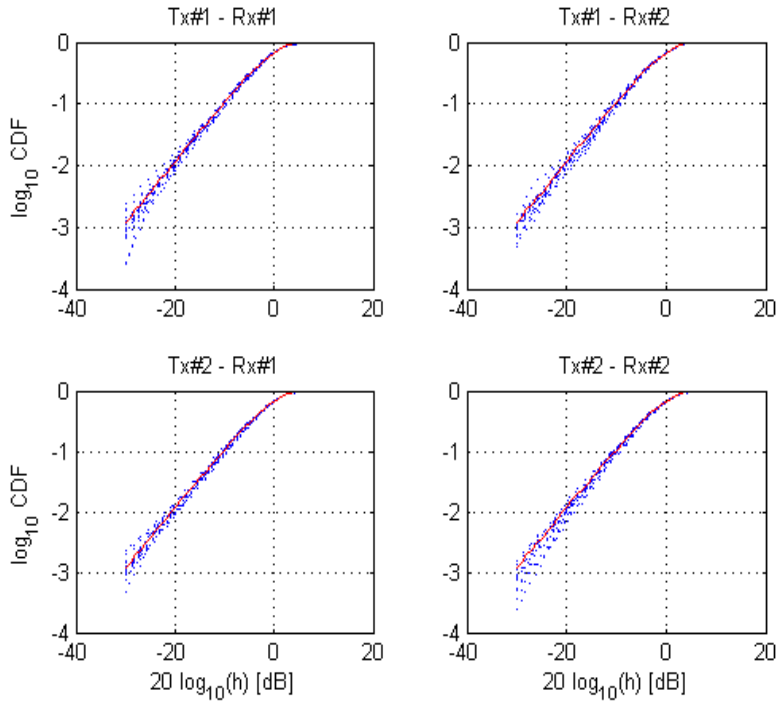

Figure 3.10 Cumulative distribution function (CDF in log scale) of capacity for a 2x2 MIMO system.

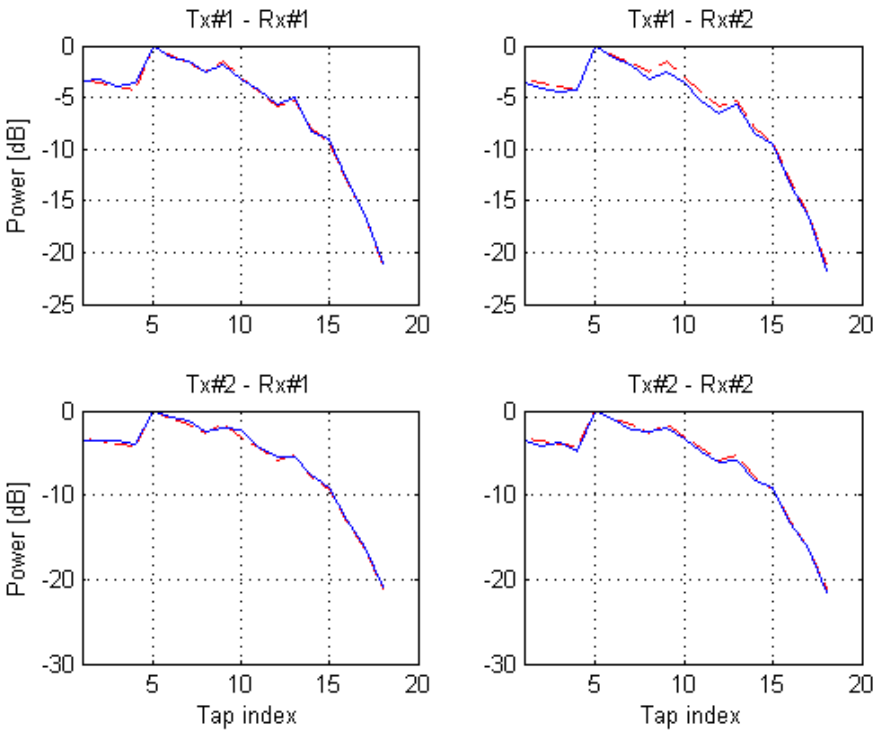

Figure 3.11 Power delay profiles of a 2x2 MIMO channel using model F.

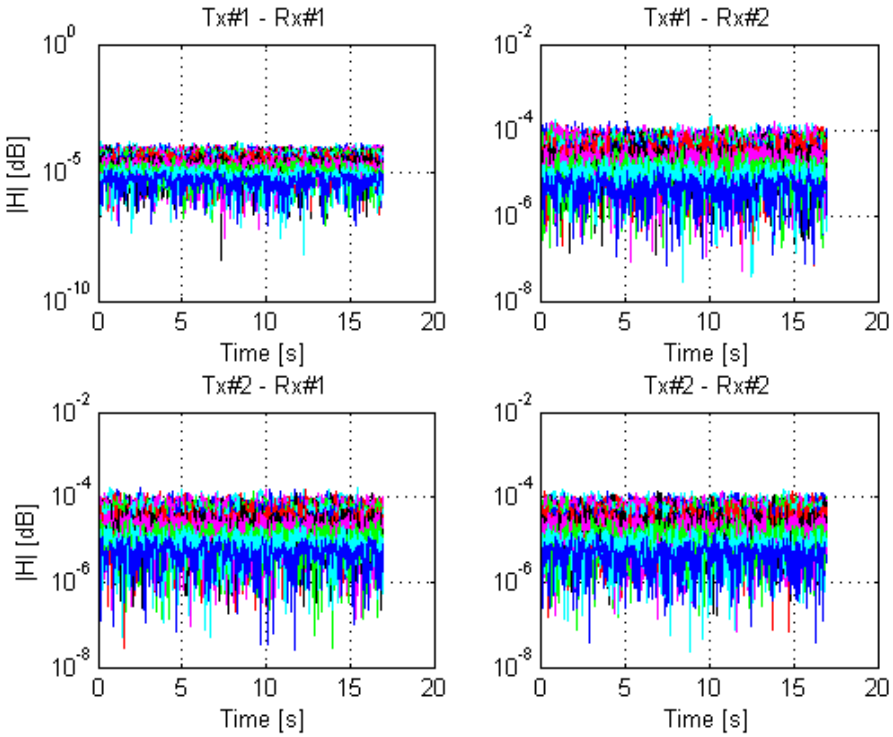

Figure 3.12 Narrowband impulse responses of a 2x2 MIMO channel using model F.

3.6 Comparison of simulation results with the GBSB approach

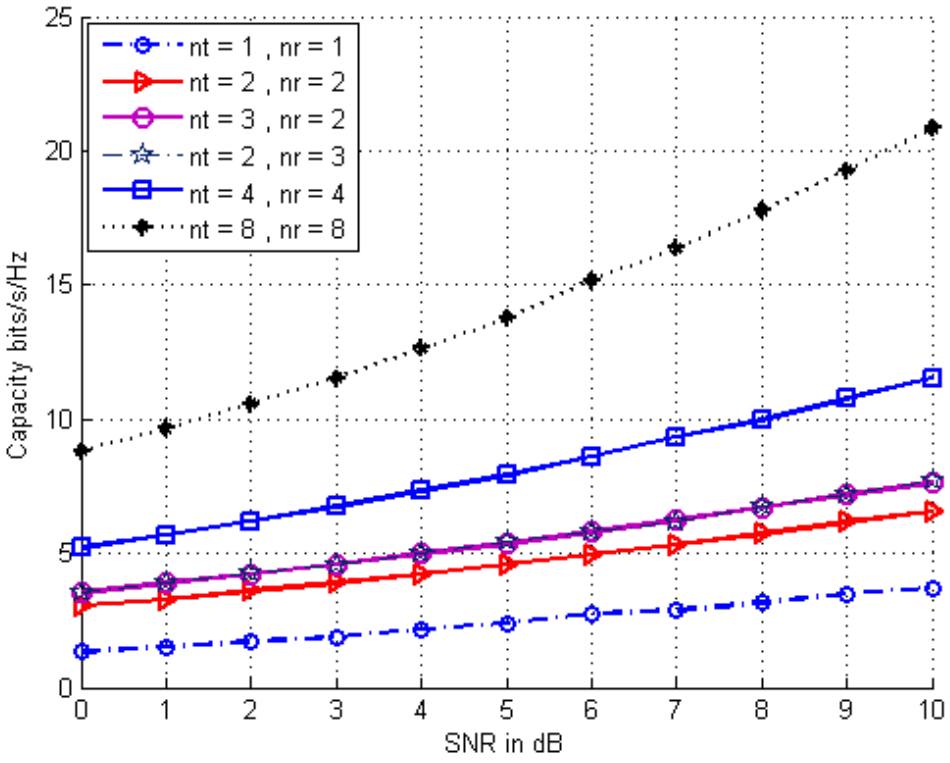

Figure 3.13 Capacities versus SNR for various transmit and receive array configurations.

Fig. 3.13 shows the capacities for various example configurations of transmit and receive arrays. The following antenna configurations have been chosen: nt=1 and nr=1 (SISO), nt=2 and nr=2, nt=3 and nr=2, nt=2 and nr=3, nt=4 and nr=4, and nt=8 and nr=8. As can be seen from Fig. 3.13 the trends that the capacity increases as the number of antenna elements for transmit and receive array configurations increases.

3.7 Conclusions

This chapter proposed a set of channel models applicable to indoor MIMO WLAN systems. The newly developed models were based on the cluster modeling approach, where tap-dependent and cluster-dependent angular and power properties were characterized. Based on these parameters, an accurate time-domain MIMO channel matrix can be obtained from the Matlab® program in [55], with proper antenna correlation properties.

Multi-antenna transmission with multi-antenna reception brings significant improvement in spectral efficiency for wireless communication systems. The degree of improvement is directly proportional to the correlation properties of the related MIMO (Multiple Input Multiple Output) radio channel. Recently, it has been noticed that signal propagation paths appear as clusters both in the delay and spatial (azimuth) domains. Depending on the number of clusters and their directions and the corresponding angular spreading the MIMO channel characteristics, especially the correlation properties, can vary significantly. Therefore, the achievable spectrum efficiency of a MIMO channel can differ considerably from the expected maximum values.

Simulation results indicate that the degree of propagation path clustering has a significant impact on the spectral efficiency of MIMO channels.

Chapter 4 Clustering Approach of Channel Model based on Geometry

This chapter describes the double bounce approach of the Geometrically Based Elliptical Channel Model, (GBSBEM) presented in Chapter 2 regarding to the scattering areas; unlike the previous geometrical models based only on single bounce reflection, it describes a model to represent the power delay angle profiles (PDAPs) by clusters plus background single bounce scatter components, i.e. the waves arrive at the receiver by double scattering at least. Instead of analyzing number of scatterers as uniformly distributed in the whole coverage area, the scatterers are grouped in “clusters”, obtaining a cluster of scatterers in order to get the parameters of interest, e.g., time of arrival (TOA), delay spread (DS), angle of arrival, (AOA), angle spread, (AS), and the power delay angle profiles (PDAPs). The effect of far scatterer clusters in outdoor urban environments and how these clusters affect the performance of MIMO systems is also analized. Part of this chapter has been published in [40].

4.1 Introduction

In Stochastic models, the average power delay angle profiles (PDAPs) and its statistical distributions is specified by the model, the statistical parameters employed in such models are usually estimated from extensive measurement campaigns or inferred from geometrical assumptions. Classical work has demonstrated that models must account for the physical geometry of scattering objects in the vicinity of the antenna of interest [6–9]. See also [17, and 19–22]

Several measurement campaigns done in different urban environments have been reported and the measurement results e.g. in [24, 29, 31, 36, 39, 41, 47, and 93], suggest that the received PDAPs are grouped into clusters, that correspond to objects in the surrounding; i.e., the waves have undergone additional scattering before being diffracted or reflected and arrived to the receiver; this result suggest that the single bounce assumption in the geometrical based channel models, e.g. [6–8, and 21], cannot represent the characteristic of the received PDAPs. In view of the above mentioned, a model to represent the

received PDAPs by clusters plus background single bounce scatter components is modeled, i.e. the waves arrive at the receiver by double scattering at least. Simulation results for one typical outdoor scenario for urban environments are also shown.

4.2 Description of the Approach

This Section introduces the description of the model proposed to represent the PDAPs. It is assumed that the mobile station is stationary or at very low speed and therefore the Doppler effects is ignored in the analysis. Multipath propagation can be well modeled with a baseband channel impulse response as [8]:

$$h_b(\tau,\theta) = \sum_{i=1}^{L} \alpha_i \delta(\tau - \tau_i)\delta(\theta - \theta_i), \tag{4.1}$$

where $|\alpha_i|$ is the magnitude of the i^{th} MPC, θ_i is the angle of arrival of the i^{th} MPC, and τ_i is the delay associated with that component. The parameter L is the total number of MPCs. Unlike the previous geometrical models based on single bounce reflection, it looks at each cluster separately to get a relationship of the cluster shape and size in the PDAPs and the geometrical description of the model. Since it is also geometrically based, the signal statistics depend on the position of the base station, (BS), (e.g. Transmitter Tx), the mobile station, (MS), (Receiver Rx), and the geometrical distribution of the clusters. It assumes that each cluster, (which include a number of scatterers), is stationary, in the far field.

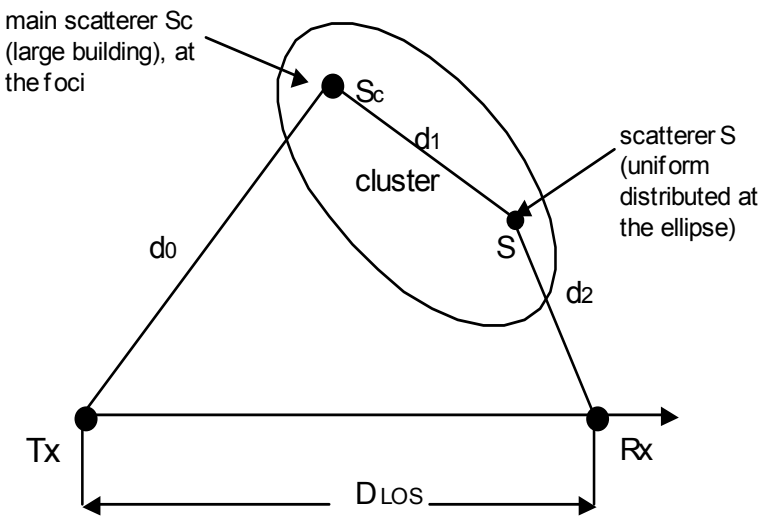

Figure 4.1 Geometrically based double bounce description (time domain).

Then the angle resolved impulse response of each cluster is defined as:

$$h_{(cluster)\,j}(\tau,\phi)=\sum_{i=1}^{L_j}\alpha_{ij}\delta(\phi-\phi_{ij})\delta(\tau-\tau_0-\tau_{ij}), \tag{4.2}$$

where, for each cluster: $|\alpha_i|$ is the magnitude of the i^{th} MPC, ϕ_i is the angle of arrival of the i^{th} MPC, τ_0 represent the extra delay due to the double scattering effect and τ_i is the delay associated with that component. The parameter L is the total number of MPCs. Then the total baseband channel impulse response is defined as:

$$h_{btotal}(\tau,\phi)=\sum_{j=1}^{J}h_{(cluster)\,j}(\tau,\phi), \tag{4.3}$$

where, the parameter J is the number of clusters. For the case of J=1, i.e., for one cluster condition is analyzed. From measurement campaigns reported in [24, 29, 36, 41, 47, and 93] in 90% of the cases, there are at most six clusters seen by the receiver, then it uses as a reference for the parameter J, i.e. $\mathrm{J}\leq\mathrm{L}$. Fig. 4.1 shows in more details the clustering approach regarding to the path length and time of arrival analysis.

Fig. 4.1 illustrates the geometry of the model. The following is assumed: the cluster region has an elliptical shape, and the main scatterer, (Sc), which is a large far away obstacle from the receiver, (e.g. a large building), is situated at one of the foci of the ellipse as shown in Fig. 4.1. Besides, there is line of sight (LOS) between the main scatterer and the receiver (Rx), and all scatterers (S) that belong to the same cluster are uniform distributed inside the cluster.

It is further assumed that the propagation takes place in the horizontal plane containing the receiver (Rx), in this case the mobile station (MS), and the transmitter (Tx), in this case the base station (BS) are placed in the same plane. D_{LOS} represent the Tx-Rx separation distance. From Fig. 4.1 the following geometrical relations can be obtained: the total path length (l), and the time of arrival (τ) of the ray resulting from the kth scatterer are given by

$$l = \|Tx - Sc\| + \|S - Sc\| + \|Rx - S\| = d_0 + d_1 + d_2, \tag{4.4}$$

and

$$\tau = \frac{l}{c}, \tag{4.5}$$

where, c represents the speed of light. Although the approach proposed is applicable for uplink (UL) as well, (just changing the position of the major axis of the cluster in the direction of the transmitter), the downlink (DL) environment is only analyzed. In the next Section the relationship between the cluster and the PDAPs is analyzed.

4.3 Analysis of the approach

In the previous Section, it was presented the description of the model based on the double scattering effect grouped into clusters. These clusters are present in the delay, as well as in the angle domain, and in general, cluster in the far field leads to a significant increase in the delay and angular dispersion. This Section presents the analysis of the approach based on the size and shape of each cluster and derives the relationship between a cluster and the PDAPs.

Fig. 4.2 shows the details regarding the angle of arrival of the MPCs of the cluster at the receiver (Rx). The line joining the main scatterer Sc and the receiver (Rx) makes an angle α with respect to the *x'-axis*, as it can be seen that the line path through the major axis of the ellipse, then, there is symmetry about that line.

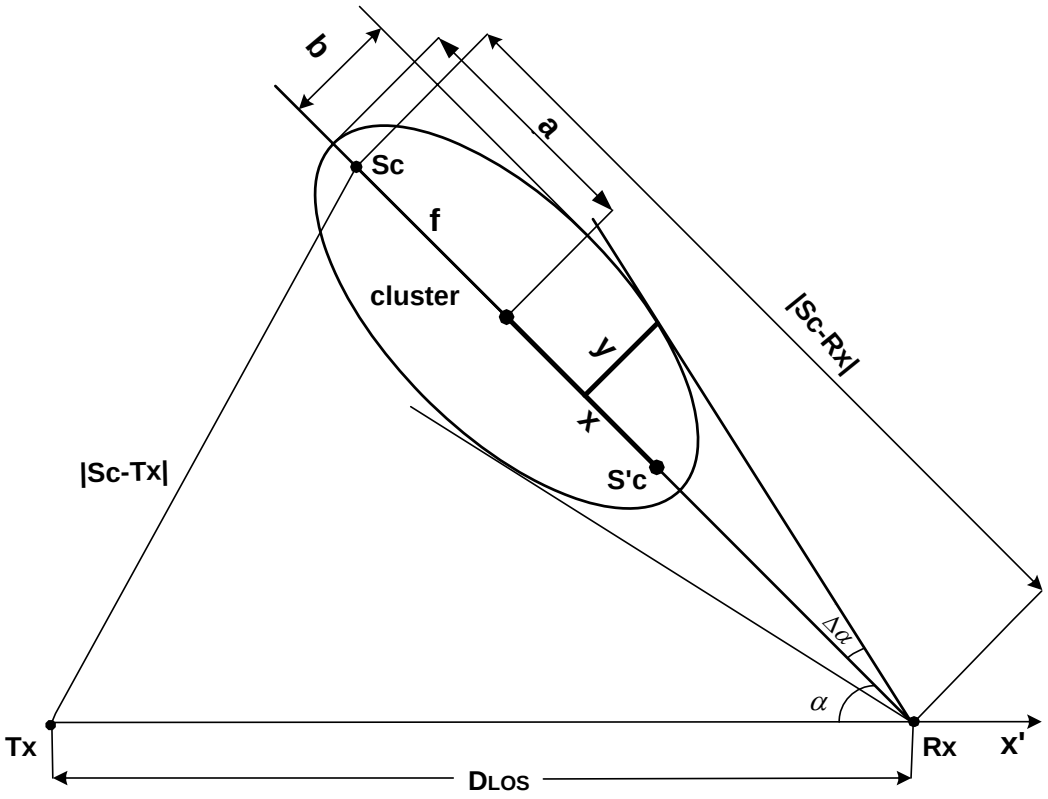

Figure 4.2 The geometry of the model (angle of arrival analysis).

The angle formed with respect to that line and one of the lines tangents to the ellipse is $\Delta\alpha$, i.e. the angle formed between the lines tangent to the ellipse is $2\Delta\alpha$. The ratio of the ellipse is also defined as:

$$r_{ab} = \frac{b}{a}, 0 < r_{ab} \leq 1, \tag{4.6}$$

i.e. the quotient from dividing the minor axis (b) by the major axis (a), (assuming $a>b$), the parameter *"a"* and the ratio r_{ab} define the size of each cluster.

The geometrical properties of the ellipse with center at origin and major axis along the *x-axis* is defined as follows

$$\frac{x^2}{a^2} + \frac{y^2}{b^2} = 1. \tag{4.7}$$

It is well-known that the foci is defined by $f = (a^2 - b^2)^{1/2}$, and f can be expressed in function of the elliptical ratio r_{ab} described earlier as follow

$$f = a\sqrt{1 - r_{ab}^2} \tag{4.8}$$

For any pair (x, y) of the ellipse described in Fig. 4.2, for a fixed given value of *"a"* the angle $\Delta\alpha_{xy}$ is

$$\Delta\alpha_{xy} = \arctan\frac{y}{|Sc - Rx| - f - x} \tag{4.9}$$

Equation (4.9) is valid for the case when the separation distance between the cluster and the receiver (Rx) is referred to the focus of the ellipse as Sc, which is at larger distance from the receiver, as illustrated in Fig. 4.2. The analysis when it uses as a reference the other focus of the ellipse, i.e. S′c, (the one that is closer to the receiver (Rx)) is presented later in this Section. The last case is useful when it has channel parameters with large excess delay and *rms* delay spread respectively, that can be found in urban scenarios for Non Line-Of-Sight (NLOS) as found in [29, 36, and 47], where the receiver is close to a large open square.

To obtain the maximum angle of the cluster, defined by $\Delta\alpha$ and illustrated in Fig. 4.2, it takes the derivative of equation (4.9) and equating to zero the following expression is obtained

$$\Delta\alpha = \arctan\left(\frac{r_{ab}\ a}{\sqrt{\left(|Sc - Rx| - f\right)^2 - a^2}}\right) \tag{4.10}$$

Based on the geometrical assumptions, the following relationship between the PDAP and the cluster is inferred and deduced from Fig. 4.2. The elliptical shape obtained in the PDAP from each cluster, and illustrated in Fig. 4.3, is verified with a numerical example in the next Section.

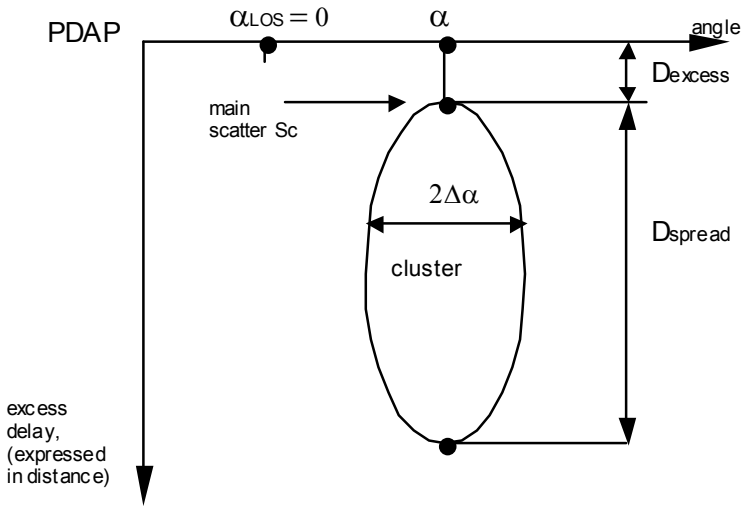

Figure 4.3 Relationship between the power delay angle profile (PDAP) and the cluster.

In Fig. 4.3, α represents the angle of arrival and $2\Delta\alpha$, represents the angle spread calculated from equation (4.10) and by the property of symmetry. The excess delay and the delay spread (both expressed in terms of distance) are represented by the following expressions deduced from Fig. 4.2:

$$D_{excess} = |Tx - Sc| + |Sc - Rx| - D_{los}, \tag{4.11}$$

$$D_{spread} = 2a\left(1 - \sqrt{1 - r_{ab}^2}\right), \tag{4.12}$$

where, equations (4.11) and (4.12), represent the excess delay and the delay spread respectively, both expressed in terms of distance.

In order to demonstrate the applicability of the proposed channel model described in Section 4.2, the position and shape of each cluster can be determined through the extraction of parameters from the PDAPs (that should be obtained from measurement campaigns): D_{excess}, α, $\Delta\alpha$, and D_{spread}, as shown in Fig. 4.3.

The position of each cluster depends on the parameters D_{excess} and α. For a fix value of each excess delay τ corresponds to a certain ellipse, which is focused on transmitter (Tx) and receiver (Rx), whereas, the angle α, is associated with a certain DOA. See [6–8, 21, and 22]. The foci, (f_{TR}), the major axis (a_{TR}) and the

minor axis (b_{TR}) of this ellipse can be defined in function of D_{LOS} and D_{excess} as follows:

$$f_{TR} = \frac{D_{los}}{2}, \tag{4.13}$$

$$a_{TR} = \frac{D_{excess}}{2} + f_{TR}, \tag{4.14}$$

$$b_{TR} = \sqrt{a^2 - f_{TR}^2}, \tag{4.15}$$

Then, the position of the cluster is obtained from equations (4.13)-(4.15) transformed into Cartesian coordinates [21]:

$$x_{Sc} = a_{TR}\left(\frac{f_{TR} - a_{TR}\cos(\alpha)}{a_{TR} - f_{TR}\cos(\alpha)}\right), \tag{4.16}$$

$$y_{Sc} = \frac{b_{TR}^2 \sin(\alpha)}{a_{TR} - f_{TR}\cos(\alpha)} \tag{4.17}$$

The size of each cluster depends on the parameters $\Delta\alpha$ and D_{spread}. As stated at the beginning of this Section the size of the cluster is defined by the parameters *"a"*, (the major axis of the ellipse), and the ratio of the ellipse *"r_{ab}"*.

Then, using equations (4.10) and (4.12) and rearranging the equations in function of a and r_{ab} the following system of nonlinear equation is obtained:

$$\begin{cases} a^2\left(1+\tan^2(\Delta\alpha)\right)r_{ab}^2 + 2a\tan^2(\Delta\alpha)\left(\left|Sc-Rx\right|\right)\sqrt{1-r_{ab}^2} - \tan^2(\Delta\alpha)\left(\left|Sc-Rx\right|^2\right) = 0 \\ \\ r_{ab} = \sqrt{\dfrac{D_{spread}}{a} - \dfrac{\left(D_{spread}\right)^2}{4a^2}}, \end{cases} \tag{4.18}$$

the shape of each cluster now is found by solving this system of equations. Due to the nonlinearity of the system, its solution can also be verified iteratively.

$$a = \frac{1}{4}\frac{4D_{spread}\tan^2(\Delta\alpha)(\left|Sc-Rx\right|) + \left(D_{spread}\right)^2\tan^2(\Delta\alpha) + 4\tan^2(\Delta\alpha)(\left|Sc-Rx\right|)^2 + \left(D_{spread}\right)^2}{2\tan^2(\Delta\alpha)(\left|Sc-Rx\right|) + D_{spread} + D_{spread}\tan^2(\Delta\alpha)} \tag{4.19}$$

$$r_{ab} = \left(\sqrt{\frac{\left(2\tan^2(\Delta\alpha)\left(\left|Sc-Rx\right|\right) + D_{spread} + D_{spread}\tan^2(\Delta\alpha)\right)\left(D_{spread} + 2\left(\left|Sc-Rx\right|\right)\right)D_{spread}\tan^2(\Delta\alpha)\left(\left|Sc-Rx\right|\right)}{\left(4D_{spread}\tan^2(\Delta\alpha)\left(\left|Sc-Rx\right|\right) + \left(D_{spread}\right)^2\tan^2(\Delta\alpha) + 4\tan^2(\Delta\alpha)\left(\left|Sc-Rx\right|\right)^2 + \left(D_{spread}\right)^2\right)^2}}\right)2\sqrt{2}. \tag{4.20}$$

The expressions in (4.19) and (4.20) are the solution of the system of equations given in (4.18) for *"a"* and *"r_{ab}"* respectively.

In a similar way, the clustering approach is analyzed for the case when the separation distance between the cluster and the receiver (Rx) is referred to the other focus of the ellipse ($S'c$) that is closer to the receiver (Rx) as illustrated in Fig. 4.2. The analysis is as follows:

Using the same approach as before, but taken into account the other focus of the ellipse, i.e. (S′c), for any pair (x, y) of the ellipse described in Fig. 4.2, the angle $\Delta\alpha_{xy}$ is

$$\Delta\alpha_{xy} = \arctan\frac{y}{\left|Sc-Rx\right| + f - x} \tag{4.21}$$

Then in this case, (as in the first case), to obtain the maximum angle of the cluster, defined by $\Delta\alpha$ and illustrated in Fig. 4.2, taking the derivative of equation (4.21) and equating to zero the following expression is obtained

$$\Delta\alpha = \arctan\left(\frac{r_{ab}\ a}{\sqrt{\left(\left|Sc-Rx\right|+f\right)^2-a^2}}\right) \tag{4.22}$$

As in the analysis for the first case, in Fig. 4.3, α represents the angle of arrival and $2\Delta\alpha$, represents the angle spread calculated now from equation (4.21) and by the property of symmetry. The excess delay and the delay spread (both expressed in terms of distance) are represented by the following expressions deduced from the same Fig. 4.2:

$$D_{excess} = \left|Tx-Sc\right|+\left|Sc-Rx\right|-D_{los}, \tag{4.23}$$

$$D_{spread} = 2a\left(1+\sqrt{1-r_{ab}^2}\right), \tag{4.24}$$

where, for this case equations (4.23) and (4.24), represent the excess delay and the delay spread respectively, both expressed in terms of distance.

Then, (as the previous case), using equations (4.22) and (4.24) and rearranging the equations in function of a and r_{ab} the following system of nonlinear equations is obtained:

$$\begin{cases} a^2\left(1+\tan^2(\Delta\alpha)\right)r_{ab}^2-2a\tan^2(\Delta\alpha)\left(\left|Sc-Rx\right|\right)\sqrt{1-r_{ab}^2}-\tan^2(\Delta\alpha)\left(\left|Sc-Rx\right|^2\right)=0 \\ r_{ab}=\sqrt{\dfrac{D_{spread}}{a}-\dfrac{\left(D_{spread}\right)^2}{4a^2}}, \end{cases} \tag{4.25}$$

Note that the system of equations in (4.25) is similar to the system of equations in (4.18), they only differ in the sign of the second term of the first equation, note also that the second equation of the systems in (4.18) and (4.25) is the same,

due to the equations (4.12) and (4.24) are very similar, from which are deduced the second equations of the systems (4.18) and (4.25), respectively. The shape of each cluster now is found by solving the system of equations in (4.25). Due to the nonlinearity of the system, the solution is also verified iteratively. The next Section illustrates a numerical example to show the application of the approach, for the cases analyzed in this Section.

4.4 Numerical Examples

This Section illustrates through numerical examples the application of the approach described in the previous section. Data are generated according to the model defined by equation (4.3), where only direction of arrival (DOA) and time of arrival (TOA) are considered (the Doppler effect has been neglected). A group of five clusters of $\mathrm{L} = 100$ scatterers uniformly distributed inside the clusters is considered, the parameters are shown in Table 4.1.

Fig. 4.4 shows the localization and boundaries of the generated group of clusters with the elliptical shape and sizes according to the parameters of Table 4.1. Then using equations (4.10)–(4.12), and (4.22)–(4.24) respectively, the excess delay (D_{excess}), delay spread (D_{spread}), angle of arrival (α), and angle spread ($2\Delta\alpha$) are obtained. All these parameters are summarized in Table 4.2.

Fig. 4.5 shows the PDAPs for each cluster, obtained from the set of parameters defined in Table 4.1. As shown in Fig. 4.4, different shape and size of clusters found in the PDAPs from measurement campaigns published in the literature can be described.

Table 3.1 Parameters of the five clusters defined by the (x,y) position, main radius (a) and the ratio (b/a).

***Tx-Rx* and No. Clusters (*Sc*)**	**x-y position [m]**		**Main radius *a* [m]**	**Ratio $r_{ab} = b/a$**
	x	**y**		
Tx (BS)	0	0	-	-
Rx (MS)	600	0	-	-
Sc 1	400	100	50	1
Sc 2	600	100	40	0.4
Sc 3	200	0	40	0.9
Sc 4	400	-100	60	0.7
Sc 5	600	-150	70	0.5

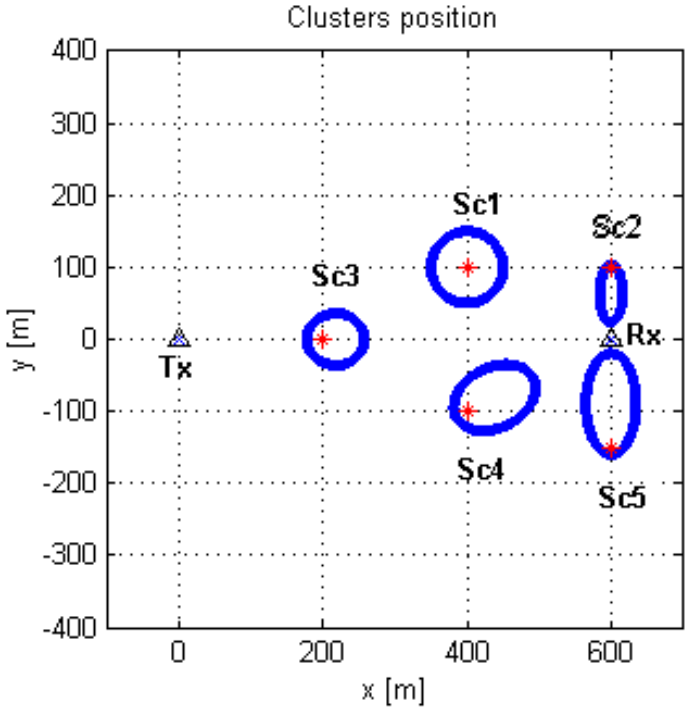

Figure 4.4 x-y cluster's position generated from Table 4.1.

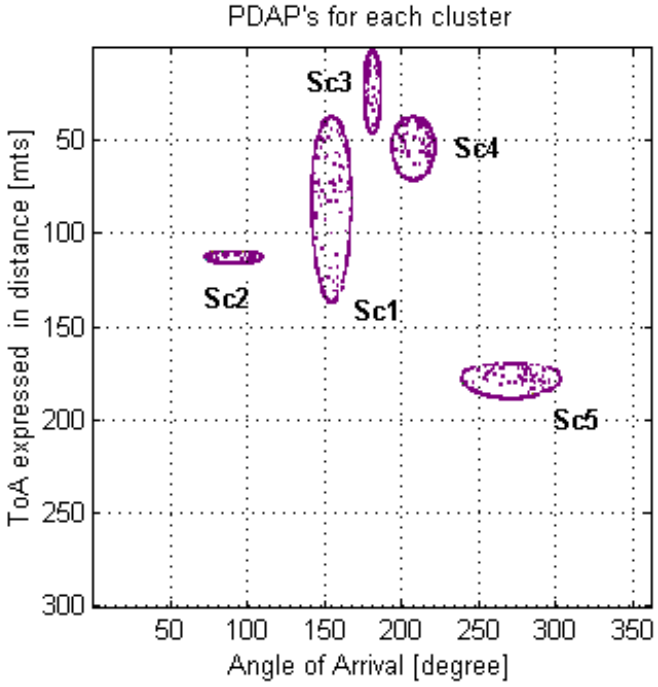

Figure 4.5 PDAPs: horizontal axis "α", vertical axis "delay" (expressed in terms of distance), and α_{LOS}=180 degrees.

Table 4.2 Results in angle (degree) and delay (expressed in distance) of the PDAPs for each cluster.

No. of Cluster	Dist. |Sc-Rx| [m]	Excess delay [m]	Delay spread [m]	Angle α (deg)	Angle spread $2\Delta\alpha$ (deg)
Sc 1	224	35.9	100	26.6	25.8
Sc 2	100	108.9	6.7	90	36.1
Sc 3	400	0	45 1	0	10.8
Sc 4	224	35.92	34.3	-26.6	27.7
Sc 5	150	168.5	18.8	-90	64.4

4.5 Delay Spread and Angle Spread Boundaries

In the previous Section, it was presented the analysis of the clustering approach of the model based on the double scattering effect grouped into clusters. These clusters are present in the delay, as well as in the angle domain, and in general, cluster in the far field leads to a significant increase in the delay and the angular dispersion. This Section presents the boundaries of the delay spread and angle spread based on the theoretical distributions in angle and time domain respectively, from a cluster of scatterers derived in the previous Section.

Boundaries of the delay spread and angle spread respectively, are shown for the two cases analyzed in the previous Section, i.e., when it is used as a reference the focus of the ellipse (Sc) that is a larger distance from the receiver and the focus of the ellipse ($S'c$) that is a closer distance to the receiver as well, as illustrated in Fig. 4.2.

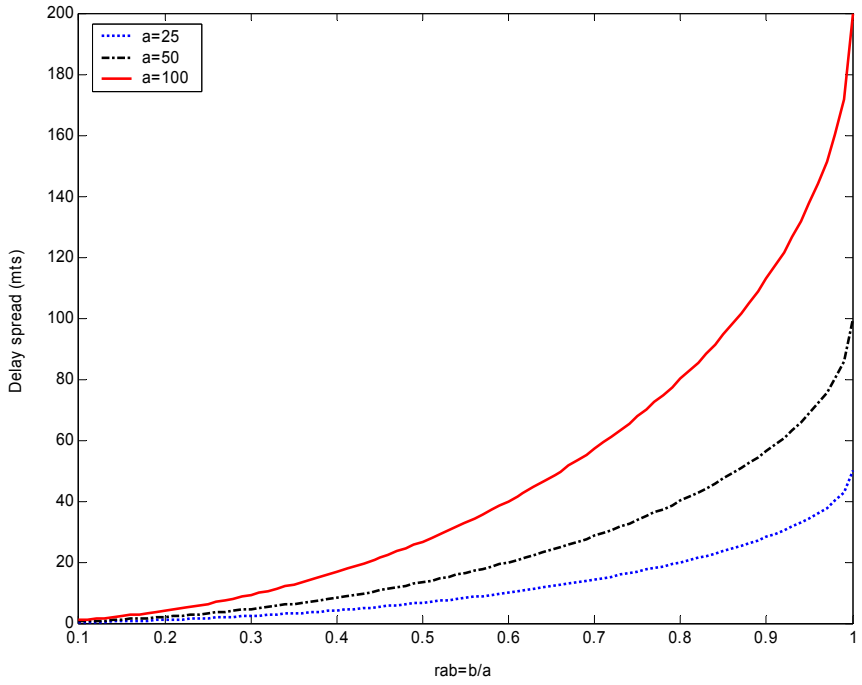

Figure 4.6 Boundaries plot of delay spread (DS), obtained from equation (4.12) for three different sizes of fixed values of "a".

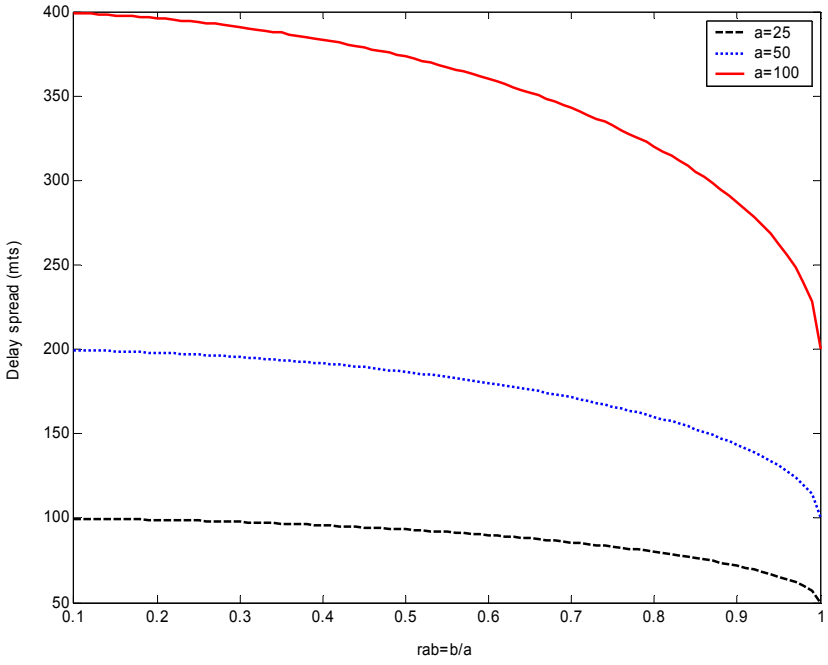

Figure 4.7 Boundaries plot of delay spread (DS), obtained from equation (4.24) for three different sizes of fixed values of "a".

Fig. 4.6 shows the boundaries of the delay spread (DS) for the case when it is used as a reference the focus of the ellipse (Sc) that is at larger distance from the receiver derived in equation (4.12). In this case for $r_{ab}=1$ (circular case) the maximum $D_{spread} = 2a$, *i.e.* $D_{spread} < 2a$.

Fig. 4.7 shows the boundaries of the delay spread (DS) for the case when it is used as a reference the focus of the ellipse ($S'c$) that is at closer distance from the receiver derived in equation (4.24). In this case for $r_{ab}=1$ (circular case) the minimum $D_{spread} = 2a$, *i.e.* $D_{spread} > 2a$.

As stated in the previous Section, this case is useful when the channel has parameters with large excess delay and rms delay spread respectively that can be found in urban scenarios for Non Line-Of-Sight (NLOS) as found in [29, 36, and 47], where the receiver is close to a large open square.

For the case of angle spread when it is used as reference the focus of the ellipse (Sc) that is larger distance from the receiver the boundaries are illustrated

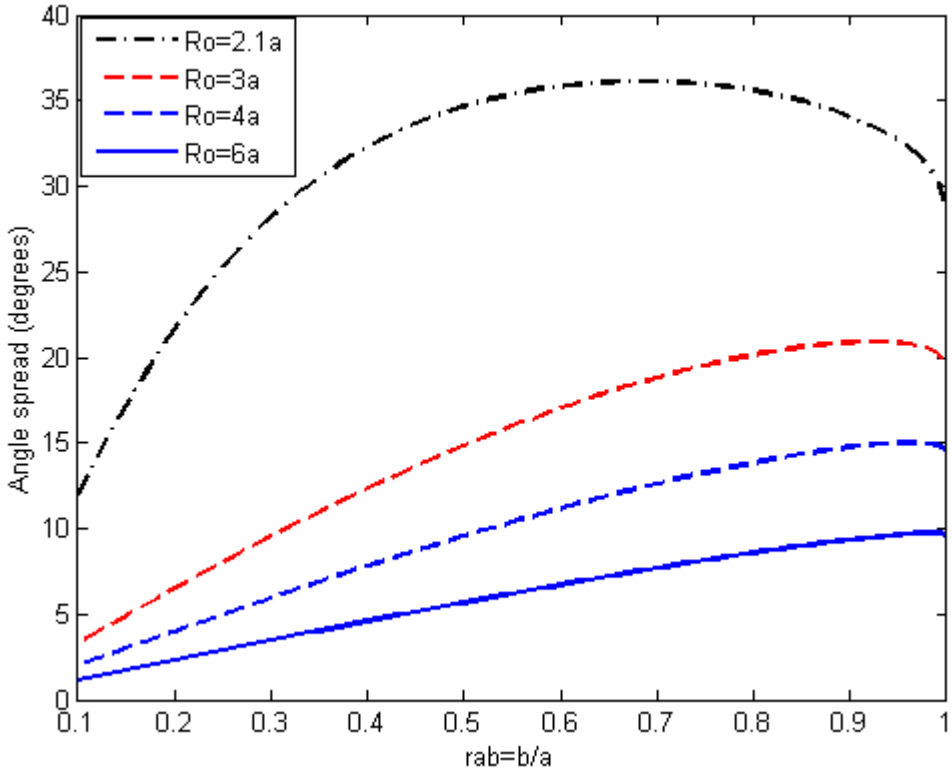

Figure 4.8 Boundaries plot of angle spread (AS), obtained form equation (4.10) for four different distances in function of size of fixed values of "a".

in Fig. 4.8. On the other hand when it is used as reference the focus of the ellipse (S′c) that is closer distance from the receiver the boundaries are illustrated in Fig. 4.9.

Fig. 4.8 shows the boundaries of the angle spread (AS) for the case when it is used as a reference the focus of the ellipse (Sc) that is at larger distance from the receiver derived in equation (3.10). The solid line in Fig. 4.8 is for the case when the cluster is in a closer distance to the receiver.

Fig. 4.9 shows the boundaries of the angle spread (AS) for the case when it is used as a reference the focus of the ellipse (S′c) that is at closer distance from the receiver derived in equation (3.22).

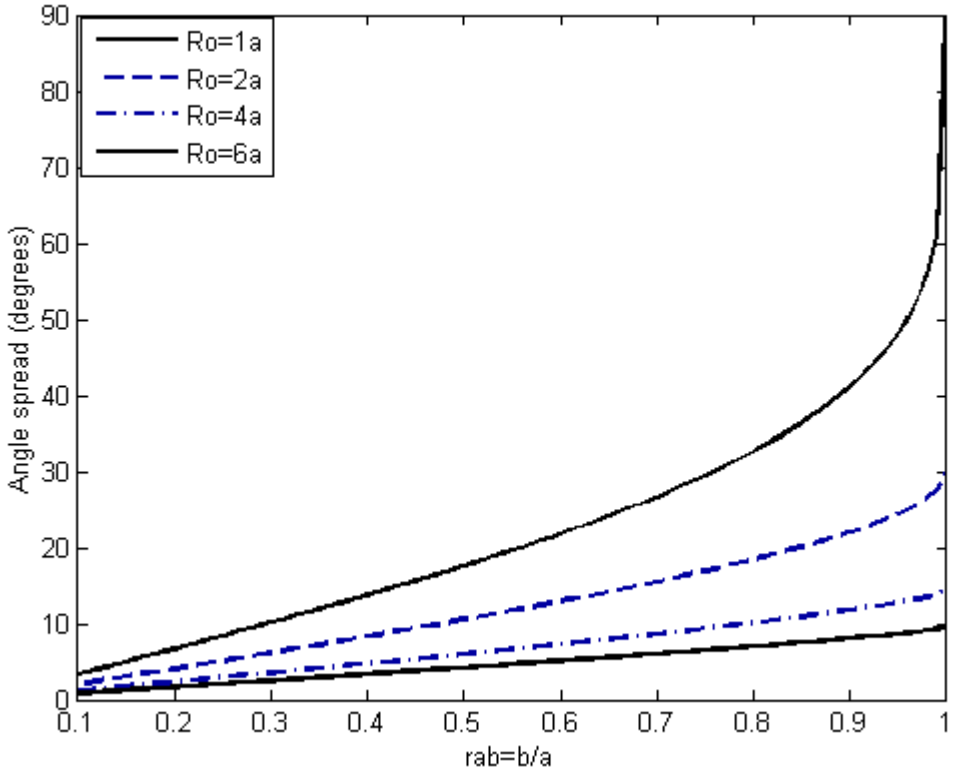

Figure 4.9 Boundaries plot of angle spread (AS) from equation (4.22) for four different distances *Ro* in function of the size of fixed values of *"a"*.

4.6 Effect of far scatterer clusters

In this Section, the clustering structures of wireless MIMO channels are considered, and the impact that multiple clusters have on the performance of MIMO systems. It is shown that multiple clusters frequently occur in urban environments. Then it proceeds to demonstrate that a channel with multiple scatterer clusters behaves differently than a channel with one cluster and the same rms angle spread. The differences are quantified in terms of correlation coefficients, information-theoretic capacity, and interference-suppression capabilities. This demonstrates the necessity of correctly taking into account the clustering structure.

First the physical channel modeling with and without far scatterer clusters is described. The basic form is also known as “local scatterer model” where all relevant scatterers are located around the mobile station (MS). The probability density function (PDF) of the scatterer location is often assumed to be uniform in a disk around the MS, Gaussian, or Rayleigh distributed. Alternatively, the power delay angular profile spectrum shows an exponential behavior in delay and Laplacian behavior in angle, around the (quasi) Line-Of-Sight component [31–33], see also [84–88, and 98].

Reference [29] suggested to additionally modeling far scatterer clusters that are far away from both the MS and the base station BS, see Fig. 4.10 for illustration. These far clusters represent e.g. high-rise buildings, in urban environments, mountains in rural environments, etc. While the local scatterers are always centered around the MS, the position of the far scatterers are fixed at an absolute position in space.

Actually, it is necessary to distinguish between two types of far scatterers. One is discrete reflectors, which gives rise essentially to a single, specular, MPC. Such a discrete reflector could be, e.g., a high-rise building with a smooth surface. The other type is a far scatterer cluster, where a group of high rise buildings or a mountain surface gives raise to several, closely spaced, MPCs. The distinction between specular reflectors and scatterer clusters is of special importance for the MIMO capacity.

For microcellular environments, the propagation processes leading to far scatterers are somewhat different. Waves get from the transmitter to the receiver via waveguiding. Different waveguides thus give rise to different clusters due to different propagation times and/or angles of incidence at the transmitter and receiver. A local cluster, representing over-the-rooftop propagation, is not necessarily present, especially if the BS antenna is significantly below the height of the surrounding rooftops [36 and 47].

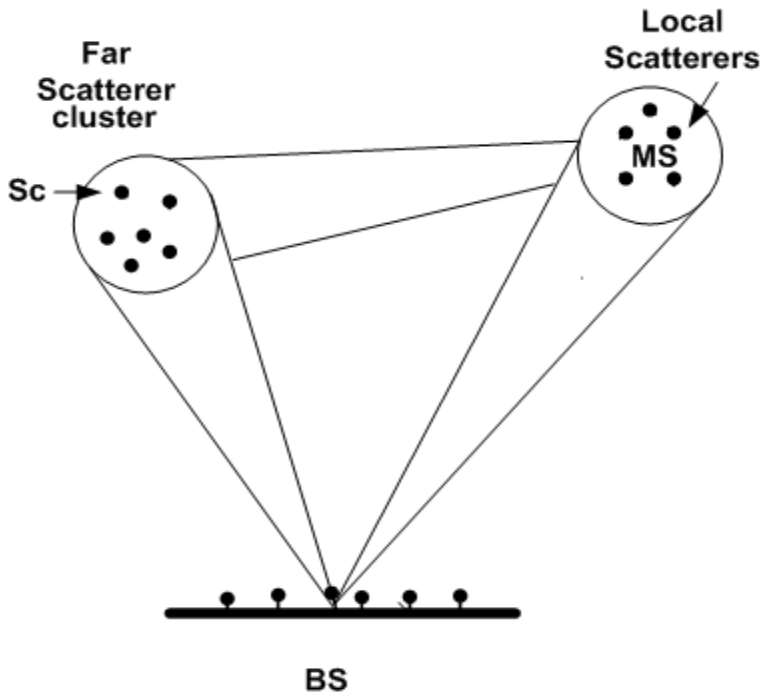

Figure 4.10 Principle of far scatterer clusters.

The identification of clusters in a measured of power delay angular profile (PDAPs) always involves a certain degree of arbitrariness. It either has to identify an (arbitrary) threshold of the arriving power that determines the boundary of a cluster, or it has to use “cluster identification algorithms”, which are well known from image processing problems, and which give different results according which algorithm is used. In many cases, a visual inspection, together with knowledge of the morphology of the environments and the possible propagation processes, gives the best results. Naturally, cluster boundaries can be defined better in a channel model.

4.6.1 Available Data of Measurement Campaigns

There have been several measurement campaigns that determine the angular spectrum of the signals arriving at the BS:

Reference [29] describes a measurement campaign in Frankfurt, Germany. This city has a strong resemblance to many American cities, with a high-rise city

center, surrounded by low-rise buildings. The paper clearly identifies many skyscrapers as “far scatterer clusters”.

Reference [24] reports measurements in Paris, France, and is notable in that the directions-of-arrival at the mobile station, but not the BS, are resolved. Also here, several locations are identified where a far scatterer cluster leads to increased delay dispersion. Reference [63], contains measurements in urban small cells in Mulhouse and Paris, France. The authors observe both cases where there is only a single cluster (with a very small angle spread), as well as cases with several clusters. In one “atypical” case, there was even hardly any energy from the direction of the mobile. However, the case with both a “local” cluster and “far clusters” is judged to be most typical.

Extensive measurements in Helsinki, Finland [47] have shown that for macrocellular situations (as well as micro and picocellular), several clusters are present. 2-3 clusters have to be taken into account to cover 75% of the energy in 90% of the cases.

On the other hand, reference [36] reports measurements in Stockholm, Sweden. This city is characterized by large areas without buildings (e.g., water), between the built-up areas. Again, multiple clusters have been observed.

Only the measurement campaign reported in [31 and 39], in Bristol, UK, and near Aalborg, Denmark, found the “multiple scatterer cluster” case to be the exception rather than the rule. This can also be explained in terms of the morphology of the measurements; those towns contain fewer irregular structures than the big cities mentioned earlier.

The importance of far scatterer clusters has been recognized also by different standardization bodies. Most notably, the use of far clusters has been recommended (for specific environments) both in the European COST259, which developed a generic spatial channel model that is suitable for a wide range of systems, and by the joint “spatial channel modeling” group of 3GPP and 3GPP2, the standardization organizations for third-generation cellular systems.

The incorporation of the far scatterers in the COST259 model is more realistic, and more complicated. The number of far scatterer clusters in macrocells is treated as a random variable. Far clusters appear and disappear in a kind of birth/death process, depending on whether a mobile station has Line-Of-Sight to the far scatterer cluster. The mean number of far scatterer clusters depends on the radio environment. For more details, please see references [4 and 5].

4.6.2 Impact of scatterer clusters on system performance

Having established in the previous subsection that far scatterers occur in practice, now turn to the question whether a far scatterer cluster can be represented by an "equivalent" increase in the *rms* angle spread of the cluster around the MS.

It is well-established in [58] that the spatial signature of an antenna array, and thus the correlation coefficient for signals at the elements of a smart antenna, is determined only by the *rms* angle spread, and not the exact shape of the PAS (power azimuth spectrum) if the angle spread, and the aperture of the array, is small. This was shown in [58] by using a truncated Taylor expansion of the steering vector. From this point of view, it is thus possible to replace a multiple-cluster model by a single cluster with the same *rms* angle spread.

However, it is important to keep in mind the following restrictions of the derivation (which are also mentioned or implied in [58]):

- This independence of the shape of the PAS is valid only for the flat-fading case. For the wideband case, multiple clusters give rise to higher frequency selectivity, and also show different angular spectra for different delays. Thus, different types of spatio-temporal Rake receivers work differently in a single cluster and multiple-cluster scenarios.

- The independence is only fulfilled if both the *rms* angle spread and the maximum angle spread are small. Thus, far-off components with small power cannot be represented correctly by increasing the spread of the local cluster.

- It is required that the antenna pattern is isotropic within the range of occurring angles of incidence. This is especially important when comparing different types of antenna elements, e.g., for different sectorizations of a cell.

- The independence is true only for complete channel information (CI), where the instantaneous channel characteristics are assumed to be known. This is usually fulfilled on the receiver side. In the Frequency Division Duplex (FDD) case, where the transmitter knows only the average channel characteristics (unless there is a dedicated feedback channel), the most popular approach to exploit the partial channel knowledge is beamforming in the direction of the clusters. This implies that a single-cluster channel exhibits beamforming gain, but not diversity gain.

As analyzed in Chapter 3, the channel capacity is the central quantity in the consideration of MIMO systems. First an argument why the capacity should

depend only on the angle spread is presented, and then the restriction of that derivation is discussed.
Assume a flat-fading system where scattering processes lead to signal correlations at transmitter and receiver that are independent of each other. In that case, the channel transfer function matrix can be written as:

$$H = R_{Rx}^{1/2} G R_{Tx}^{1/2} \tag{4.26}$$

where G is a matrix with $i.i.d.$ complex Gaussian entries, and R_{Rx} and R_{Tx} are the correlation matrices at transmitter and receiver side respectively. If the correlation matrix depends only on the rms angle spread, then this holds also for the matrix H, and thus for the ergodic capacity as defined in equation (3.4) [10, and 15]:

$$C = E\left[\log_2\left(\left|I + \frac{SNR}{N_t} H H^{*T}\right|\right)\right] \quad \text{b/s/Hz} \tag{4.27}$$

where $|\cdot|$ is the matrix determinant, N_t is the number of transmit antennas, SNR is the mean receive signal-to-noise ratio (SNR), I is an identity matrix, and H^{*T} is the conjugate transpose of the normalized channel transfer matrix H.

From this derivation, it can be concluded that the necessary conditions for the capacity to depend only on the rms angle spread as follows:

- The conditions mentioned in the previous Section (flat fading, small rms angle spread, small maximum angle spread) must hold.

- The channel matrix must allow decomposition in the form of equation (4.26). This implies that the angular spreading at transmitter (Tx) and receiver (Rx) must be independent of each other. A similar condition is also derived in [57] for the limiting case of very large arrays.

- The considered channel must be a dense multipath channel;, i.e., the channel rank must be larger than the number of used antenna elements. If this is not the case, the number of MPCs with large energy (positive SNR) limits the capacity.

- The computation was done for the capacity of a single link MIMO system without co-channel interference.

In the following it assumes that the angular spectrum at the MS is uniform for all delays (this does not correspond to physical reality in the majority of cases, but is sufficient to point out the most essential aspects). Now three channel configurations that all have 5.8 (or 30) degree angle spread are compared:

- A single-cluster model with a Laplacian power azimuth spectrum (PA)S at the BS, with an angle spread of 5.8 and 30 degrees.

- Two equal-power specular sources, one at broadside, and one at 11.6 (or 60) degree angle

- Two scatterer clusters, each with a Laplacian PAS with 3 degree angle spread. These clusters have a mean angle of arrival of 0 and 10 (or 60) degrees respectively.

Fig. 4.11 shows the cumulative distribution functions of the capacity for 2*2, 4*4, and 8*8 antenna arrays. It can be noted that for a 2*2 array, the capacity is independent of the shape of the power azimuth spectrum (PAS), even for the relatively large angle spread of 30 degree. However, for a four-antenna array, this independence is fulfilled only for a small angle spread (5.8 degree), and for an 8*8 array, the capacity shows considerable variations even for a small angle spread. Similar results are found in [60].

This behavior of the channel can be explained intuitively. A channel with two specular sources can have at most two significant eigenvalues. Thus, even an increase in the number of antenna elements increases the capacity only by a small amount (by improving the SNR). Note also that for an 8*8 array, the capacities for the two angle spreads coincide almost completely. A single-cluster channel, on the other hand, shows a continuous increase in the effective degrees of freedom (EDF) as the angle spread increases. Since the number of possible propagation paths is much larger, the capacity also exhibits an increase with the number of antenna elements.

Not surprisingly, a two-cluster channel (with a fixed small but finite angle spread for each cluster) exhibits an intermediate behavior. The capacity does depend on the angle spread, but since the paths within a cluster are so strongly correlated, the effective degree of freedom is mainly determined by the number of clusters, i.e., two. Note also that for large antenna spacing and/or large cluster spread, the capacities of the one-cluster and the two-cluster model become similar (both reduce effectively to an $i.i.d.$ model), capacity [bit/s/Hz]

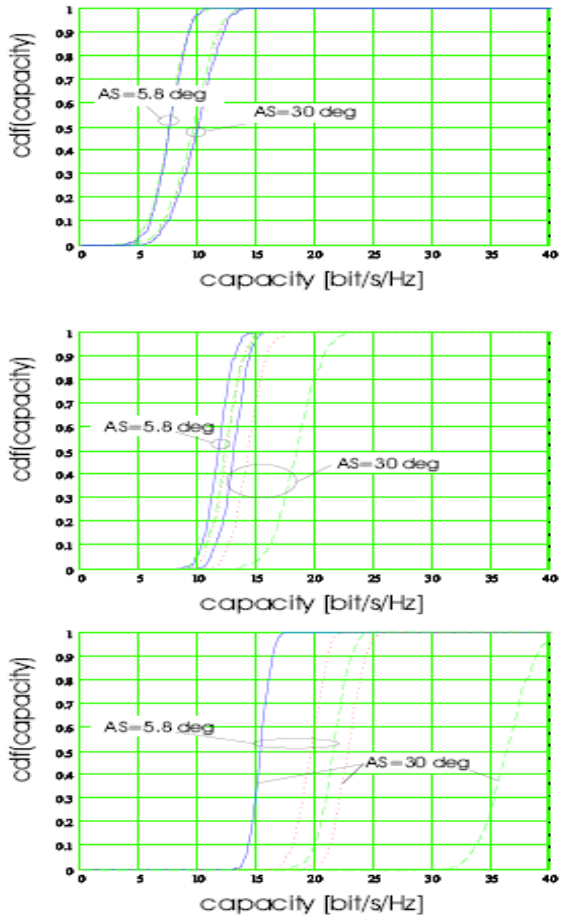

Figure 4.11 cdf of the capacity for 2x2 (top), 4x4 (middle), and 8x8 (bottom) antenna arrays and different channels. Two specular sources (solid), single cluster (dashed), two clusters (dotted).

cdf (capacity) while the model with two specular paths shows a much smaller capacity determined by the number of significant eigenvalues.

Next consider the capacity as a function of the signal-to-noise ratios for high values of the SNR. An approximate measure for the capacity is the number of eigenvalues of the channel matrix that is larger than the noise variance; this number in the following is called the *"effective rank"*. For the two path channel, the rank is always two as long as the SNR is larger than the power ratio of the two paths. Increasing the SNR more is not going to change the rank, only the mean SNR. For the one-cluster model, the number of effective eigenvalues is unity as long as the SNR is smaller than the ratio of the first two eigenvalues of the product HH^{*T} [89]. However, as the SNR is increased to large values, it will has as many eigenvalues as there are antenna elements.

Another important point is that a two-cluster model shows significantly larger delay dispersion than a single-cluster model. Simulations results in [60] demonstrate that this leads to a steeper slope of the capacity cdf as long as the

Chapter 4 Clustering Approach of Channel Model based on Geometry

This chapter describes the double bounce approach of the Geometrically Based Elliptical Channel Model, (GBSBEM) presented in Chapter 2 regarding to the scattering areas; unlike the previous geometrical models based only on single bounce reflection, it describes a model to represent the power delay angle profiles (PDAPs) by clusters plus background single bounce scatter components, i.e. the waves arrive at the receiver by double scattering at least. Instead of analyzing number of scatterers as uniformly distributed in the whole coverage area, the scatterers are grouped in “clusters”, obtaining a cluster of scatterers in order to get the parameters of interest, e.g., time of arrival (TOA), delay spread (DS), angle of arrival, (AOA), angle spread, (AS), and the power delay angle profiles (PDAPs). The effect of far scatterer clusters in outdoor urban environments and how these clusters affect the performance of MIMO systems is also analized. Part of this chapter has been published in [40].

4.1 Introduction

In Stochastic models, the average power delay angle profiles (PDAPs) and its statistical distributions is specified by the model, the statistical parameters employed in such models are usually estimated from extensive measurement campaigns or inferred from geometrical assumptions. Classical work has demonstrated that models must account for the physical geometry of scattering objects in the vicinity of the antenna of interest [6–9]. See also [17, and 19–22]

Several measurement campaigns done in different urban environments have been reported and the measurement results e.g. in [24, 29, 31, 36, 39, 41, 47, and 93], suggest that the received PDAPs are grouped into clusters, that correspond to objects in the surrounding; i.e., the waves have undergone additional scattering before being diffracted or reflected and arrived to the receiver; this result suggest that the single bounce assumption in the geometrical based channel models, e.g. [6–8, and 21], cannot represent the characteristic of the received PDAPs. In view of the above mentioned, a model to represent the

received PDAPs by clusters plus background single bounce scatter components is modeled, i.e. the waves arrive at the receiver by double scattering at least. Simulation results for one typical outdoor scenario for urban environments are also shown.

4.2 Description of the Approach

This Section introduces the description of the model proposed to represent the PDAPs. It is assumed that the mobile station is stationary or at very low speed and therefore the Doppler effects is ignored in the analysis. Multipath propagation can be well modeled with a baseband channel impulse response as [8]:

$$h_b(\tau,\theta) = \sum_{i=1}^{L} \alpha_i \delta(\tau - \tau_i)\delta(\theta - \theta_i), \tag{4.1}$$

where $|\alpha_i|$ is the magnitude of the i^{th} MPC, θ_i is the angle of arrival of the i^{th} MPC, and τ_i is the delay associated with that component. The parameter L is the total number of MPCs. Unlike the previous geometrical models based on single bounce reflection, it looks at each cluster separately to get a relationship of the cluster shape and size in the PDAPs and the geometrical description of the model. Since it is also geometrically based, the signal statistics depend on the position of the base station, (BS), (e.g. Transmitter Tx), the mobile station, (MS), (Receiver Rx), and the geometrical distribution of the clusters. It assumes that each cluster, (which include a number of scatterers), is stationary, in the far field.

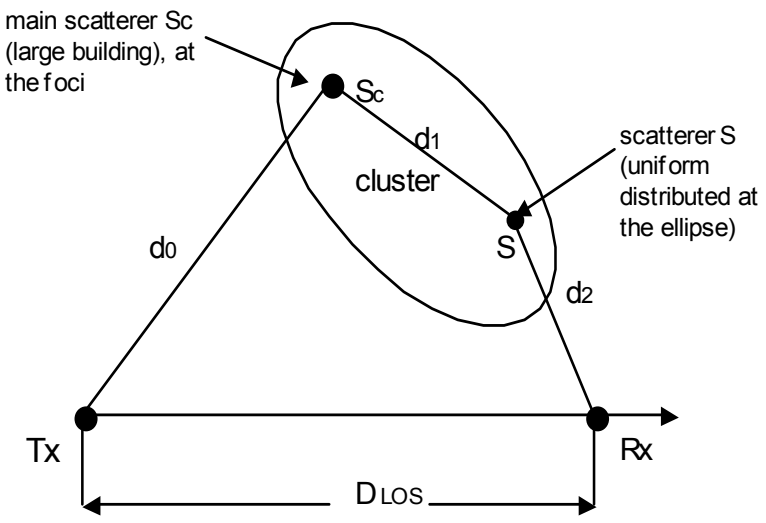

Figure 4.1 Geometrically based double bounce description (time domain).

Then the angle resolved impulse response of each cluster is defined as:

$$h_{(cluster)\,j}(\tau,\phi)=\sum_{i=1}^{L_j}\alpha_{ij}\delta(\phi-\phi_{ij})\delta(\tau-\tau_0-\tau_{ij}), \tag{4.2}$$

where, for each cluster: $|\alpha_i|$ is the magnitude of the i^{th} MPC, ϕ_i is the angle of arrival of the i^{th} MPC, τ_0 represent the extra delay due to the double scattering effect and τ_i is the delay associated with that component. The parameter L is the total number of MPCs. Then the total baseband channel impulse response is defined as:

$$h_{btotal}(\tau,\phi)=\sum_{j=1}^{J}h_{(cluster)\,j}(\tau,\phi), \tag{4.3}$$

where, the parameter J is the number of clusters. For the case of J=1, i.e., for one cluster condition is analyzed. From measurement campaigns reported in [24, 29, 36, 41, 47, and 93] in 90% of the cases, there are at most six clusters seen by the receiver, then it uses as a reference for the parameter J, i.e. $\mathrm{J}\leq\mathrm{L}$. Fig. 4.1 shows in more details the clustering approach regarding to the path length and time of arrival analysis.

Fig. 4.1 illustrates the geometry of the model. The following is assumed: the cluster region has an elliptical shape, and the main scatterer, (Sc), which is a large far away obstacle from the receiver, (e.g. a large building), is situated at one of the foci of the ellipse as shown in Fig. 4.1. Besides, there is line of sight (LOS) between the main scatterer and the receiver (Rx), and all scatterers (S) that belong to the same cluster are uniform distributed inside the cluster.

It is further assumed that the propagation takes place in the horizontal plane containing the receiver (Rx), in this case the mobile station (MS), and the transmitter (Tx), in this case the base station (BS) are placed in the same plane. D_{LOS} represent the Tx-Rx separation distance. From Fig. 4.1 the following geometrical relations can be obtained: the total path length (l), and the time of arrival (τ) of the ray resulting from the kth scatterer are given by

$$l = \|Tx - Sc\| + \|S - Sc\| + \|Rx - S\| = d_0 + d_1 + d_2, \tag{4.4}$$

and

$$\tau = \frac{l}{c}, \tag{4.5}$$

where, c represents the speed of light. Although the approach proposed is applicable for uplink (UL) as well, (just changing the position of the major axis of the cluster in the direction of the transmitter), the downlink (DL) environment is only analyzed. In the next Section the relationship between the cluster and the PDAPs is analyzed.

4.3 Analysis of the approach

In the previous Section, it was presented the description of the model based on the double scattering effect grouped into clusters. These clusters are present in the delay, as well as in the angle domain, and in general, cluster in the far field leads to a significant increase in the delay and angular dispersion. This Section presents the analysis of the approach based on the size and shape of each cluster and derives the relationship between a cluster and the PDAPs.

Fig. 4.2 shows the details regarding the angle of arrival of the MPCs of the cluster at the receiver (Rx). The line joining the main scatterer Sc and the receiver (Rx) makes an angle α with respect to the *x'-axis*, as it can be seen that the line path through the major axis of the ellipse, then, there is symmetry about that line.

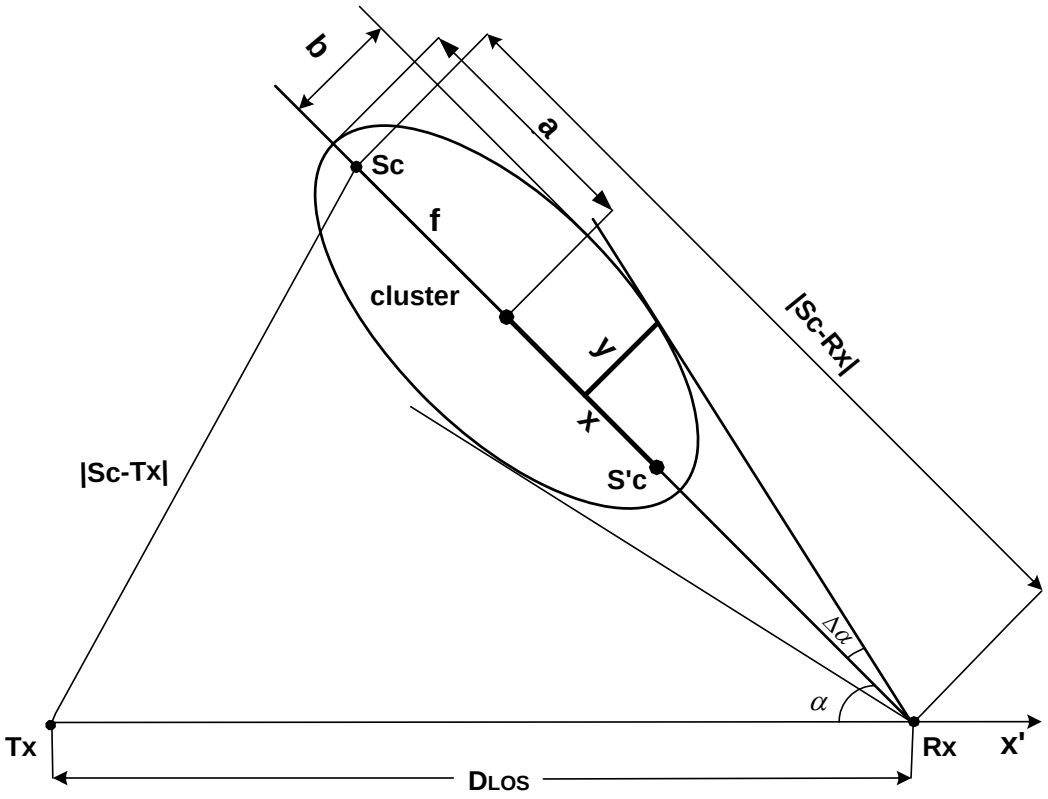

Figure 4.2 The geometry of the model (angle of arrival analysis).

The angle formed with respect to that line and one of the lines tangents to the ellipse is $\Delta\alpha$, i.e. the angle formed between the lines tangent to the ellipse is $2\Delta\alpha$. The ratio of the ellipse is also defined as:

$$r_{ab} = \frac{b}{a}, 0 < r_{ab} \leq 1, \tag{4.6}$$

i.e. the quotient from dividing the minor axis (b) by the major axis (a), (assuming $a>b$), the parameter *"a"* and the ratio r_{ab} define the size of each cluster.

The geometrical properties of the ellipse with center at origin and major axis along the *x-axis* is defined as follows

$$\frac{x^2}{a^2} + \frac{y^2}{b^2} = 1. \tag{4.7}$$

It is well-known that the foci is defined by $f = (a^2 - b^2)^{1/2}$, and f can be expressed in function of the elliptical ratio r_{ab} described earlier as follow

$$f = a\sqrt{1 - r_{ab}^2} \tag{4.8}$$

For any pair (x, y) of the ellipse described in Fig. 4.2, for a fixed given value of *"a"* the angle $\Delta\alpha_{xy}$ is

$$\Delta\alpha_{xy} = \arctan\frac{y}{|Sc - Rx| - f - x} \tag{4.9}$$

Equation (4.9) is valid for the case when the separation distance between the cluster and the receiver (Rx) is referred to the focus of the ellipse as Sc, which is at larger distance from the receiver, as illustrated in Fig. 4.2. The analysis when it uses as a reference the other focus of the ellipse, i.e. S′c, (the one that is closer to the receiver (Rx)) is presented later in this Section. The last case is useful when it has channel parameters with large excess delay and *rms* delay spread respectively, that can be found in urban scenarios for Non Line-Of-Sight (NLOS) as found in [29, 36, and 47], where the receiver is close to a large open square.

To obtain the maximum angle of the cluster, defined by $\Delta\alpha$ and illustrated in Fig. 4.2, it takes the derivative of equation (4.9) and equating to zero the following expression is obtained

$$\Delta\alpha = \arctan\left(\frac{r_{ab}\ a}{\sqrt{\left(|Sc - Rx| - f\right)^2 - a^2}}\right) \tag{4.10}$$

Based on the geometrical assumptions, the following relationship between the PDAP and the cluster is inferred and deduced from Fig. 4.2. The elliptical shape obtained in the PDAP from each cluster, and illustrated in Fig. 4.3, is verified with a numerical example in the next Section.

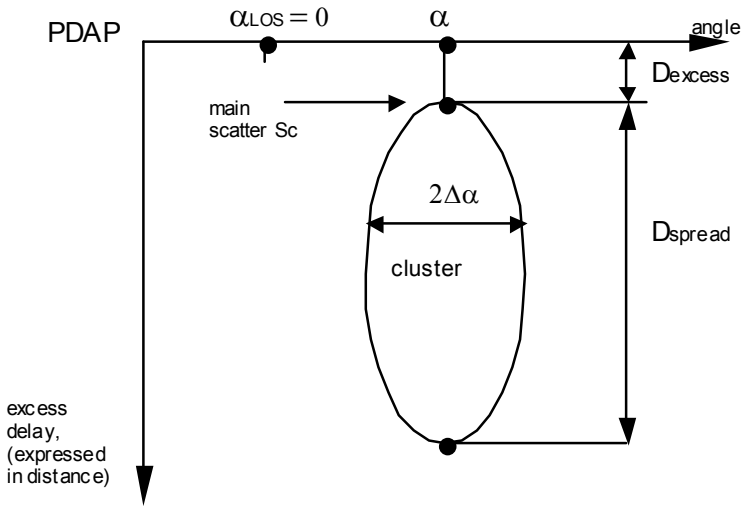

Figure 4.3 Relationship between the power delay angle profile (PDAP) and the cluster.

In Fig. 4.3, α represents the angle of arrival and $2\Delta\alpha$, represents the angle spread calculated from equation (4.10) and by the property of symmetry. The excess delay and the delay spread (both expressed in terms of distance) are represented by the following expressions deduced from Fig. 4.2:

$$D_{excess} = |Tx - Sc| + |Sc - Rx| - D_{los}, \tag{4.11}$$

$$D_{spread} = 2a\left(1 - \sqrt{1 - r_{ab}^2}\right), \tag{4.12}$$

where, equations (4.11) and (4.12), represent the excess delay and the delay spread respectively, both expressed in terms of distance.

In order to demonstrate the applicability of the proposed channel model described in Section 4.2, the position and shape of each cluster can be determined through the extraction of parameters from the PDAPs (that should be obtained from measurement campaigns): D_{excess}, α, $\Delta\alpha$, and D_{spread}, as shown in Fig. 4.3.

The position of each cluster depends on the parameters D_{excess} and α. For a fix value of each excess delay τ corresponds to a certain ellipse, which is focused on transmitter (Tx) and receiver (Rx), whereas, the angle α, is associated with a certain DOA. See [6–8, 21, and 22]. The foci, (f_{TR}), the major axis (a_{TR}) and the

minor axis (b_{TR}) of this ellipse can be defined in function of D_{LOS} and D_{excess} as follows:

$$f_{TR} = \frac{D_{los}}{2}, \tag{4.13}$$

$$a_{TR} = \frac{D_{excess}}{2} + f_{TR}, \tag{4.14}$$

$$b_{TR} = \sqrt{a^2 - f_{TR}^2}, \tag{4.15}$$

Then, the position of the cluster is obtained from equations (4.13)-(4.15) transformed into Cartesian coordinates [21]:

$$x_{Sc} = a_{TR}\left(\frac{f_{TR} - a_{TR}\cos(\alpha)}{a_{TR} - f_{TR}\cos(\alpha)}\right), \tag{4.16}$$

$$y_{Sc} = \frac{b_{TR}^2 \sin(\alpha)}{a_{TR} - f_{TR}\cos(\alpha)} \tag{4.17}$$

The size of each cluster depends on the parameters $\Delta\alpha$ and D_{spread}. As stated at the beginning of this Section the size of the cluster is defined by the parameters *"a"*, (the major axis of the ellipse), and the ratio of the ellipse *"r_{ab}"*.

Then, using equations (4.10) and (4.12) and rearranging the equations in function of a and r_{ab} the following system of nonlinear equation is obtained:

$$\begin{cases} a^2\left(1+\tan^2(\Delta\alpha)\right)r_{ab}^2 + 2a\tan^2(\Delta\alpha)\left(\left|Sc-Rx\right|\right)\sqrt{1-r_{ab}^2} - \tan^2(\Delta\alpha)\left(\left|Sc-Rx\right|^2\right) = 0 \\ \\ r_{ab} = \sqrt{\dfrac{D_{spread}}{a} - \dfrac{\left(D_{spread}\right)^2}{4a^2}}, \end{cases} \tag{4.18}$$

the shape of each cluster now is found by solving this system of equations. Due to the nonlinearity of the system, its solution can also be verified iteratively.

$$a = \frac{1}{4}\frac{4D_{spread}\tan^2(\Delta\alpha)(\left|Sc-Rx\right|) + \left(D_{spread}\right)^2\tan^2(\Delta\alpha) + 4\tan^2(\Delta\alpha)(\left|Sc-Rx\right|)^2 + \left(D_{spread}\right)^2}{2\tan^2(\Delta\alpha)(\left|Sc-Rx\right|) + D_{spread} + D_{spread}\tan^2(\Delta\alpha)} \tag{4.19}$$

$$r_{ab} = \left(\sqrt{\frac{\left(2\tan^2(\Delta\alpha)\left(\left|Sc-Rx\right|\right) + D_{spread} + D_{spread}\tan^2(\Delta\alpha)\right)\left(D_{spread} + 2\left(\left|Sc-Rx\right|\right)\right)D_{spread}\tan^2(\Delta\alpha)\left(\left|Sc-Rx\right|\right)}{\left(4D_{spread}\tan^2(\Delta\alpha)\left(\left|Sc-Rx\right|\right) + \left(D_{spread}\right)^2\tan^2(\Delta\alpha) + 4\tan^2(\Delta\alpha)\left(\left|Sc-Rx\right|\right)^2 + \left(D_{spread}\right)^2\right)^2}}\right)2\sqrt{2}. \tag{4.20}$$

The expressions in (4.19) and (4.20) are the solution of the system of equations given in (4.18) for *"a"* and *"r_{ab}"* respectively.

In a similar way, the clustering approach is analyzed for the case when the separation distance between the cluster and the receiver (Rx) is referred to the other focus of the ellipse ($S'c$) that is closer to the receiver (Rx) as illustrated in Fig. 4.2. The analysis is as follows:

Using the same approach as before, but taken into account the other focus of the ellipse, i.e. (S′c), for any pair (x, y) of the ellipse described in Fig. 4.2, the angle $\Delta\alpha_{xy}$ is

$$\Delta\alpha_{xy} = \arctan\frac{y}{\left|Sc-Rx\right| + f - x} \tag{4.21}$$

Then in this case, (as in the first case), to obtain the maximum angle of the cluster, defined by $\Delta\alpha$ and illustrated in Fig. 4.2, taking the derivative of equation (4.21) and equating to zero the following expression is obtained

$$\Delta\alpha = \arctan\left(\frac{r_{ab}\ a}{\sqrt{\left(\left|Sc-Rx\right|+f\right)^2-a^2}}\right) \tag{4.22}$$

As in the analysis for the first case, in Fig. 4.3, α represents the angle of arrival and $2\Delta\alpha$, represents the angle spread calculated now from equation (4.21) and by the property of symmetry. The excess delay and the delay spread (both expressed in terms of distance) are represented by the following expressions deduced from the same Fig. 4.2:

$$D_{excess} = \left|Tx-Sc\right|+\left|Sc-Rx\right|-D_{los}, \tag{4.23}$$

$$D_{spread} = 2a\left(1+\sqrt{1-r_{ab}^2}\right), \tag{4.24}$$

where, for this case equations (4.23) and (4.24), represent the excess delay and the delay spread respectively, both expressed in terms of distance.

Then, (as the previous case), using equations (4.22) and (4.24) and rearranging the equations in function of a and r_{ab} the following system of nonlinear equations is obtained:

$$\begin{cases} a^2\left(1+\tan^2(\Delta\alpha)\right)r_{ab}^2-2a\tan^2(\Delta\alpha)\left(\left|Sc-Rx\right|\right)\sqrt{1-r_{ab}^2}-\tan^2(\Delta\alpha)\left(\left|Sc-Rx\right|^2\right)=0 \\ r_{ab}=\sqrt{\dfrac{D_{spread}}{a}-\dfrac{\left(D_{spread}\right)^2}{4a^2}}, \end{cases} \tag{4.25}$$

Note that the system of equations in (4.25) is similar to the system of equations in (4.18), they only differ in the sign of the second term of the first equation, note also that the second equation of the systems in (4.18) and (4.25) is the same,

due to the equations (4.12) and (4.24) are very similar, from which are deduced the second equations of the systems (4.18) and (4.25), respectively. The shape of each cluster now is found by solving the system of equations in (4.25). Due to the nonlinearity of the system, the solution is also verified iteratively. The next Section illustrates a numerical example to show the application of the approach, for the cases analyzed in this Section.

4.4 Numerical Examples

This Section illustrates through numerical examples the application of the approach described in the previous section. Data are generated according to the model defined by equation (4.3), where only direction of arrival (DOA) and time of arrival (TOA) are considered (the Doppler effect has been neglected). A group of five clusters of $\mathrm{L} = 100$ scatterers uniformly distributed inside the clusters is considered, the parameters are shown in Table 4.1.

Fig. 4.4 shows the localization and boundaries of the generated group of clusters with the elliptical shape and sizes according to the parameters of Table 4.1. Then using equations (4.10)–(4.12), and (4.22)–(4.24) respectively, the excess delay (D_{excess}), delay spread (D_{spread}), angle of arrival (α), and angle spread ($2\Delta\alpha$) are obtained. All these parameters are summarized in Table 4.2.

Fig. 4.5 shows the PDAPs for each cluster, obtained from the set of parameters defined in Table 4.1. As shown in Fig. 4.4, different shape and size of clusters found in the PDAPs from measurement campaigns published in the literature can be described.

Table 3.1 Parameters of the five clusters defined by the (x,y) position, main radius (a) and the ratio (b/a).

***Tx-Rx* and No. Clusters (*Sc*)**	**x-y position [m]**		**Main radius *a* [m]**	**Ratio $r_{ab} = b/a$**
	x	**y**		
Tx (BS)	0	0	-	-
Rx (MS)	600	0	-	-
Sc 1	400	100	50	1
Sc 2	600	100	40	0.4
Sc 3	200	0	40	0.9
Sc 4	400	-100	60	0.7
Sc 5	600	-150	70	0.5

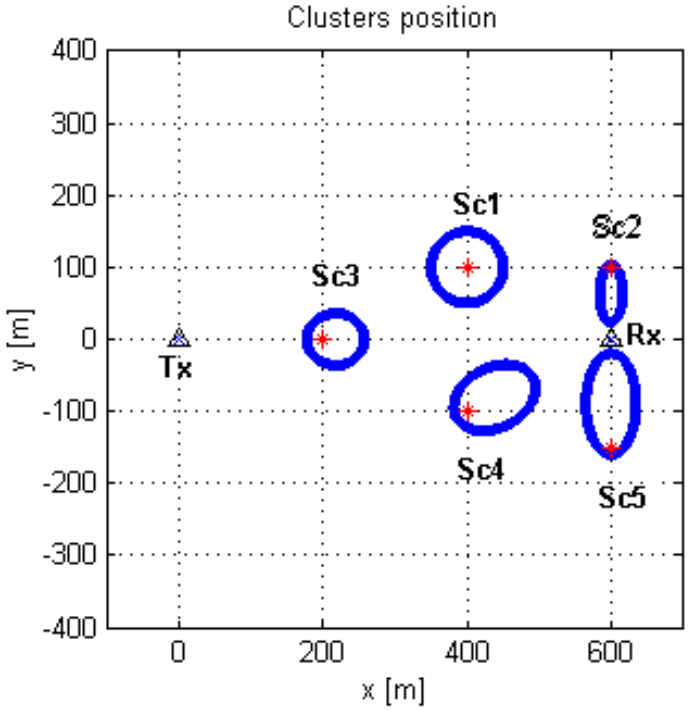

Figure 4.4 x-y cluster's position generated from Table 4.1.

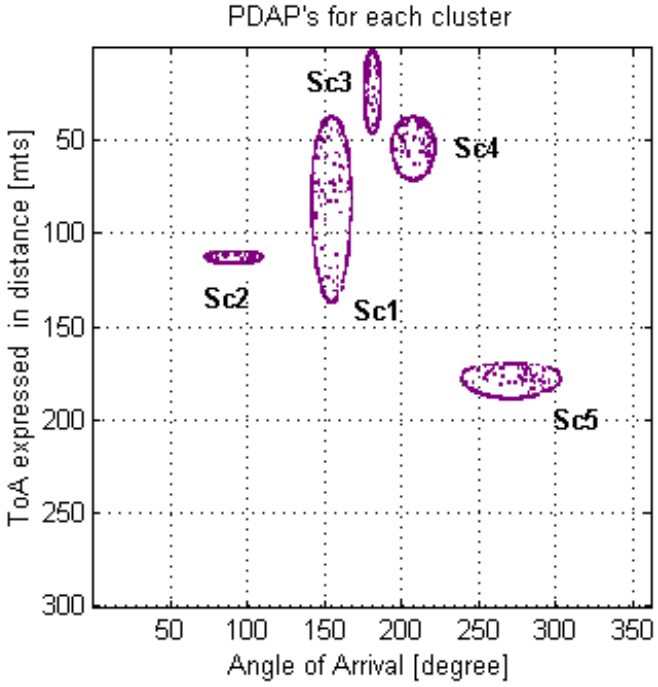

Figure 4.5 PDAPs: horizontal axis "α", vertical axis "delay" (expressed in terms of distance), and α_{LOS}=180 degrees.

Table 4.2 Results in angle (degree) and delay (expressed in distance) of the PDAPs for each cluster.

No. of Cluster	Dist. |Sc-Rx| [m]	Excess delay [m]	Delay spread [m]	Angle α (deg)	Angle spread $2\Delta\alpha$ (deg)
Sc 1	224	35.9	100	26.6	25.8
Sc 2	100	108.9	6.7	90	36.1
Sc 3	400	0	45 1	0	10.8
Sc 4	224	35.92	34.3	-26.6	27.7
Sc 5	150	168.5	18.8	-90	64.4

4.5 Delay Spread and Angle Spread Boundaries

In the previous Section, it was presented the analysis of the clustering approach of the model based on the double scattering effect grouped into clusters. These clusters are present in the delay, as well as in the angle domain, and in general, cluster in the far field leads to a significant increase in the delay and the angular dispersion. This Section presents the boundaries of the delay spread and angle spread based on the theoretical distributions in angle and time domain respectively, from a cluster of scatterers derived in the previous Section.

Boundaries of the delay spread and angle spread respectively, are shown for the two cases analyzed in the previous Section, i.e., when it is used as a reference the focus of the ellipse (Sc) that is a larger distance from the receiver and the focus of the ellipse ($S'c$) that is a closer distance to the receiver as well, as illustrated in Fig. 4.2.

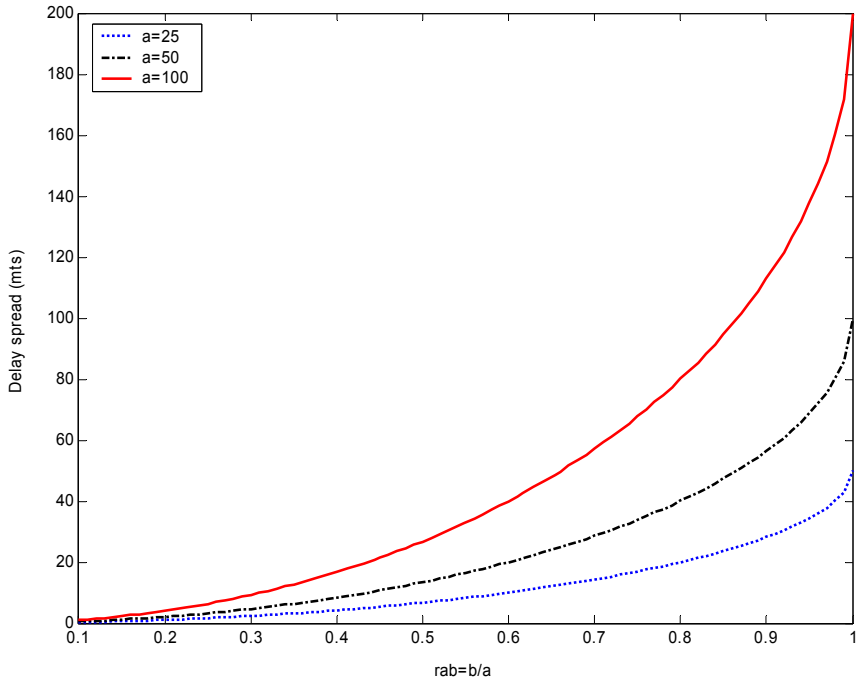

Figure 4.6 Boundaries plot of delay spread (DS), obtained from equation (4.12) for three different sizes of fixed values of "a".

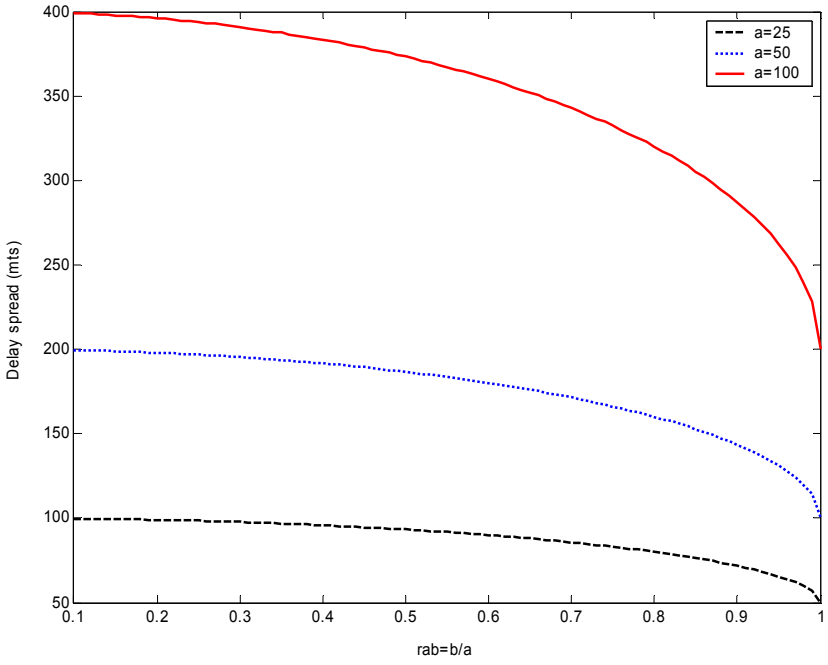

Figure 4.7 Boundaries plot of delay spread (DS), obtained from equation (4.24) for three different sizes of fixed values of "a".

Fig. 4.6 shows the boundaries of the delay spread (DS) for the case when it is used as a reference the focus of the ellipse (Sc) that is at larger distance from the receiver derived in equation (4.12). In this case for $r_{ab}=1$ (circular case) the maximum $D_{spread} = 2a$, *i.e.* $D_{spread} < 2a$.

Fig. 4.7 shows the boundaries of the delay spread (DS) for the case when it is used as a reference the focus of the ellipse ($S'c$) that is at closer distance from the receiver derived in equation (4.24). In this case for $r_{ab}=1$ (circular case) the minimum $D_{spread} = 2a$, *i.e.* $D_{spread} > 2a$.

As stated in the previous Section, this case is useful when the channel has parameters with large excess delay and rms delay spread respectively that can be found in urban scenarios for Non Line-Of-Sight (NLOS) as found in [29, 36, and 47], where the receiver is close to a large open square.

For the case of angle spread when it is used as reference the focus of the ellipse (Sc) that is larger distance from the receiver the boundaries are illustrated

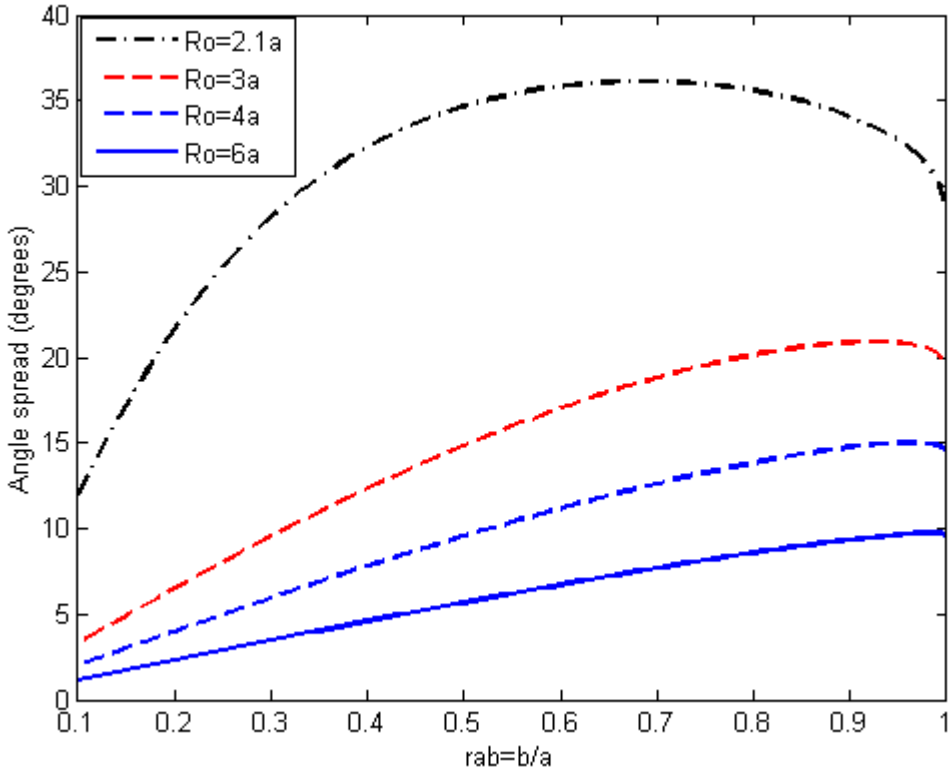

Figure 4.8 Boundaries plot of angle spread (AS), obtained form equation (4.10) for four different distances in function of size of fixed values of "a".

in Fig. 4.8. On the other hand when it is used as reference the focus of the ellipse (S′c) that is closer distance from the receiver the boundaries are illustrated in Fig. 4.9.

Fig. 4.8 shows the boundaries of the angle spread (AS) for the case when it is used as a reference the focus of the ellipse (Sc) that is at larger distance from the receiver derived in equation (3.10). The solid line in Fig. 4.8 is for the case when the cluster is in a closer distance to the receiver.

Fig. 4.9 shows the boundaries of the angle spread (AS) for the case when it is used as a reference the focus of the ellipse (S′c) that is at closer distance from the receiver derived in equation (3.22).

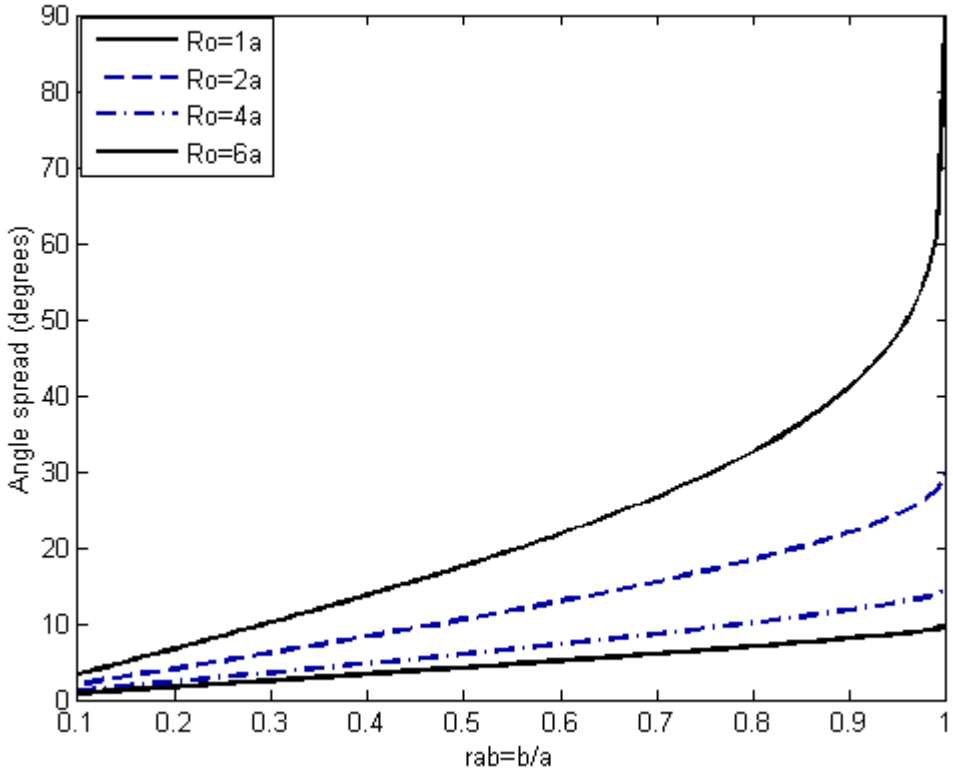

Figure 4.9 Boundaries plot of angle spread (AS) from equation (4.22) for four different distances *Ro* in function of the size of fixed values of *"a"*.

4.6 Effect of far scatterer clusters

In this Section, the clustering structures of wireless MIMO channels are considered, and the impact that multiple clusters have on the performance of MIMO systems. It is shown that multiple clusters frequently occur in urban environments. Then it proceeds to demonstrate that a channel with multiple scatterer clusters behaves differently than a channel with one cluster and the same rms angle spread. The differences are quantified in terms of correlation coefficients, information-theoretic capacity, and interference-suppression capabilities. This demonstrates the necessity of correctly taking into account the clustering structure.

First the physical channel modeling with and without far scatterer clusters is described. The basic form is also known as “local scatterer model” where all relevant scatterers are located around the mobile station (MS). The probability density function (PDF) of the scatterer location is often assumed to be uniform in a disk around the MS, Gaussian, or Rayleigh distributed. Alternatively, the power delay angular profile spectrum shows an exponential behavior in delay and Laplacian behavior in angle, around the (quasi) Line-Of-Sight component [31–33], see also [84–88, and 98].

Reference [29] suggested to additionally modeling far scatterer clusters that are far away from both the MS and the base station BS, see Fig. 4.10 for illustration. These far clusters represent e.g. high-rise buildings, in urban environments, mountains in rural environments, etc. While the local scatterers are always centered around the MS, the position of the far scatterers are fixed at an absolute position in space.

Actually, it is necessary to distinguish between two types of far scatterers. One is discrete reflectors, which gives rise essentially to a single, specular, MPC. Such a discrete reflector could be, e.g., a high-rise building with a smooth surface. The other type is a far scatterer cluster, where a group of high rise buildings or a mountain surface gives raise to several, closely spaced, MPCs. The distinction between specular reflectors and scatterer clusters is of special importance for the MIMO capacity.

For microcellular environments, the propagation processes leading to far scatterers are somewhat different. Waves get from the transmitter to the receiver via waveguiding. Different waveguides thus give rise to different clusters due to different propagation times and/or angles of incidence at the transmitter and receiver. A local cluster, representing over-the-rooftop propagation, is not necessarily present, especially if the BS antenna is significantly below the height of the surrounding rooftops [36 and 47].

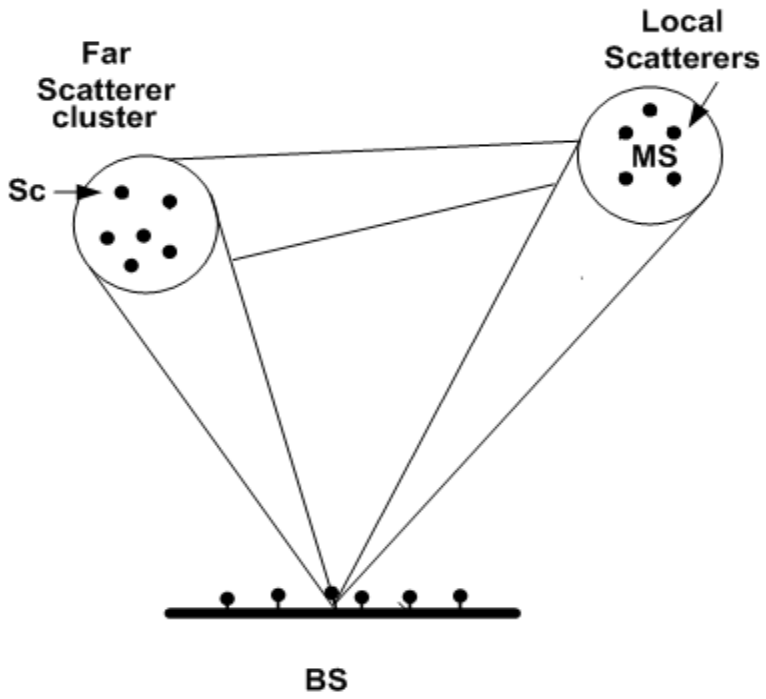

Figure 4.10 Principle of far scatterer clusters.

The identification of clusters in a measured of power delay angular profile (PDAPs) always involves a certain degree of arbitrariness. It either has to identify an (arbitrary) threshold of the arriving power that determines the boundary of a cluster, or it has to use “cluster identification algorithms”, which are well known from image processing problems, and which give different results according which algorithm is used. In many cases, a visual inspection, together with knowledge of the morphology of the environments and the possible propagation processes, gives the best results. Naturally, cluster boundaries can be defined better in a channel model.

4.6.1 Available Data of Measurement Campaigns

There have been several measurement campaigns that determine the angular spectrum of the signals arriving at the BS:

Reference [29] describes a measurement campaign in Frankfurt, Germany. This city has a strong resemblance to many American cities, with a high-rise city

center, surrounded by low-rise buildings. The paper clearly identifies many skyscrapers as “far scatterer clusters”.

Reference [24] reports measurements in Paris, France, and is notable in that the directions-of-arrival at the mobile station, but not the BS, are resolved. Also here, several locations are identified where a far scatterer cluster leads to increased delay dispersion. Reference [63], contains measurements in urban small cells in Mulhouse and Paris, France. The authors observe both cases where there is only a single cluster (with a very small angle spread), as well as cases with several clusters. In one “atypical” case, there was even hardly any energy from the direction of the mobile. However, the case with both a “local” cluster and “far clusters” is judged to be most typical.

Extensive measurements in Helsinki, Finland [47] have shown that for macrocellular situations (as well as micro and picocellular), several clusters are present. 2-3 clusters have to be taken into account to cover 75% of the energy in 90% of the cases.

On the other hand, reference [36] reports measurements in Stockholm, Sweden. This city is characterized by large areas without buildings (e.g., water), between the built-up areas. Again, multiple clusters have been observed.

Only the measurement campaign reported in [31 and 39], in Bristol, UK, and near Aalborg, Denmark, found the “multiple scatterer cluster” case to be the exception rather than the rule. This can also be explained in terms of the morphology of the measurements; those towns contain fewer irregular structures than the big cities mentioned earlier.

The importance of far scatterer clusters has been recognized also by different standardization bodies. Most notably, the use of far clusters has been recommended (for specific environments) both in the European COST259, which developed a generic spatial channel model that is suitable for a wide range of systems, and by the joint “spatial channel modeling” group of 3GPP and 3GPP2, the standardization organizations for third-generation cellular systems.

The incorporation of the far scatterers in the COST259 model is more realistic, and more complicated. The number of far scatterer clusters in macrocells is treated as a random variable. Far clusters appear and disappear in a kind of birth/death process, depending on whether a mobile station has Line-Of-Sight to the far scatterer cluster. The mean number of far scatterer clusters depends on the radio environment. For more details, please see references [4 and 5].

4.6.2 Impact of scatterer clusters on system performance

Having established in the previous subsection that far scatterers occur in practice, now turn to the question whether a far scatterer cluster can be represented by an "equivalent" increase in the *rms* angle spread of the cluster around the MS.

It is well-established in [58] that the spatial signature of an antenna array, and thus the correlation coefficient for signals at the elements of a smart antenna, is determined only by the *rms* angle spread, and not the exact shape of the PAS (power azimuth spectrum) if the angle spread, and the aperture of the array, is small. This was shown in [58] by using a truncated Taylor expansion of the steering vector. From this point of view, it is thus possible to replace a multiple-cluster model by a single cluster with the same *rms* angle spread.

However, it is important to keep in mind the following restrictions of the derivation (which are also mentioned or implied in [58]):

- This independence of the shape of the PAS is valid only for the flat-fading case. For the wideband case, multiple clusters give rise to higher frequency selectivity, and also show different angular spectra for different delays. Thus, different types of spatio-temporal Rake receivers work differently in a single cluster and multiple-cluster scenarios.

- The independence is only fulfilled if both the *rms* angle spread and the maximum angle spread are small. Thus, far-off components with small power cannot be represented correctly by increasing the spread of the local cluster.

- It is required that the antenna pattern is isotropic within the range of occurring angles of incidence. This is especially important when comparing different types of antenna elements, e.g., for different sectorizations of a cell.

- The independence is true only for complete channel information (CI), where the instantaneous channel characteristics are assumed to be known. This is usually fulfilled on the receiver side. In the Frequency Division Duplex (FDD) case, where the transmitter knows only the average channel characteristics (unless there is a dedicated feedback channel), the most popular approach to exploit the partial channel knowledge is beamforming in the direction of the clusters. This implies that a single-cluster channel exhibits beamforming gain, but not diversity gain.

As analyzed in Chapter 3, the channel capacity is the central quantity in the consideration of MIMO systems. First an argument why the capacity should

depend only on the angle spread is presented, and then the restriction of that derivation is discussed.
Assume a flat-fading system where scattering processes lead to signal correlations at transmitter and receiver that are independent of each other. In that case, the channel transfer function matrix can be written as:

$$H = R_{Rx}^{1/2} G R_{Tx}^{1/2} \tag{4.26}$$

where G is a matrix with $i.i.d.$ complex Gaussian entries, and R_{Rx} and R_{Tx} are the correlation matrices at transmitter and receiver side respectively. If the correlation matrix depends only on the rms angle spread, then this holds also for the matrix H, and thus for the ergodic capacity as defined in equation (3.4) [10, and 15]:

$$C = E\left[\log_2\left(\left|I + \frac{SNR}{N_t} H H^{*T}\right|\right)\right] \quad \text{b/s/Hz} \tag{4.27}$$

where $|\cdot|$ is the matrix determinant, N_t is the number of transmit antennas, SNR is the mean receive signal-to-noise ratio (SNR), I is an identity matrix, and H^{*T} is the conjugate transpose of the normalized channel transfer matrix H.

From this derivation, it can be concluded that the necessary conditions for the capacity to depend only on the rms angle spread as follows:

- The conditions mentioned in the previous Section (flat fading, small rms angle spread, small maximum angle spread) must hold.

- The channel matrix must allow decomposition in the form of equation (4.26). This implies that the angular spreading at transmitter (Tx) and receiver (Rx) must be independent of each other. A similar condition is also derived in [57] for the limiting case of very large arrays.

- The considered channel must be a dense multipath channel;, i.e., the channel rank must be larger than the number of used antenna elements. If this is not the case, the number of MPCs with large energy (positive SNR) limits the capacity.

- The computation was done for the capacity of a single link MIMO system without co-channel interference.

In the following it assumes that the angular spectrum at the MS is uniform for all delays (this does not correspond to physical reality in the majority of cases, but is sufficient to point out the most essential aspects). Now three channel configurations that all have 5.8 (or 30) degree angle spread are compared:

- A single-cluster model with a Laplacian power azimuth spectrum (PA)S at the BS, with an angle spread of 5.8 and 30 degrees.

- Two equal-power specular sources, one at broadside, and one at 11.6 (or 60) degree angle

- Two scatterer clusters, each with a Laplacian PAS with 3 degree angle spread. These clusters have a mean angle of arrival of 0 and 10 (or 60) degrees respectively.

Fig. 4.11 shows the cumulative distribution functions of the capacity for 2*2, 4*4, and 8*8 antenna arrays. It can be noted that for a 2*2 array, the capacity is independent of the shape of the power azimuth spectrum (PAS), even for the relatively large angle spread of 30 degree. However, for a four-antenna array, this independence is fulfilled only for a small angle spread (5.8 degree), and for an 8*8 array, the capacity shows considerable variations even for a small angle spread. Similar results are found in [60].

This behavior of the channel can be explained intuitively. A channel with two specular sources can have at most two significant eigenvalues. Thus, even an increase in the number of antenna elements increases the capacity only by a small amount (by improving the SNR). Note also that for an 8*8 array, the capacities for the two angle spreads coincide almost completely. A single-cluster channel, on the other hand, shows a continuous increase in the effective degrees of freedom (EDF) as the angle spread increases. Since the number of possible propagation paths is much larger, the capacity also exhibits an increase with the number of antenna elements.

Not surprisingly, a two-cluster channel (with a fixed small but finite angle spread for each cluster) exhibits an intermediate behavior. The capacity does depend on the angle spread, but since the paths within a cluster are so strongly correlated, the effective degree of freedom is mainly determined by the number of clusters, i.e., two. Note also that for large antenna spacing and/or large cluster spread, the capacities of the one-cluster and the two-cluster model become similar (both reduce effectively to an $i.i.d.$ model), capacity [bit/s/Hz]

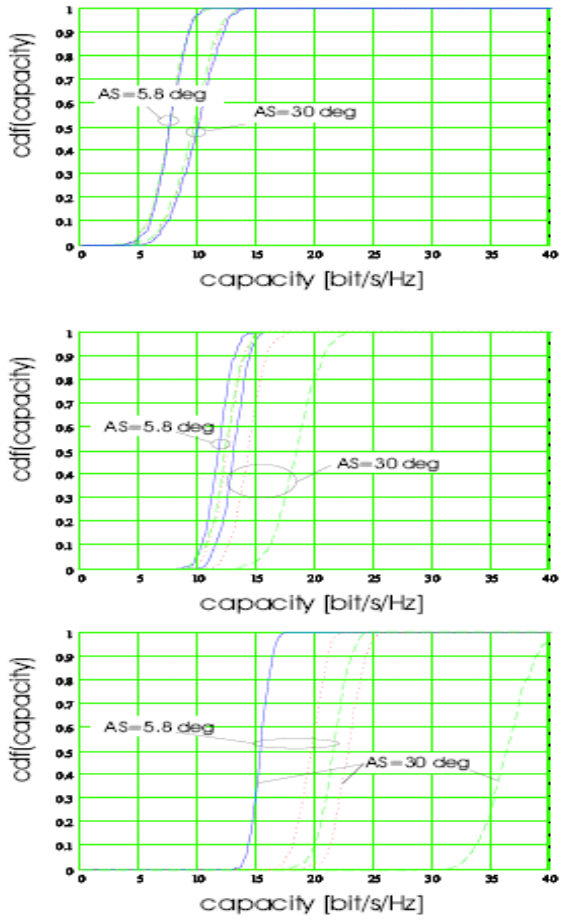

Figure 4.11 cdf of the capacity for 2x2 (top), 4x4 (middle), and 8x8 (bottom) antenna arrays and different channels. Two specular sources (solid), single cluster (dashed), two clusters (dotted).

cdf (capacity) while the model with two specular paths shows a much smaller capacity determined by the number of significant eigenvalues.

Next consider the capacity as a function of the signal-to-noise ratios for high values of the SNR. An approximate measure for the capacity is the number of eigenvalues of the channel matrix that is larger than the noise variance; this number in the following is called the *"effective rank"*. For the two path channel, the rank is always two as long as the SNR is larger than the power ratio of the two paths. Increasing the SNR more is not going to change the rank, only the mean SNR. For the one-cluster model, the number of effective eigenvalues is unity as long as the SNR is smaller than the ratio of the first two eigenvalues of the product HH^{*T} [89]. However, as the SNR is increased to large values, it will has as many eigenvalues as there are antenna elements.

Another important point is that a two-cluster model shows significantly larger delay dispersion than a single-cluster model. Simulations results in [60] demonstrate that this leads to a steeper slope of the capacity cdf as long as the

system bandwidth is larger than the excess delay between the two clusters. For systems with very large bandwidth (where the delay spread within a cluster is comparable to the system bandwidth) that difference vanishes.

Finally, the difference between the two clusters and the single-cluster model can also be explained in the framework of Ref. [61].

4.7 Conclusions

In this Chapter it has proposed a clustering approach to represent the power delay angle profiles (PDAPs) of the MPCs in urban environments, based on the double bounce approach. Unlike the previous geometrical models based only on single bounce reflection, a model to represent the PDAPs by clusters plus background single bounce scatter components was described, i.e. the waves arrive at the receiver by double scattering at least.

Closed-form expressions for the parameters employed for each cluster, have been derived, i.e. the angle spread (AS) and the time excess delay expressed in terms of distance. The values of the parameters were based on results published in the open literature from extensive measurement campaigns. In the next chapter analytical expressions are derived for the time delay and angle of arrival PDFs respectively, for the channel modeling based on the clustering approach described in this chapter.

The importance of far scatterer clusters for the correct modeling of MIMO channels has also been demonstrated. Far scatterer clusters frequently occur in urban environments and that they cannot be replaced by an “equivalent” increase of the angle spread of the scatterer cluster around the MS.

Chapter 5 Statistical Analysis of the Clustering Approach

The computer simulation approach with an emphasis on the propagation modeling for wireless channels for current and future communication systems is a powerful tool to assess the performance of systems without the need of building them. This chapter uses the clustering approach for geometry-based channel model proposed in the previous chapter, and employs it to derive analytical expressions for the angle of arrival (AOA) PDF and time of arrival (TOA) PDF (expressed in terms of distance) respectively of the multipath signal components. To evaluate the theoretical clusters PDFs in angular and time domain proposed, computer simulations of the geometry-based channel model propose in Chapter 4 are carried out. Then simulation results can be compared to experimental results published in the literature showing good agreement. Part of this chapter has been published in [87 and 88].

Introduction

For the analysis of channel propagation, design, and simulation of many practical mobile radio systems (e.g. third generation systems and beyond like the wideband-CDMA), is necessary to model channel models that provide the required spatial and temporal information necessary for studying such systems. Besides, these models must be easy to implement as well as to accomplish with practical important requirements such as simplicity and adaptivity [1–3]. Various models, such as empirical models and stochastic modeling based on geometry [1–8, 21–24, 27–31, and 70–73] are commonly used. Geometric models thus attempt to embed measurable fading metrics integrally into the propagation channel's idealized geometry, such that the geometric parameters would affect these various fading metrics in an inter-connected manner to reveal conceptually the channel's underlying fading dynamics.

Accurate and, if possible, simple propagation models would lead to an effective design and evaluation of modern communication systems, the physical channel

is characterized by multipath propagation. The differences in propagation delays among these multiple propagation paths causes delay spread (DS), which in turn induces *intersymbol interference* (ISI). The *rms* delay spread is one of the basic modeling parameters, since it is directly connected to the capacity of a specific communication system and gives a rough estimation on the complexity of a receiver [1].

Typically, several versions of the transmitted signal impinge on the receiving antenna from different directions because of multipaths. In fact, the directions from which the signals arrive, the direction of arrival (DOA) is an important property when characterizing the channel as well as designing receiver algorithms. For instance, the wireless channel changes very rapidly resulting from movement of both the users as well as changes in the surrounding environment. However, the main direction of arrival does not change nearly as rapidly [16]. Thus, characterization of the channel in terms of DOA is an interesting alternative to standard models.

Another important channel property that determines the quality of the communication link is the angle spread, among others, essentially determines the diversity gain by using an antenna array [7]. Also, it has been proposed to employ antenna arrays to reduce the co-channel interference by transmitting energy only in the direction of a specific user and essentially no energy in the directions of other users. In most situations, a certain angle spread occurs when a base station antenna receives the signal from a mobile user, where this spreading is due to multipaths in the environment. The spread is important for diversity schemes and also for the determination of the angle of arrival. It is an accepted model now that an angular spread occurs from a cluster of scatterers; where the total signal may come from several clusters; see [24, 29, 36, 41, 47 and 93–96]. As mentioned in [16], in order to understand the basic mechanism of propagation, a statistical approach is necessary.

5.2 Clustering of PDF of Angle of Arrival

This Section presents an approach to derive simple general formulas to model the probability density function (PDF) of the direction of arrival (DOA), between the receiver (Rx) and the far scatterer clusters. Assuming an elliptical shape of the clusters and bounded by a circular shape, the approach is described as follows: firstly, Fig 5.1 illustrates the details regarding the direction of arrival (DOA) of the MPCs of the cluster at the receiver (Rx).

The scatterer's density function is expressed with respect to the polar coordinates (r,θ). The polar coordinates are related to the rectangular coordinates via the following set of equations:

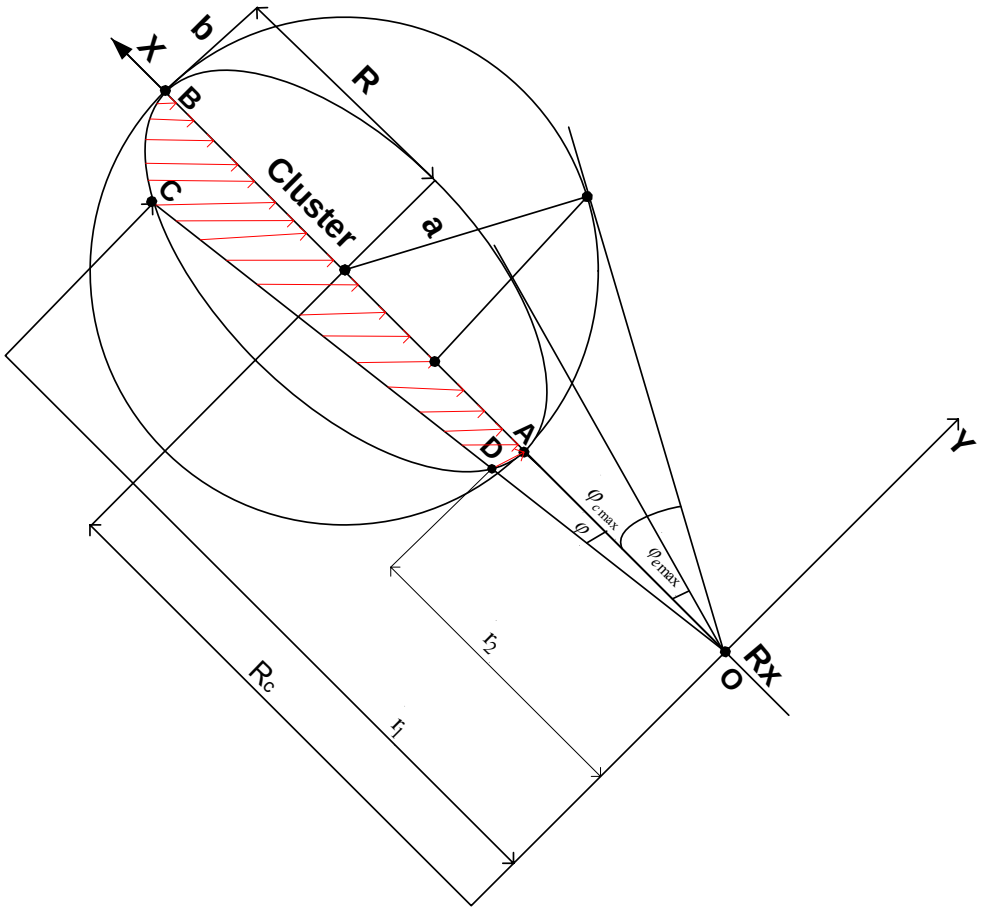

Figure 5.1 Geometry of the model for the calculation of the PDF of DOA.

$$
\begin{aligned}
r &= \sqrt{x^2 + y^2}, \\
\theta &= \arctan\left(\frac{y}{x}\right), \\
x &= r\cos(\theta), \\
y &= r\sin(\theta),
\end{aligned}
\tag{5.1}
$$

where, (x,y) denotes the position of the cluster. As shown in Fig. 5.1, the maximum angle of arrival for the circular case is given by.

$$\varphi_{c\max} = \arcsin\left(\frac{a}{R_c}\right), \tag{5.2}$$

where *"a"* is the radius of the circle and R_c is the distance between the center of the circle and the Receiver (Rx). Squeezing in the vertical dimension by a factor $r_{ab}=b/a$, $0 < r_{ab} \leq 1$, forms the ellipse inside the circle, i.e., the axes of the ellipse produced are major axis $a = R$ and minor axis $b = r_{ab}*R$.

From Fig. 5.1, it is possible to relate the new maximum angle of arrival of the ellipse with the maximum angle of arrival of the circle case by the following expression:

$$r_{ab}\tan(\varphi_{c\max}) = \tan(\varphi_{e\max}), \tag{5.3}$$

Using equations (5.2) and (5.3) a general expression of the maximum angle of arrival for both cases can be obtained as follows:

$$\varphi_{e\max} = \arctan\left(r_{ab}\tan\left(\arcsin\left(\frac{a}{R_c}\right)\right)\right), \tag{5.4}$$

Note from equation (5.4) that for the particular case for $r_{ab} = 1$, this equation becomes identically to equation (5.2), (circular case). Note also that the area defined by the *x-axis* and the line described by the points ODC as it illustrates in Fig. 5.1, defines an area ABCD (the shaded area) within the ellipse that is a function of the angle φ, within the range $0 < \varphi \leq \varphi_{emax}$, i.e., $A(\varphi)$. Then for a uniform distribution of the scatterers inside the cluster the cumulative density function (CDF) of the angle of arrival can be defined as follows:

$$F_{\varphi}(\varphi) = \frac{A(\varphi)}{\frac{1}{2}A_e} = \frac{2A(\varphi)}{ab\pi}, \tag{5.5}$$

where $A_e = ab\pi$ denotes the area of the ellipse. The equation of the ellipse defined in Fig. 5.1 is given by:

$$\frac{(x - R_c)}{a^2} + \frac{y^2}{b^2} = 1. \tag{5.6}$$

Transforming equation (5.6) into polar coordinates and using the relations defined in equation (5.1) and rearranging it, a second order equation is obtained:

$$r^2\left(\frac{\cos^2(\varphi)}{a^2} + \frac{\sin^2(\varphi)}{b^2}\right) - r\left(\frac{2R_c\cos(\varphi)}{a^2}\right) + \frac{R_c^2}{a^2} - 1 = 0 \tag{5.7}$$

Solving the equation (5.7) with respect to *"r"* the following expressions are obtained, corresponding to the two radii r_1 and r_2 shown in Fig. 5.1:

$$r_1 = \frac{R_c b^2\cos(\varphi) + \sqrt{b^4a^2\cos^2(\varphi) - b^2a^2\sin^2(\varphi)R_c^2 + b^2a^4\sin^2(\varphi)}}{b^2\cos^2(\varphi) + a^2\sin^2(\varphi)}, \tag{5.8}$$

and

$$r_2 = \frac{R_c b^2\cos(\varphi) - \sqrt{b^4a^2\cos^2(\varphi) - b^2a^2\sin^2(\varphi)R_c^2 + b^2a^4\sin^2(\varphi)}}{b^2\cos^2(\varphi) + a^2\sin^2(\varphi)}, \tag{5.9}$$

then, an area bounded in function of $r_1(\varphi)$ and $r_2(\varphi)$ in polar coordinates is given by the following expression:

$$A(\varphi) = \tfrac{1}{2}\int_0^{\varphi}\left(r_1^2(\xi) - r_2^2(\xi)\right)d\xi, \tag{5.10}$$

next, inserting equations (5.8) and (5.9) into equation (5.10), and the result into equation (5.5) the cumulative density function (CDF) of the angle of arrival (AOA) is obtained and can be defined by the following integral:

$$F_{\varphi}(\varphi) = \int_0^{\varphi}\frac{4bR_c\cos(\xi)\sqrt{-a^2b^2(-\cos^2(\xi)b^2 + R_c^2 - R_c^2\cos^2(\xi) - a^2 + a^2\cos^2(\xi))}}{a\pi(\cos^2(\xi)b^2 + \sin^2(\varphi)a^2)^2}, \tag{5.11}$$

finally, the probability density function (PDF) of the angle of arrival can be calculated by taking the derivative of the CDF with respect to φ, and solving it, the following expression is obtained:

$$f_{\varphi}(\varphi)=\frac{d}{d\varphi}F_{\varphi}(\varphi)=\begin{cases}\dfrac{4r_{ab}R_c\cos(\varphi)\sqrt{-a^2b^2(-\cos^2(\varphi)b^2+R_c^2-R_c^2\cos^2(\varphi)-a^2+a^2\cos^2(\varphi))}}{\pi(\cos^2(\varphi)b^2+\sin^2(\varphi)a^2)^2}, \\ for-\varphi_{\max}<0\le\varphi_{\max} \\ 0, elsewhere\end{cases} \tag{5.12}$$

Since the clusters are bounded by a circle when $r_{ab}=1$, i.e., for the case $b=a$, the direction of arrival (DOA) of the MPCs, (that conform the same cluster), at the receiver (Rx) is restricted to an angular region of $2\varphi_{cmax}$, as illustrated in Fig. 5.1.

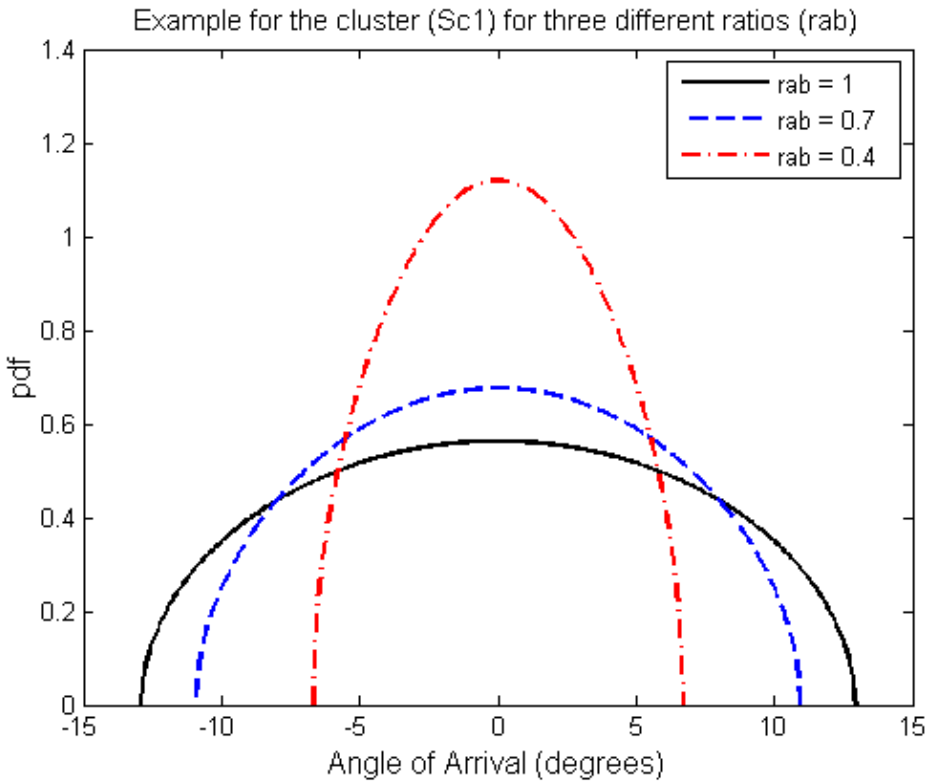

Figure 5.2 PDF of DOA for a cluster with three different ratios $r_{ab}=1$, $r_{ab}=0.7$, *and* $r_{ab}=0.4$ bounded by a circular shape cluster, using as a reference the center of the ellipse as shown in Fig. 5.1.

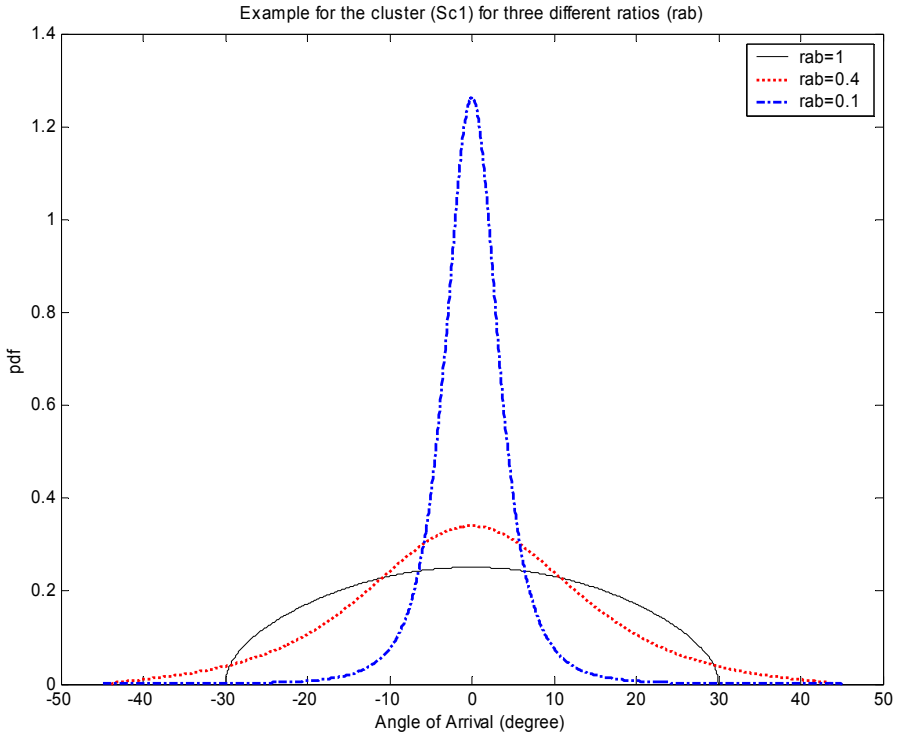

Figure 5.3 PDF of DOA for a cluster with three different ratios r_{ab}=1, r_{ab} = 0.7, *and* r_{ab}=0.1 bounded by a circular shape cluster, using as a reference the center of the ellipse as shown in Fig. 5.1.

Fig. 5.2 shows one example for the PDF of the direction of arrival (DOA), for two different shapes of clusters as follows: for the case of circular cluster (r_{ab}=1), and for two elliptical shape clusters for the cases r_{ab}=0.4 and r_{ab}=0.7, respectively. In a similar way, Fig. 5.3 shows another example, for the circular case (r_{ab}=1), and for two elliptical cases: r_{ab}=0.4, and r_{ab}=0.1 respectively. Note that from Fig. 5.2 for the circular case the DOA is maximum, as expected from equation (5.4) and Fig. 5.1. For the elliptical cases, note also that the DOA is decreasing as the ratio r_{ab} is decreasing. This is always valid when the circular cluster bound the ellipses, i.e. when r_{ab}=1, in other words, when the separation distance between the center of the cluster and the receiver (Rx) is fixed, as illustrated in Fig. 5.1.

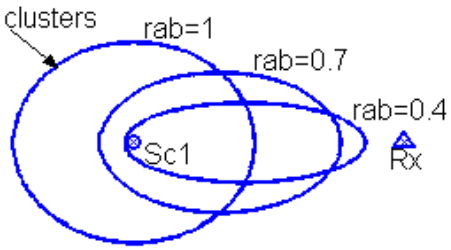

(a) Reference: focus of the ellipse at larger distance from Rx

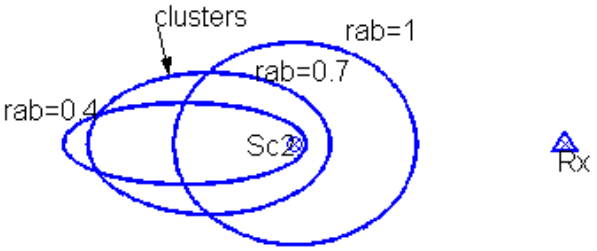

(b) Reference: focus of the ellipse at closer distance from Rx

Figure 5.4 Area of a cluster with three different ratios r_{ab}=1, r_{ab} = 0.7, *and* r_{ab}=0.4 using as a reference the separation distances between the cluster (*Sc*) and the receiver (Rx), the foci of the ellipses (a) Sc1 and (b) Sc2 respectively.

On the other hand, for the application it is also considered two cases based on the foci of the ellipses as illustrated in Fig. 5.4. One case is when it uses as a reference the distance between the cluster and receiver (Rx) the focus of the ellipse (Sc1) is situated at larger distance from the receiver as shown in Fig. 5.4(a). This case is taken from the simulations results in [47]. The other case is when it uses as a reference the focus of the ellipse (Sc2) situated at closer distance from the receiver as shown in Fig. 5.4(b).

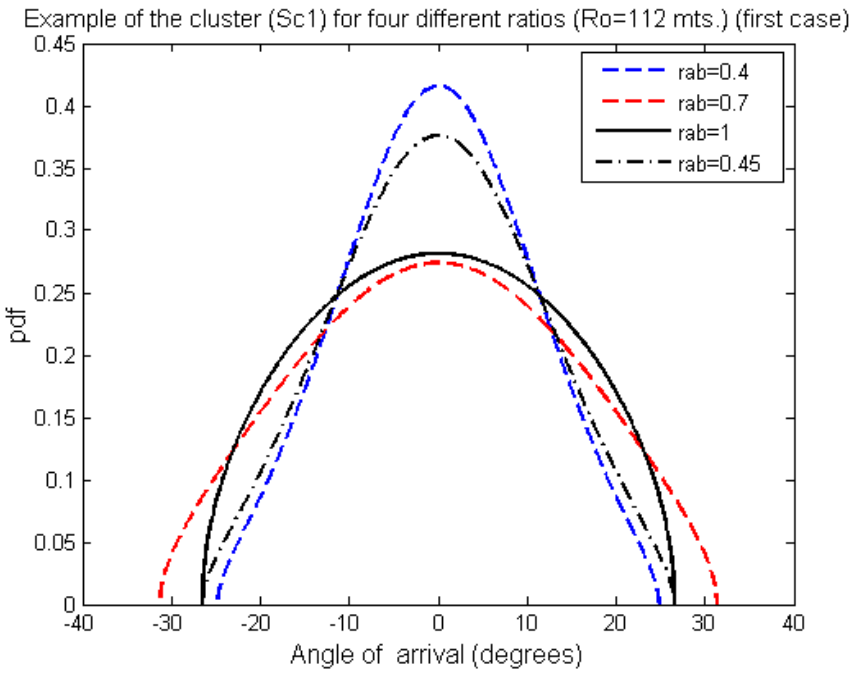

Figure 5.5 PDF of DOA for four different ratios using as a reference the separation distance between the cluster and receiver (Rx), the focus of the ellipse (Sc1) that is at larger distance to the receiver as illustrated in Fig. 5.3 (a).

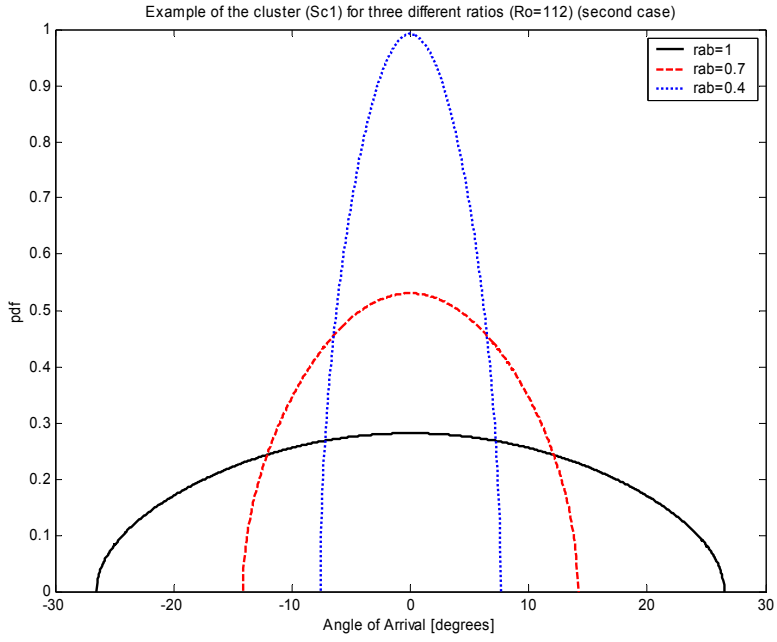

Figure 5.6 PDF of DOA for three different ratios using as a reference the separation distance between the cluster and receiver (Rx), the focus of the ellipse (Sc2) that is at closer distance to the receiver as illustrated in Fig. 5.3 (b).

Figures 5.5 and 5.6 show examples for the PDF of the direction of arrival (DOA), for two different shapes of clusters for the two cases illustrated in Fig. 5.4: (a) when it uses as a reference the distance between the cluster and receiver (Rx) the focus of the ellipse (Sc1) is situated at larger distance from the receiver as shown in Fig. 5.5. The other case (b) is when it uses as a reference the focus of the ellipse (Sc2) situated at closer distance from the receiver as shown in Fig. 5.6. Note that from Figures 5.5 and 5.6 respectively, for the circular case in both cases, the DOA is maximum, as expected from equation (5.4) and Fig. 5.1

5.3 Clustering of PDF of Time of Arrival

Deriving a general time of arrival (TOA) PDF for an arbitrary scatterer density function is more difficult. Integrating the joint TOA/AOA PDF over AOA, even for the case of a uniform scatterer density function, is nearly intractable and does not yield manageable results [28]. Then a similar approach likes in the previous section is used to derive a probability density function (PDF) of the time of arrival (TOA), between the receiver (Rx) and the far clusters ($P(\tau)$). The following is assumed: the cluster region has an elliptical shape because anything outside the ellipse has a large excess delay, i.e., the physical interpretation is that only MPCs with time delay smaller than the specified maximum time delay (bounded by the ellipse), are considered. Therefore, providing that the maximum delay is sufficiently large, nearly all of the power of the multipath signals of a physical channel will be accounted for by the model:

The area of the shaded region (see Fig. 5.7), is calculated integrating that region bounded by the cluster in order to get the cumulative distribution function (CDF) and then taking the derivative of the CDF the PDF is obtained. From Fig. 5.7 it can be observed that the maximum delay occurs when the ellipse just encloses all points of the cluster region.

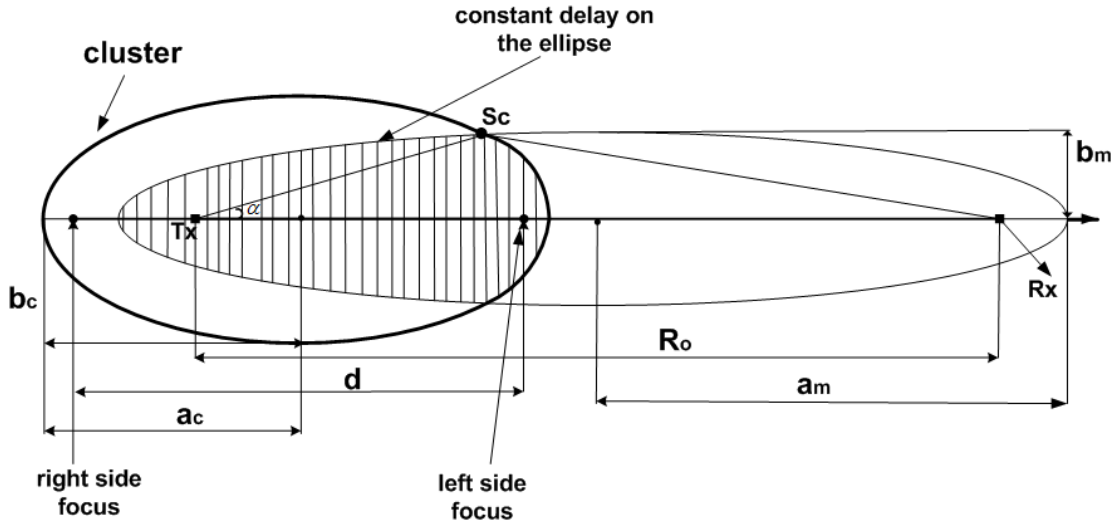

Figure 5.7 Geometry of the model for the calculation of the PDF of TOA.

As stated in [28 and 37–39], if the cluster region extends to infinity, the maximum delay correspondingly becomes infinity. The scatterer's density function is expressed with respect to the polar coordinates (r,θ). The polar coordinates are related to the rectangular coordinates via the same set of equations defined in equation 5.1, where, (x, y) denotes the position of the cluster. Then for a uniform distribution of the scatterers inside the cluster the CDF of the TOA can be defined as follows:

$$F_{\tau}(\tau) = \frac{A_{\tau}(\tau)}{A_c}, \tag{5.13}$$

where $A_c = a_c b_c \pi$ denotes the area of the elliptical cluster, a_c and b_c are the semimajor and semiminor axes values respectively as shown in Fig. 5.7. The ratio of the ellipse is also defined as a factor $r_{ab}=b/a,\ 0 < r_{ab} \leq 1$ *for* $a>b$. The equation of the bounding ellipse illustrated in Fig. 5.7 is defined as follows:

$$\frac{\left(x - R_0/2\right)^2}{a_m^2} + \frac{y^2}{b_m^2} = 1, \tag{5.14}$$

where the parameters a_m and b_m are the semimajor and semiminor axes values respectively, and f is the focus of the ellipse, which are given by [8]

$$
\begin{aligned}
a_m &= \frac{c\tau_m}{2}, \\
b_m &= \frac{1}{2}\sqrt{c^2\tau_m^2 - d^2}, \\
f &= \sqrt{a^2 - b^2} = a\sqrt{1 - r_{ab}^2},
\end{aligned}
\tag{5.15}
$$

where c is the speed of light, and τ_m is the maximum TOA which intersect with the cluster at the point Sc, located at angle α as shown in Fig. 5.7 Thus using equations (5.1) and (5.15) equation (5.14) can be rewritten as:

$$
\frac{\left(R_0/2 - r_m\cos\phi\right)^2}{a_m^2} + \frac{r_m^2\sin^2\phi}{b_m^2} = 1, \tag{5.16}
$$

then equation (5.16) can be rewritten for r_m as follows:

$$
r_m = \frac{4a_m^2 - R_0^2}{2(2a_m - R_0\cos\phi)} = \frac{c^2\tau_m{}^2 - R_0^2}{2(c\tau_m - R_0\cos\phi)}. \tag{5.17}
$$

In a similar way, the equation of the elliptical cluster region illustrated in Fig. 5.7 is defined as follows:

$$
\frac{\left(x - d_0\right)^2}{a_c^2} + \frac{y^2}{b_c^2} = 1, \tag{5.18}
$$

and, equation (5.18) can be rewritten as:

$$
\frac{\left(r_c\cos\phi\right)^2}{a_c^2} + \frac{r_c^2\sin^2\phi}{b_c^2} = 1, \tag{5.19}
$$

Then, equation (5.19) can be rewritten for r_c as follows:

$$
r_c = \frac{a_c b_c}{\sqrt{a_c^2\sin^2\phi + b_c^2\cos^2\phi}}, \tag{5.20}
$$

Thus calculating the area of the overlap between the bounding ellipse and the elliptical cluster $A_\tau(\tau)$, as follows:

$$A_\tau(\tau) = 2\int_0^{\alpha} \tfrac{1}{2} r_c^2(\phi) d\phi + 2\int_{\alpha}^{\pi} \tfrac{1}{2} r_m^2(\phi) d(\phi), \tag{5.21}$$

Then substituting equation (5.17) and equation (5.19) into to equation (5.21) the following expression is obtained

$$A_\tau(\tau) = \int_0^{\alpha} \left[\frac{a_c b_c}{a_c^2 \sin^2\phi + b_c^2 \cos^2\phi} \right]^2 d\phi + \int_{\alpha}^{\pi} \left[\frac{c^2\tau^2 - R_0^2}{2(c\tau - R_0 \cos\phi)} \right]^2 d\phi, \tag{5.22}$$

and solving for α, equation (5.22) an approximation of the CDF of the TOA is obtained:

$$\begin{aligned} A_\tau(\tau) &= a_c^2 r_{ab} \tan^{-1}\left(\frac{\tan\alpha}{r_{ab}}\right) + \frac{c^2\tau^2(e_\tau^2 - 1)}{4} \\ &\cdot \left[\frac{-\pi}{\sqrt{1-e_\tau^2}} + \frac{e_\tau^2 \sin\alpha}{1 - e_\tau \cos\alpha} + \frac{2}{\sqrt{1-e_\tau^2}} \tan^{-1}\left(\frac{\sqrt{1+e_\tau}\tan(\frac{\alpha}{2})}{\sqrt{1-e_\tau}} \right) \right], \end{aligned} \tag{5.23}$$

Where e_τ represents the eccentricity of the bounding ellipse corresponding to time delay τ defined as: $e_\tau = \frac{R_0}{c\tau}$.

Finally, the approximation of the CDF of TOA is obtained substituting equation (5.23) into equation (5.13), and then taking the derivative of the CDF of TOA, the deisired PDF of TOA is obtained.

Fig. 5.8 shows one example for the PDF of the time of arrival (TOA), for two different shape of clusters for the case of circular cluster (r_{ab}=1), and elliptical shape cluster for the case r_{ab}=0.8. Theses cases are taken from the simulations results in [88]. Note from Fig. 5.8 that for the circular case the time of arrival is maximum. For the elliptical case, note also from the same Fig. 5.8 that the time of arrival is decreasing as the ratio r_{ab} is decreasing. This is always valid for the elliptical cases when the circular cluster bound the ellipses, i.e. for r_{ab}=1. The delay spread is less than or equal $2a$ in this case it uses as a reference the focus of the ellipse that is at larger distance (left side) from the receiver (Rx) as illustrated in Fig. 5.4.

On the other hand, Fig. 5.8 shows one example of the time of arrival (TOA), for the case when it uses as a reference the focus of the ellipse that is at closer distance from the receiver (right side) as illustrated in Fig. 5.4. In this case the delay spread is greater than $2a$ and bounded by approximated value of $4a$. As in Fig. 5.7 for the elliptical case, note that the time of arrival is decreasing as the ratio r_{ab} is decreasing, and is maximum for $r_{ab}=1$. The plots in Figures 5.8 and 5.9 respectively, show that there is a high density of scatterers with relatively small delays.

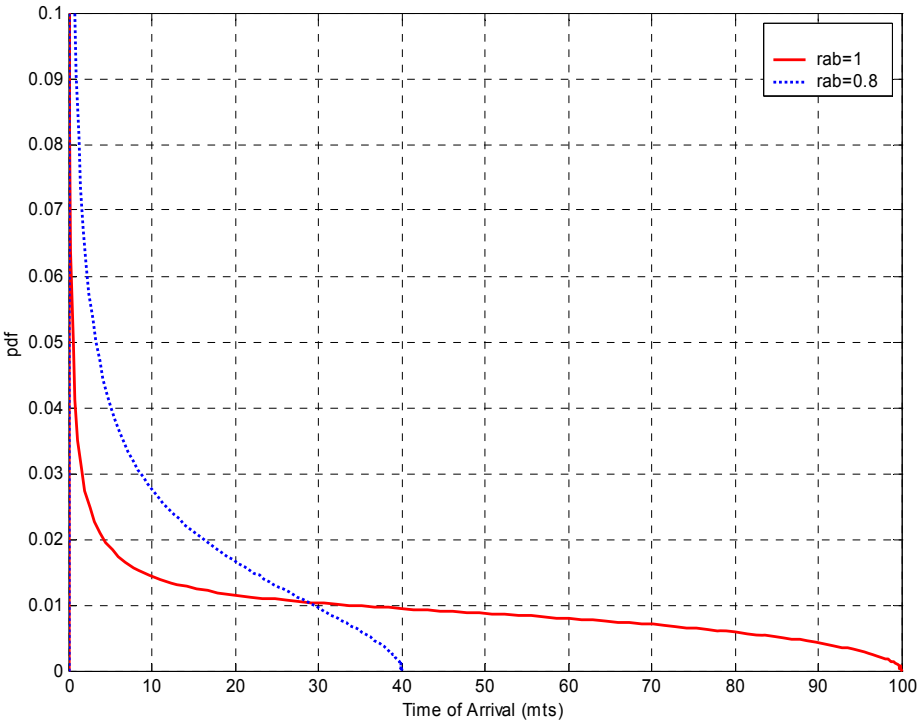

Figure 5.8 Example of PDF of TOA for a cluster with two different ratios $r_{ab}=1$, and $r_{ab}=0.8$ respectively, using as a reference the left side of the focus of the ellipse as shown in Fig. 5.4.

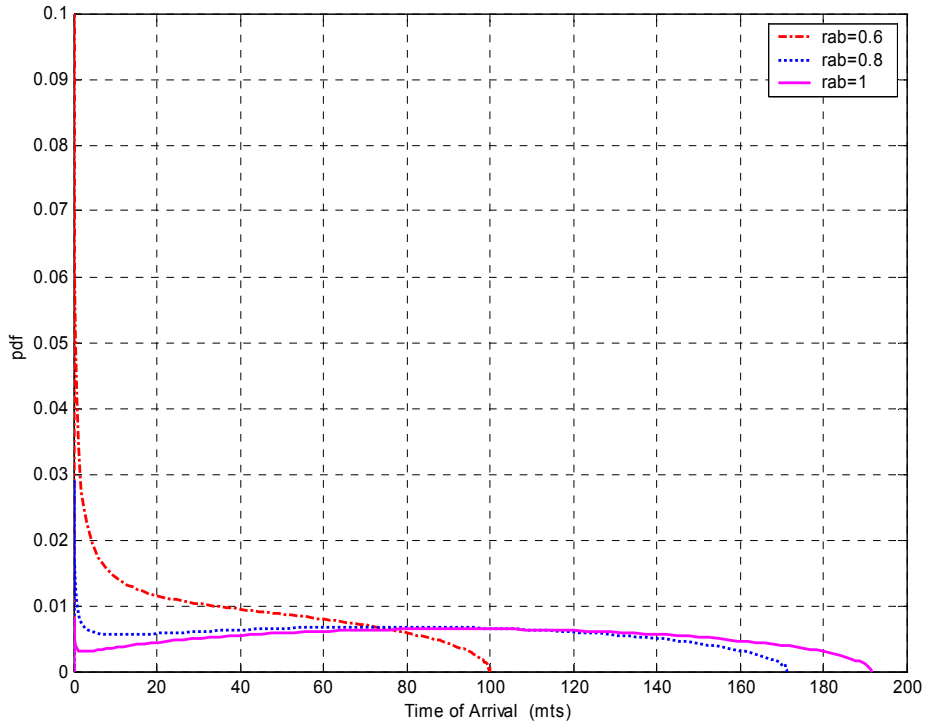

Figure 5.9 Example of PDF of TOA for a cluster with three different ratios r_{ab}=1, r_{ab} = 0.8, *and* r_{ab}=0.6 respectively, using as a reference the right side of the focus of the ellipse as shown in Fig. 5.4.

5.4 Numerical Results

In order to validate the theoretical PDFs, some numerical examples are used. The theoretical PDF for angle of arrival described in equation (5.12) is evaluated for a test case where the separation distance between the base station as (Tx), and the mobile unit as (Rx), is 600 meters, and the separation distance between the cluster and the mobile unit (Rx) is assumed 224 meters. The (x, y) position of two clusters at the same distance from the receiver (Rx) is showing the two cases analyzed in the previous Section as illustrated in Fig. 5.4, the results of the power delay angle profiles (PDAPs) obtained from the cluster's positions generated are presented in Fig. 5.10.

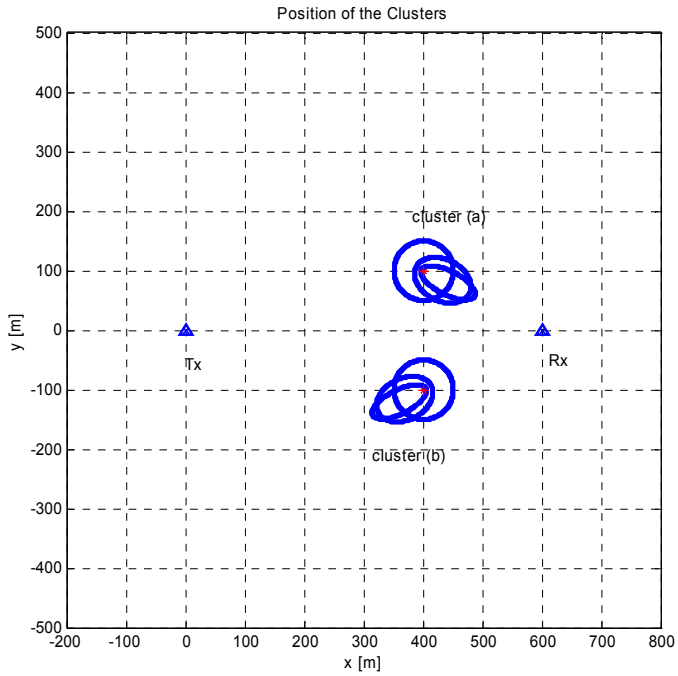

Figure 5.10 X-Y Position of two clusters for three different ratios: r_{ab}=0.4, r_{ab}=0.7, *and* r_{ab}=1 respectively.

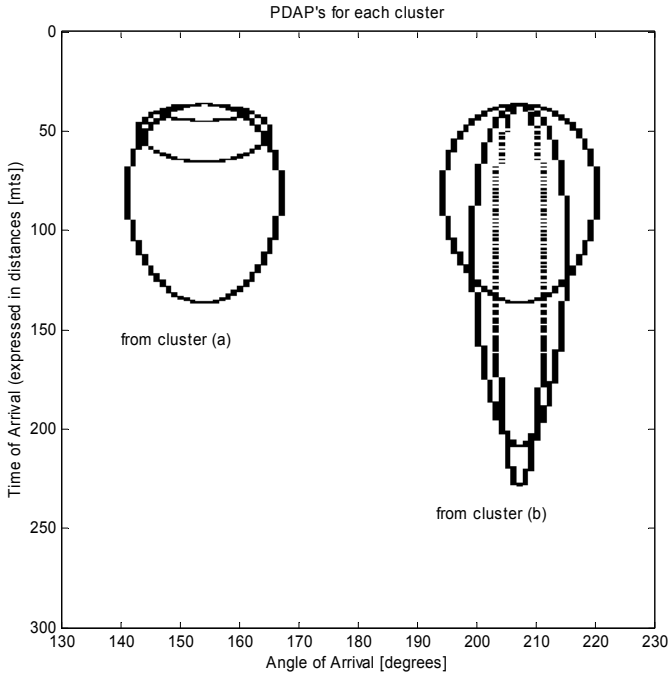

Figure 5.11 PDAPs: horizontal axis α, vertical axis delay expressed in meters, and α_{LOS}= 180 degrees.

5.5 Comparison with Experimental Results

Several experimental results are available to which is possible to compare the theory. In the indoor case, Chong et al. [41] have characterized the indoor wideband channel model to the angular domain through experimental results obtained by a wideband vector channel sounder together with an eight-element uniform linear array (ULA) receiver (Rx). MPCs parameters were estimated using a super-resolution frequency domain algorithm Space Alternating Generalised Expectation (FD-SAGE) and clusters were identified in the spatio-temporal domain by a nonparametric density estimation procedure. The clustering effect also gives rise to two classes of channel power density spectra PDS intercluster and intracluster PDS, which are shown to exhibit exponential and Laplacian functions in the delay and angular domain respectively.

In the outdoor case, Toeltsch et al. [47] used a wideband channel sounder together with a planar antenna array to determine the parameters of the incident waves. A super-resolution algorithm Unitary Estimation of Signal Parameters via Rotational Invariance Tecniques (U-ESPRIT) allows resolving individual MPCs in such clusters and hence enables a detailed statistical analysis of the propagation properties.
Comparisons to experimental results published in [47] are summarized in Tables 5.1, 5.3 and 5.5 respectively. These Tables presents the parameters of the clusters extracted from measurement campaign, i.e., the excess delay, delay spread (DS), (both in terms of distance), DOA, and angle spread (AS), (both in degrees). Then from these experimental results it uses the solution of the system of equations (4.18) from the channel modeling based on the clustering approach proposed in the previous chapter, in order to get the parameters *"a"* and *"r_{ab}"*, and from there obtain the position of each cluster and the separation distance between each cluster (Sc) and the receiver (Rx). These results are obtained numerically in order to compare the results obtained using the analytical tractable solution. The theoretical parameters obtained from Chapter 4 are also verified, the boundaries of the delay spread (DS) and angle spread (AS) plotted in Figures 4.6 and 4.7 for time domain and Figures 4.8 and 4.9 for angular domain respectively. The results obtained from Tables 5.1, 5.3, and 5.5 are summarized in Tables 5.2, 5.4, and 5.6 respectively.

Figures 5.12, 5.14, and 5.16 respectively, show the position of each cluster based on the measurements of the power delay angle profiles (PDAPs) published in [47]. Tables 5.2, 5.4, and 5.6 respectively, summarize the parameters using analytical tractable solution as derived in details in [40, 87, and 88] for the angular and time domain parameters respectively.

Table 5.1 Experimental results from [47] in angle (degrees) and delay (expressed in distance) of the PDAPs for each cluster.

No. of Cluster	Excess delay [m]	Delay spread [m]	Angle α (deg)	Angle spread $2\Delta\alpha$ (deg)
Sc 1	150	60	-8	25
Sc 2	45	60	-6	6
Sc 3	15	60	0	8
Sc 4	210	180	0	8

Figures 5.13, 5.15, and 5.17 respectively, show the boundaries of PDAPs for each cluster obtained from the set of parameters extracted from [47] and defined in Tables 5.1, 5.3, and 5.5 respectively. As shown in Figures 5.13, 5.15, and 5.15, respectively, describe different shapes and sizes of clusters found in the PDAPs from measurement campaigns published in the literature, as reported in [24, 29, 41, 47, and 93]. Comparison of theoretical with experimental results reported in the literature shows that the average number of clusters and MPCs distribution within a cluster is heavily dependent on the resolution of the parameter estimation algorithm. This also depends on the type of scenario, (indoor or outdoor); e.g., from experimental results for indoor scenarios, Chong et al. [41], and Yu et al. [93], they reported as most nine and five cluster respectively.

On the other hand, from experimental results in outdoor scenarios (including above, at, and below rooftop level of the base station locations), Toeltsch *et al*. [47] found at most four clusters. Furthermore, as stated in [41], the number of clusters and MPCs detected were also dependent on several others factors such as the Tx-Rx separation and location, the physical layout of the environment, as well as the dynamic range of the channel sounder. Furthermore, Table 5.1 indicates that within each cluster, the angular statistics is almost independent of the time delay. Fig. 5.13 shows the positions of the MPCs derived from [47] in the delay-angular domain. It can be seen that the MPCs arrive in several clusters.

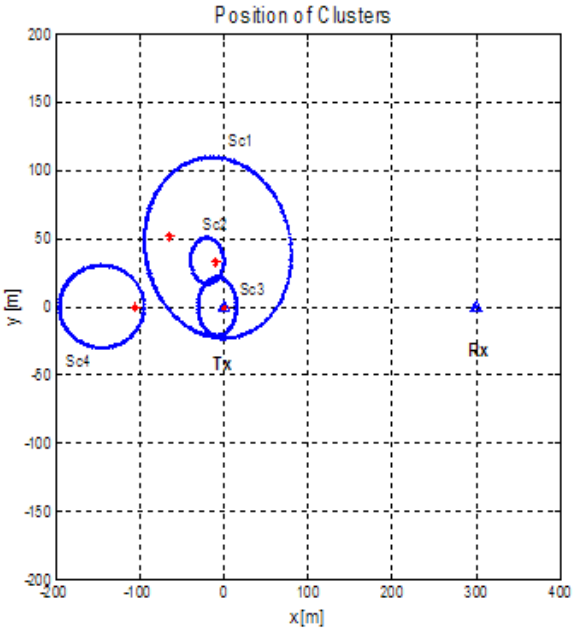

Figure 5.12 X-Y Cluster's position obtained using the experimental results PDAPs from [47].

Table 5.2 Parameters of the four clusters obtained from Table 5.1. The (x-y) position, main radius (a), and the ratio (b/a).

Tx-Rx and No. Clusters (Sc)	**x-y position [m]**		**Main radius a [m]**	**Dist. |Sc-Rx| [m]**	**Ratio $r_{ab} = b/a$**
	x	**y**			
Tx (BS)	0	0	–	–	–
Rx (MS)	300	0	–	–	–
Sc 1	–64.3	–51.2	87.6	367.8	0.75
Sc 2	–9.4	–32.5	19.7	311	0.85
Sc 3	–7.5	0	23	307.5	0.95
Sc 4	–105	0	50.3	405	0.6

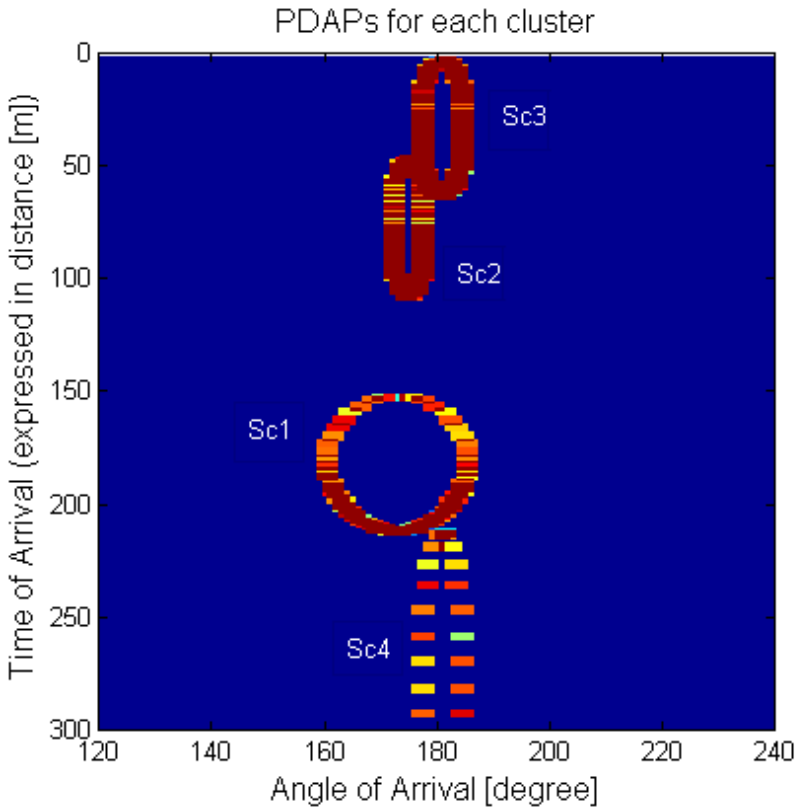

Figure 5.13 PDAPs: horizontal axis α, vertical axis delay expressed in meters, and α_{LOS}= 180 deg.

Table 5.3 Experimental results from [47] in angle (deg) and delay (expressed in distance) of the PDAPs for each cluster.

No. of Cluster	Excess delay [m]	Delay spread [m]	Angle α (deg)	Angle spread $2\Delta\alpha$ (deg)
Sc 1	15	90	-8	11
Sc 2	30	105	6	7
Sc 3	195	120	6	7

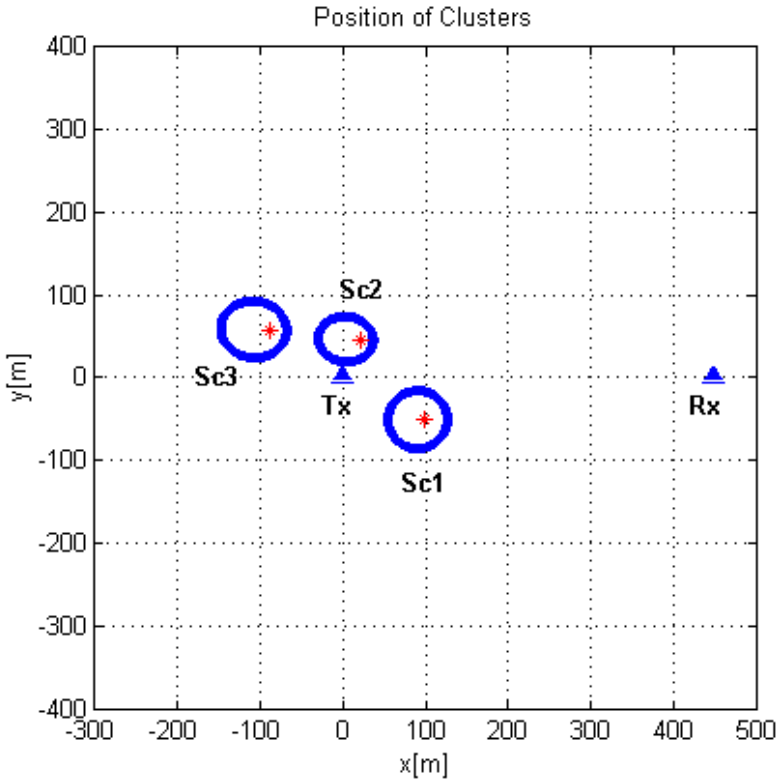

Figure 5.14 X-Y Cluster's position obtained using the experimental results PDAPs from [47].

Table 5.4 Parameters of the three clusters obtained from parameters of Table 5.3.

Tx-Rx and No. Clusters (Sc)	**x-y position [m]**		**Main radius a [m]**	**Dist. |Sc-Rx| [m]**	**Ratio $r_{ab} = b/a$**
	X	**y**			
Tx (BS)	0	0	-	-	-
Rx (MS)	450	0	-	-	-
Sc 1	99.3	-49.3	36	354	0.97
Sc 2	22.6	44	33.4	429.7	0.82
Sc 3	-87.7	56.5	39.8	540.7	0.86

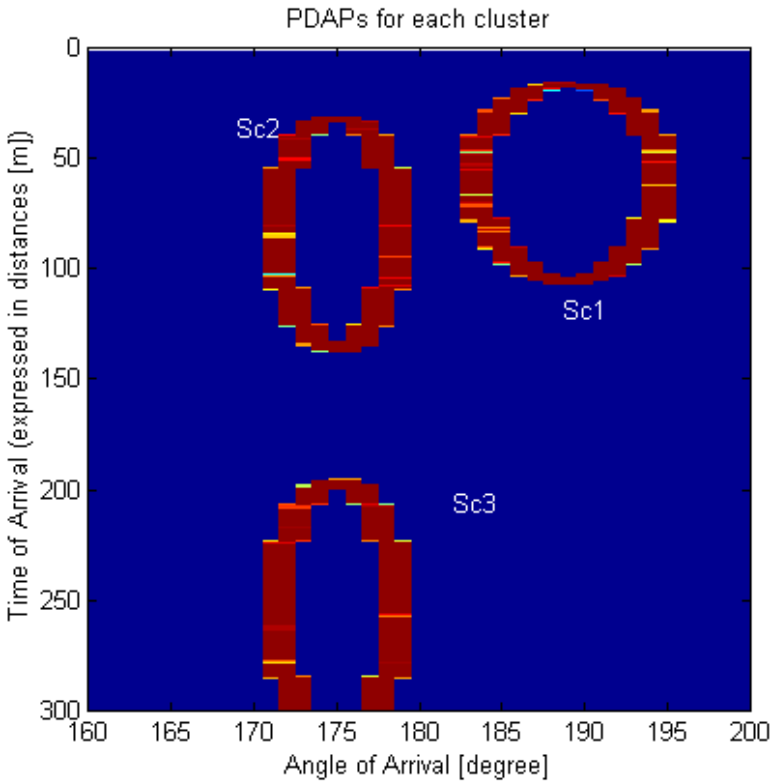

Figure 5.15 PDAPs: horizontal axis α, vertical axis delay expressed in meters, and α_{LOS}= 180 deg.

Table 5.5 Experimental results from [47] in angle (deg) and delay (expressed in distance) of the PDAPs for each cluster.

No. of Cluster	Excess delay [m]	Delay spread [m]	Angle α (deg)	Angle spread $2\Delta\alpha$ (deg)
Sc 1	60	60	6	5.5
Sc 2	60	60	-8	5.5
Sc 3	255	60	-8	5.5
Sc 4	420	60	-1	3.5

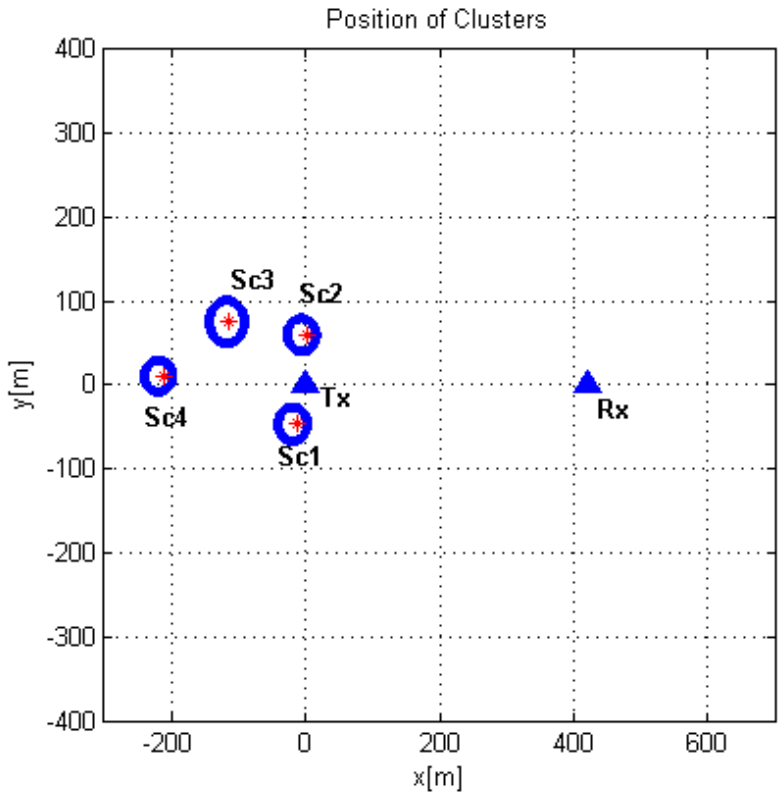

Figure 5.16 X-Y Cluster's position obtained using the experimental results PDAPs from [47].

Table 5.6 Parameters of the four clusters obtained from parameters of Table 5.5.

Tx-Rx and No. Clusters (Sc)	**x-y position [m]**		**Main radius *a* [m]**	**Dist. |Sc-Rx| [m]**	**Ratio $r_{ab} = b/a$**
	X	**y**			
Tx (BS)	0	0	-	-	-
Rx (MS)	420	0	-	-	-
Sc 1	-11.0	-45.3	21.9	433.4	0.93
Sc 2	2.8	58.6	21.5	421.3	0.92
Sc 3	-113.6	75.0	26.0	538.9	0.99
Sc 4	-209.8	11.0	21.0	629.9	0.90

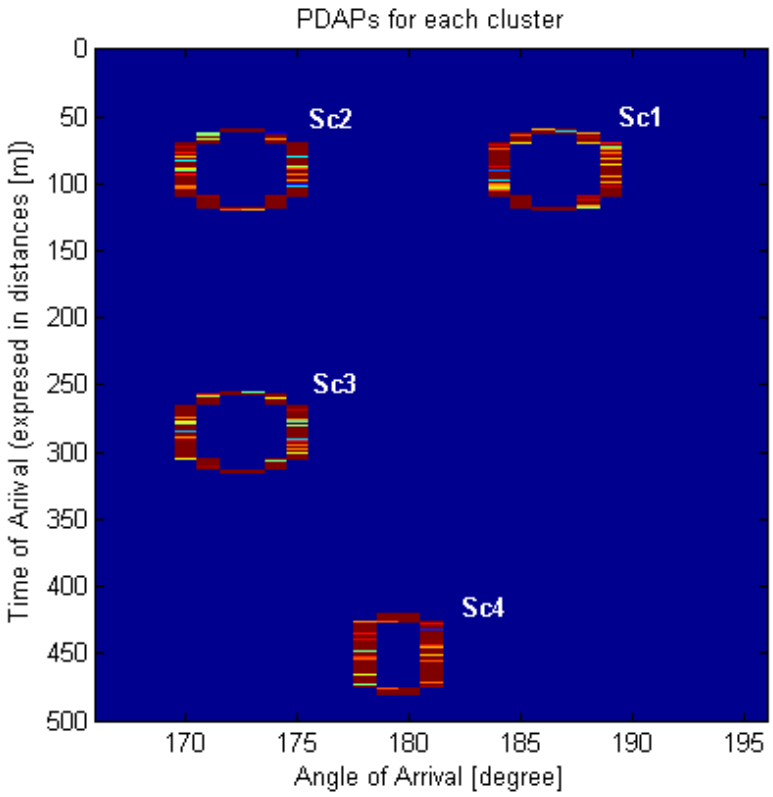

Figure 5.17 PDAPs: horizontal axis α, vertical axis delay expressed in meters, and α_{LOS}= 180 deg.

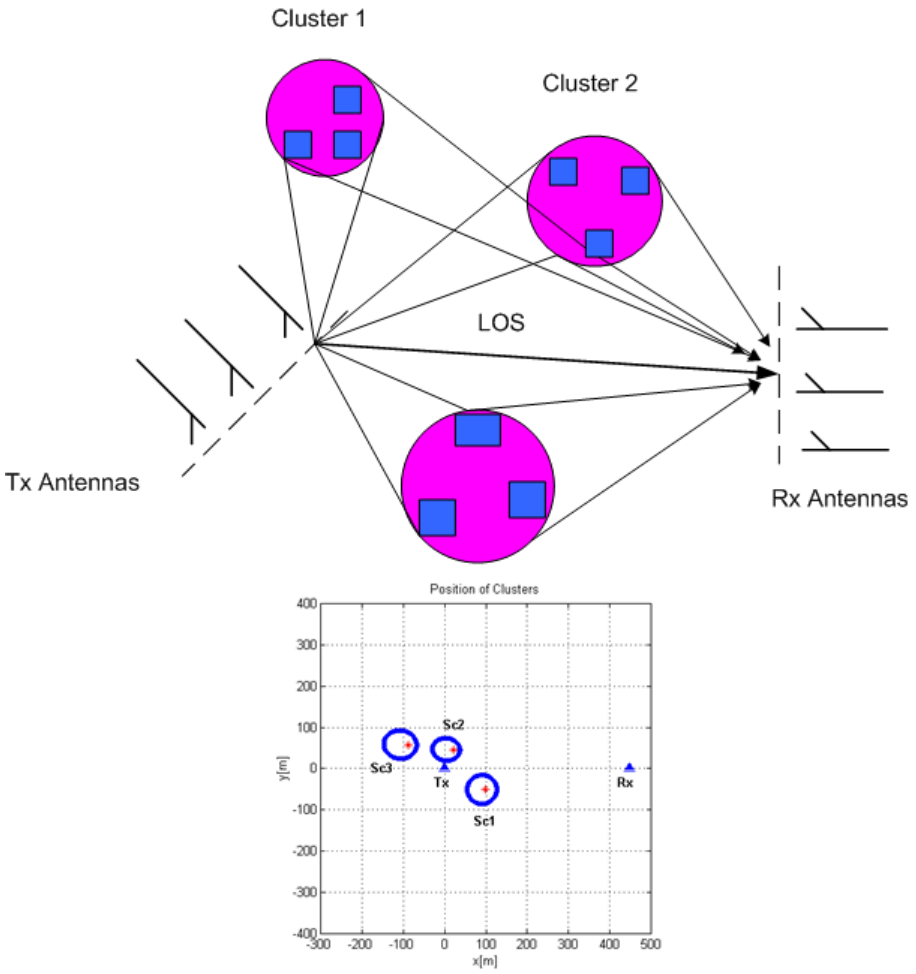

(a)

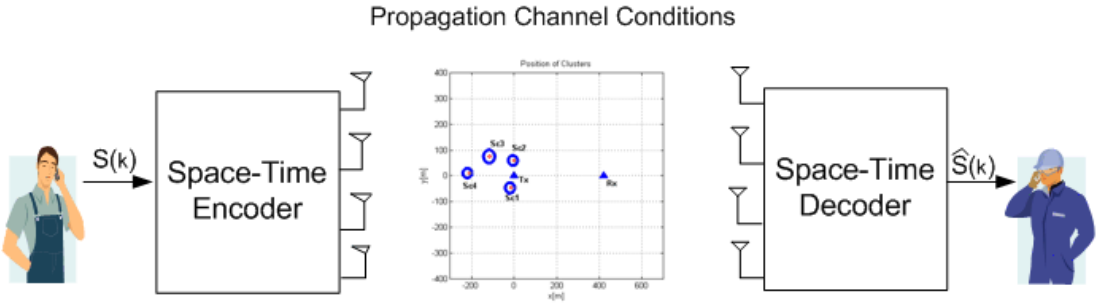

(b)

Figure 5.18 Illustrative example application: (a) spatial multiplexing and (b) Space-Time Coding (STC) for spatial diversity in Clustered MIMO channel model from results presented in Figures 5.14 and 5.16 respectively.

In this example (Fig. 5.18), uniform linear arrays with antenna separation of λ/2 of the carrier wavelength were assumed both at the Tx and Rx. The clusters seen from the Rx are at completely different directions which guarantee uncorrelated fading between the Rx antennas. The angular spread is about 4-6 degrees per cluster.

The multiple receive antenna elements are used for separating the different data streams at the receiver, having Nr combinations of the Nt transmit signals. If the channel is well-behaved, so that the Nr received signals represent linearly independent combinations that can recover the transmit signals as long as Nt≤ Nr [13].

In rich scattering environments, as shown in Fig. 5.18 (a), independent data signals transmitted from different antennas can be uniquely decoded to yield an increase in channel capacity. This increase in capacity os referred to as spatial multiplexing gain. This gain is linear and at most equal to the minimum of the number of transmit and receive antennas used in the MIMO system, (in the example equal to three) with no coding. It requires no additional power or bandwith.

More generally, however, the individual streams should be encoded jointly (as shown in Fig. 5.18 (b), in order to protect transmission caused by channel fading and noise plus interference. In tis case, the multiple antennas are only used as a source of spatial diversity and not to increase data rate.The set of schemes aimed at realizing joint encoding of multiple Tx antennas are called Space Time Coding (STC). The symbols are generated by the space-time encoder such that by using the appropriate signal processing and decoding procedure at the receiver, the diversity gain is maximized.

5.6 Conclusions

The study of wireless communications is based on the signal propagated from Tx to Rx. The performance of the Rx depends on the time of arrival (TOA), direction of arrival (DOA) and angle of departure (AOD) from clusters containing group of MPCs which scatterers the signal.

In this chapter a probability density function (PDF) of DOA and TOA respectively, has been derived for an elliptical and circular scattering for MPC's using the channel modeling based on the clustering approach. Assuming Rx and clusters are stationary (i.e., no Doppler effects), then the total base band channel impulse response is given by equation (4.3) in Chapter 4.

Here, the MPC's with smaller delay than maximum delay (bounded by ellipse) is considered and also a circle is bounded to the ellipse shape cluster. So, DOA is

maximum for circle than ellipse. It decreases with the ratio minor and major axes (r_{ab}) and also the distance between the focus of ellipse to Rx.

Comparison of theoretical with experimental results is done in two cases. In Indoor, MPC parameters were estimated using an algorithm and DOA is calculated. There gets the two classes of power density spectra (PDS) through clustering effect: Inter-cluster and Intracluster PDS which exhibit the Laplacian function in angular domain like power angular spectrum.

In outdoor, the incident wave parameters are determined by wide band channel with planar array. The individual MPC's in the clusters are given by an algorithm by which the analysis of detailed statistics of the propagation properties are enabled.

Advantages:

- Simple model in which the number of clusters and their descriptive parameters (TOA, DOA, DS, AS), is limited.
- Energy is clustered into isolated intervals in delay and angle at the BS and MS.
- Clustering in the angular domain influences the MIMO techniques (beamforming, spatial multiplexing, and diversity), while in the delay domain influences the design of receivers.
- The maximum DOA of the signals to the receiver can be calculated with lower time delay.

Disadvantages:

- This cannot explain about the signals received out of the ellipse which are of huge time delay. This cannot explain the signal statistics in presence of the Doppler effects.
- The average number of cluster and MPCs within a cluster is heavily dependent of the parameter estimation algorithm.

Regarding to the average number of clusters and MPCs distribution within a cluster is heavily dependent on the resolution of the parameter estimation algorithm. This also depends on the type of scenario, (indoor or outdoor); e.g., from experimental results for indoor scenarios, Chion et al., [41], found as most nine clusters. On the other hand from experimental results in outdoor scenarios, (including above, at, and below rooftop level of the base station locations), Toeltsch et al., [47] found as most four clusters. Furthermore, as stated in [41], the number of clusters and MPCs detected are also dependent on several others factors such as the Tx-Rx separation, and location, the physical layout of the environment, as well as the dynamic range of the channel sounder.

Chapter 6 Conclusions and Future Work

This chapter is a summary of the results presented in the thesis and contains general conclusions and discussions around the results presented in the earlier chapters. The thesis has dealt with the analysis and design of geometrically based channel models for MIMO wireless communications that provide the required spatial and temporal information through the clustering approach and their relationship to the power delay angle profiles (PDAPs), necessary for studying such systems as a potential technique to improve access to telecommunication services in urban areas. Taking into account the clustering approach the spatio-temporal properties of the channel is described. So far urban areas have been attractive to private investors due to high population density, large coverage areas, in perhaps no difficult terrain together with the high income of potential users.

6.1 Discussions

Geometric modeling with some stochastic features has becomes popular in describing the characteristics of spatio-temporal radio propagation channel [3–8] even if in some respects stochastic MIMO channels are easier to create from radio channel measurements [48]. One important merit of the geometric approach is that it enables accurate modeling of the correlation between different antenna branches, which is essential for multi-antenna applications such as diversity transmission or reception, beamforming, and the MIMO technique.

The spatio-temporal characteristics of urban environments have been studied using experimental results published in the literature for stationary conditions of the channel, and the environment to be slowing time-varying. Some important conclusions can be made that the comparisons with experimental results have good agreement with the clustering approach proposed. From the comparisons with experimental results, the following observations can be made. First, more clusters are observed at LOS environments or when the Tx–Rx separations are smaller because in such a case, MPCs impinging on the Rx have stronger power. If their path weights are beyond the channel sounder noise threshold,

they will be observable, thereby leading to an increased number of effective clusters. Second, the cluster AS and DS are much smaller for LOS-propagation scenarios due to the smaller feature sizes of the pertinent structure. Third, the correlation between the system operating frequency and the number of clusters is weak.

The average number of clusters and MPCs distribution within a cluster is heavily dependent on the resolution of the parameter estimation algorithm. This also depends on the type of scenario, (indoor or outdoor); e.g., from experimental results for indoor scenarios, Chion et al., [41], found as most nine clusters. On the other hand from experimental results in outdoor scenarios, (including above, at, and below rooftop level of the base station locations), Toeltsch et al., [47] found as most four clusters. This investigation has shown that for each individual data set, four-six clusters can be identified with 7°-25° cluster angle spread (AS).

The statistical modeling approach can in turn be used to analyze different smart antenna configuration in UMTS, which fully exploit the characteristics of UMTS as well as the environment that the system operates in. The channel modeling based on the clustering approach described in Chapter 4 and analyzed in more details in Chapter 5 can be useful to simulate the cases of the appearance or disappearance of cluster due to the relative change in position due to small movements between the transmitter (Tx) or receiver (Rx); i.e., is possible to describe the change in the environments due to the different positions between the transmitter (Tx) and receiver (Rx). As also stated in Chapter 5, the derived PDF can be used to simulate a power delay angle profile (PDAP) and to quantify second order statistics, i.e., angle spread and delay spread for a given circular or elliptical shape of the cluster using the r_{ab} ratio parameter.

As mentioned before, the aim of this thesis is to propose the channel modeling based on the clustering approach and use it for analysis in the space-time domains for stationary conditions to represent the power delay angle profiles (PDAPs) of the MPCs in urban environments. Closed-form expressions have been derived in angular and time domains respectively, however the modeling approach analyzed in this thesis has some limitations compared to others models because is limited to stationary conditions, i.e., the clustering approach proposed does not incorporate the Doppler effect in the analysis.

Furthermore, in Chapter 4, unlike the previous geometrical models based only on single bounce reflection, a model to represent the PDAPs by clusters plus background single bounce scatter components has been described, i.e. the waves arrive at the receiver by double scattering at least. The relationship between the power delay angle profiles (PDAPs) and the clusters have been inferred through the parameters delay spread (DS), angle spread (AS), direction of arrival (DOA), and excess delay, extracted from the PDAPs.

6.2 Contributions

The thesis deals with the analysis and design of geometrically based channel models for MIMO wireless communications, with advanced antenna systems (AAS) as a potential technology to improve access to telecommunication services in urban areas. Taking into account the clustering approach, the spatio-temporal properties of the channel have been described. So far urban areas have been attractive to private investors due to high population density, large coverage areas, in perhaps no difficult terrain together with the high income of potential users.

Furthermore, a new channel model is proposed. Unlike the previous geometrical models based only on single bounce reflection, the model represents the PDAPs by clusters plus background single bounce scatter components, i.e. the waves arrive at the receiver by double scattering at least.

A fundamental insight behind the present thesis is that certain channel characteristics (such as multipath power, angle, and delay) are substantially constant in time but vary gradually as a function of location. Thus, the dependence of the channel characteristics upon location can be used together with (Tx-Rx) location information to improve channel estimation, and hence to improve wireless communication performance between Tx-Rx.

The statistical geometry based channel model proposes can in turn be used to analyze different smart antenna configuration in UMTS, which fully exploit the characteristics of UMTS as well as the environment that the system operates in.

Key contributions:

- In this thesis a channel modeling based on the clustering approach is proposed and used for analysis in the space-time domains for stationary conditions, and employ it to represent the power delay angle profiles (PDAPs) of the MPCs in urban environments.

- A new methodology is proposed for evaluating the performance of MIMO communications systems through the geometry-based channel models.

- Through comparisons with measurements results available in the literature, the performance gain of the MIMO system has been evaluated utilizing different physical urban scenarios that comprise the wireless channel model.

- Derivation of probability density functions (PDFs) in the angular and time domain respectively through direction of arrival (DOA) and time of arrival (TOA) for the channel modeling based on the clustering approach. In order to evaluate the theoretical PDFs derived and compared those to

experimental results published in the literature. The comparison to experimental results shows good agreement.

6.3 Scope and Limitations

The emphasis of the thesis lies in MIMO channel models based on geometry. However, analyses in angular and time domain for transmission scheme are shortly presented to get a better overview of the overall channel and communication systems. As mentioned before the scope of this thesis is the analysis of the spatio-temporal properties for MIMO systems using the clustering approach model proposed under stationary conditions, so, it does not take in to account the Doppler effect in the analysis presented. Assuming stationary conditions; however, the channel models consider the effect of local scatterers, which are grouped into clusters for the analysis. Besides, in Chapter 4, the far scatterers (again grouped into clusters), are analyzed assuming that the path loss will tend to limit their contribution to the overall channel. In addition, because of local scatterers introduce multipath differences that are small compared to the transmit-receive range, the focus is laid on microscopic (Rayleigh) fading only.

6.4 List of Publications

Parts of the contents of this thesis have been published or accepted for publication in IEEE international conference contributions proceedings and journal papers detailed as follows:

Journal Articles:

- M.R. Arias and B. Mandersson, “Clustering approach for geometrically based channel model in urban environments”, IEEE Antennas and Wireless Propagation Letters, Vol. 5 pp 290-293, Dec. 2006. Available in the Institute for Scientific Information database (ISI Thomson).

- M. R. Arias, “Derivación Analítica del Tiempo de Llegada en Modelos de Canal Basados en Geometría para Sistemas Inalámbricos”, “Revista Científica de la Universidad Nacional de Ingeniería, Nexo Vol. 20, No. 02, pp. 69-77/Noviembre 2007. Available in the Directory of Open Access Journals, (DOAJ).

International Conferences Contributions (Available in IEEE *Xplore* database):

- M.R. Arias and B. Mandersson, “An approach of the Geometrical-based single bounce elliptical channel model for mobile environments,” Proceedings of The 8th International Conference on Communication Systems, (ICCS 2002), vol.1, pp 11-16, Singapore, Nov. 2002.

- M.R. Arias and B. Mandersson, “Clusters PDF in Angle and Time Domain for Geometrically Based Channel Model”, Proceedings of International Symposium on Intelligent Signal Processing and Communication Systems (ISPACS 2004), pp 433-438, Seoul, Korea, Dec. 2004.

- M.R. Arias and B. Mandersson, “A Generalized Angle Domain Clusters PDF and Its Application in Geometrically Based Channel Models”, Proceedings of International Conference on Information, Communications and Signal Processing (ICICS 2005), pp 1339-1343, Bangkok, Thailand, Dec. 2005.

- M.R. Arias and B. Mandersson, “Time Domain Cluster PDF and Its Application in Geometry-Based Statistical Channel Models”, Proceedings of The 18th Annual IEEE International Symposium on Personal, Indoor and Mobile Radio Communications (PIMRC 2007), pp 1-5, Athens, Greece, Sept. 2007.

6.5 Future Work

This thesis has addressed aspects and issues regarding the use of statistical channel models based on geometry for MIMO wireless communications, however there is still a number of further research questions considered relevant for future work. In particular further research is still required in the MIMO channel modeling area, the following issues deserve more thorough investigation: Narrowband model errors are large when both the BS and MS have high covariances between neighboring antenna elements. Similar simulation results are reported in [61] using electromagnetic (EM) scattering model to simulate both microcell and indoor environments. Therefore theoretical analysis of the non-physical models and validation of the physical models from measurements are required to bridge the gap between these two groups of models. An initial theoretical derivation of the Kronecker structure for non-physical model under certain conditions can be found in [58]. A validated physical model can greatly reduce the number of required measurements and thus decrease the research and development costs when designing and evaluating a system.

References

1. T. S. Rappaport, “Wireless Communications Principles and Practice”. Prentice Hall PTR, Second Edition, 2002, ISBN 0-13-099572-X.

2. J. G. Proakis, “Digital Communications,” McGrall-Hill Fourth Edition, 2000, ISBN 0-07-232111-3.

3. M. Paetzold, “Mobile Fading Channels: Modeling, Analysis & Simulations” John Wiley & Sons, Inc. 2002, ISBN 0471-49549-2.

4. A. F. Molisch, H. Asplun, R. Heddergott, M. Steinbauer, and T. Zwick “The Cost259 Directional Channel Model- Part I: Overview and Methodology,” IEEE Transactions on Wireless Communications, vol. 5 No. 12, pp 3421-3433 Dec. 2006.

5. H. Asplund, A. Alayón, A. F. Molisch, K. I. Pedersen, and M. Steinbauer, “The COST 259 Directional Channel Model- Part II: Macrocells,” IEEE Transactions on Wireless Communications, vol. 5 No. 12, pp 3434-3450, Dec. 2006.

6. R. B. Ertel, P. Cardieri, K. W. Sowerby, T. S. Rappaport, and J. H. Reed, “Overview of spatial channel models for antenna array communication systems,” IEEE Pers. Commun. Magn, pp. 10-22, Feb. 1998.

7. J. C. Liberti and T. S. Rappaport, “Smart Antennas for Wireless Communications: IS-95 and Third Generation CDMA Applications,” Prentice Hall PTR, 1999, ISBN 0-13-719287-8.

8. J. C. Liberti and T. S. Rappaport, “A geometrically based model for Line-Of-Sight multipath radio channels,” in Proc. IEEE Veh. Tech. Conf., Spring 1996, pp. 844-848.

9. A. F. Molisch, “Wireless Communications” John Wiley & Sons, Inc. 2005, ISBN 10-0-470-84888-X.

10. G. J. Foschini, and M. J. Gans, “On limits of wireless communications in a fading environment,” IEEE Trans. Wireless Personal Communications, vol. 6, pp 311-335, Mar. 1998.

11. G. J. Foschini, “Layered space-time architecture for wireless communication in a fading environment when using multiple antennas” Bell Laboratories Technical Journal, vol. 1, no.2, pp. 41-59, Autumn 1996.

12. W. H. Tranter, K. S. Shanmugan, T. S. Rappaport, and K. L. Kosbar, “Principles of Communication Systems Simulation with Wireless Applications,” Prentice Hall PTR, 2004, ISBN 10-01-3494790-8.

13. D. Gesbert, M. Shafi, D. S. Shiu, P. J. Smith, and A. Naguib, “From theory to practice: an overview of MIMO space-time coded wireless systems,” IEEE J. Selected Areas Comm., vol. 21, pp. 281–302, 2003.

14. J. H. Winters, “On the capacity of radio communications systems with diversity in Rayleigh fading environments,” IEEE J. Selected Areas Comm., vol. 5, pp. 871–878, June 1987.

15. I. E. Telatar, “Capacity of multi-antenna Gaussian channels,” European Trans. Telecomm., vol. 10, pp. 585–595, 1999.

16. D. Piazza, N.J. Kirsch, A. Forenza, R.W. Heath, and K.R. Dandecar, “Design and Evaluation of a Reconfigurable Antenna Array for MIMO Systems,” IEEE Trans. On Antennas and Propagation, vol. 56 No. 3, pp 869-881, March 2008.

17. A. Paulraj, D. Gore, and R. Nabar, Multiple antenna systems. Cambridge, U.K.: Cambridge University Press, 2003.

18. G. J. Foschini, D. Chizhik, M. J. Gans, C. Papadias, and R. A. Valenzuela, “Analysis and performance of some basic space-time architectures,” IEEE J. Selected Areas Comm., vol. 21, pp. 303–320, 2003.

19. G. J. Foschini, G. D. Golden, R. A. Valenzuela, and P. W. Wolniansky, “Simplified processing for high spectral efficiency wireless communication employing multi-element arrays,” IEEE J. Selected Areas Comm., vol. 17, pp. 1841–1852, 1999.

20. V. Tarokh, N. Seshadri, and A. R. Calderbank, “Space-time codes for high data rate wireless communication: Performance criterion and code construction,” IEEE Trans. Information Theory, vol. 44, No. 2, pp. 744–765, March 1998.

21. A. F. Molisch, A. F. Kuchar, J. Laurila, K. Hugl, and E. Boneck, “Efficient implementation of a geometry-based directional model for mobile radio channels,” in Proc. IEEE Veh. Tech. Conf., Fall 1999, pp. 1449-1453.

22. M. Matthaiou, D. I. Laurenson, and J. Thompson, “A MIMO Channel Model Based on Nakagam-Faded Spatial Eigenmodes,” IEEE Transactions on Antennas and Propagation, vol. 56 No. 5, pp 1494-1497, May 2008.

23. P. Suvikunna, J. Salo, and P. Vainikainen, “Impact of Power Normalization in Experimental MIMO Antenna Peroformance Studies,” IEEE Antennas and Wireless Propagation Letters, Vol. 6, pp 43-46, Dec. 2007.

24. A. Kuchar, J. P. Rossi, and E. Bonek, “Directional Macro-cell channel characterization from urban measurements,” IEEE Trans. On Antennas and Propagation, vol. 48 No. 2, pp 137-146, Feb. 2000.

25. G. L. Siqueira and E. J. A. Vásquez, “Local and Global Signal Variability Statistics in a Mobile Urban Environment,” Kluwer Wireless Personal Communications, vol. 15, pp. 61–78, Feb. 2000.

26. Y. Chen, and V. K. Dubey, “Dynamic Simulation Model of Indoor Wideband Directional Channels,” IEEE Trans. On Vehicular and Technol., Vol. 55, No. 2, pp 417-430, March 2006.

27. P. P. Petrus, J. H. Reed, and T. S. Rappaport, “Geometrical-based statistical macrocell channel model for mobile environments,” IEEE Trans. On Communications, vol. 50, No. 3, 495-502, March 2002.

28. R. B. Ertel and J. H. Reed, “Angle and Time of Arrival Statistics for Circular and Elliptical Scattering Models,” IEEE Journal on Selected Areas in Communications, vol. 17, No. 11, pp 1829-1840, Nov. 1999.

29. U. Martin, J. Fuhl, I. Gaspard, M. Haardt, A. Kuchar, C. Math, A. F. Molisch, and R. Thomä, “Model scenarios for direction-selective adaptive antennas in cellular mobile communication systems—Scanning the literature,” Kluwer Wireless Personal Communications, vol. 11, no. 1, pp. 109–129, Oct. 1999.

30. X. Zhao, J. Kivinen, P. Vainikainen, and K. Skog, “Propagation Characteristics for Wideband Outdoor Mobile Communications at 5.3 GHz,” IEEE J. Select. Areas Commun., vol. 20, No. 3 pp. 507–514, Apr. 2002.

31. K. I. Pedersen, P. E. Mogensen, and B. H. Fleury, “A stochastic model of the temporal and azimuthal dispersion seen at the base station in outdoor propagation environments,” IEEE Trans. Veh. Technol., vol. 49, pp. 437–447, Mar. 2000.

32. H. Nishimoto, Y. Ogawn, T. Nishimura, and T. Ohgane, “Measurement-Based Performance Evaluation of MIMO Spatial Multiplexing in a Multipath-Rich Indoor Environment,” IEEE Transactions on Antennas and Propagation, vol. 55 No. 12, pp 3677-3689, Dec. 2007.

33. B. H. Fleury, M. Tschudin, R. Heddergott, D. Dahlhaus, and K. I. Pedersen, “Channel parameter estimation in mobile radio environments using the SAGE algorithm,” IEEE J. Select. Areas Commun., vol. 17, pp. 438–450, Mar. 1999.

34. M. R. Arias and B. Mandersson, “An approach of the Geometrical-based single bounce elliptical channel model for mobile environments,” in Proc. 8th IEEE ICCS2002 Conf. vol.1, Singapore, Nov. 2002, pp 11-16.

35. A. Alcocer-Ochoa, R. Parra-Michel, and V. Kontorovitch, “Geometrical Modeling of Wideband MIMO Channels,” Computación y Sistemas, CIC-IPN, vol. 9 No. 4, pp 326-339, April 2006.

36. H. Asplund, A. F. Molisch, and N. B. Mehta, “Clustering of Scatterers in Mobile Radio Channels- Evaluation and Modeling in the COST259 Directional Channel Model,” In Proc. IEEE ICC 2002 Conf., vol. 2, May 2002, pp 901-905.

37. R. Janaswamy, “Angle and Time of Arrival Statistics for the Gaussian Scatter Density Model,” IEEE Transactions on Wireless Communications, vol. 1 No. 3, pp 488-497, July 2002.

38. A. Algans, K. I. Pederssen, and P.E. Mogensen, “Experimental Analysis of the Joint Statistical Properties of Azimuth Spread, Delay Spread, and Shadow Fading,” IEEE Journal on Selected Areas in Communications, vol. 20 No. 3, pp 523-531, April 2002.

39. J. B. Andersen, and K.I. Pedersen, “Angle-of-Arrival Statistics for Low Resolution Antennas,” IEEE Transactions on Antennas and Propagation, vol. 50 No. 3, pp 391-395, March 2002.

40. M. R. Arias and B. Mandersson, “Clustering Approach for Geometrically Based Channel Model for Mobile Environments,” IEEE Antennas and Wireless Propagation Letters, Vol. 5, pp 290-293, Dec. 2006.

41. C. C. Chong, C.M. Tan, D. I. Laurenson, S. McLaughlin, M. A. Beach, and A. R. Nix, “A New Statistical Wideband Spatio-Temporal Channel Model for 5-GHz Band WLAN Systems,” IEEE Journal on Selected Areas in Communications, vol. 21 No. 2, pp 139-150, Feb. 2003.

42. A. M. Saleh and R.A. Valenzuela, “A statistical model for indoor multipath propagation,” IEEE J. Select. Areas Commun., vol. 5, pp. 128-137, Nov. 1987.

43. Q. H. Spencer, et al., “Modeling the statistical time and angle of arrival characteristics of an indoor environment,” IEEE J. Select. Areas Commun., vol. 18, No. 3, pp. 347-360, March 2000.

44. R. J-M. Cramer, R.A. Scholtz, and M.Z. Win, “Evaluation of an ultra-wide-band propagation channel,” IEEE Trans. Antennas Propagat., vol. 50, No.5, pp. 561-570, May 2002.

45. G. German, Q. Spencer, L. Swindlehurst, and R. Valenzuela, “Wireless indoor channel modeling: Statistical agreement of ray tracing simulations and channel sounding measurements,” in proc. IEEE Acoustics, Speech, and Signal Proc. Conf., vol. 4, 2001, pp. 2501-2504.

46. S. Wyne, A. F. Molisch, P. Almers, G. Eriksson, J. Karedal, and F. Tufvesson,” Outdoor-to-Indoor Officle MIMO Measurements and Analysis at 5.2 GHz,” IEEE Trans. On Vehicular Techn., Vol. 57, No. 3, pp 1374-1386, May 2008.

47. M. Toeltsch, J. Laurilla, K. Kalliola, A. F. Molisch, P. Vainikainen, and E. Bonek, “Statistical characterization of urban spatial radio channels,” IEEE Journal on selected areas in Communications, vol. 20, No. 3, pp 539-549, April 2002.

48. J.P. Kermoal, L. Schumacher, K.I. Pedersen, P.E. Mogensen and F. Frederiksen, “A Stochastic MIMO Radio Channel Model With Experimental Validation”, IEEE Journal on selected areas in Communications, vol. 20, No. 6, pp 1211-1226, August 2002.

49. P. Kyritsi and D.C. Cox, “Correlation properties of MIMO radio channels for indoor scenarios,” in proc. Signal Systems and Computers 35th Asilomar Conf., vol. 2, 2001.

50. J. Medbo, M. Riback, and J-E. Berg, “Validation of 3GPP spatial channel model including WINNER wideband extension using measurements,” in Proc. VTC-Fall Conf., vol. 1, pp. 1-5, Sept. 2006.

51. J. Medbo, M. Riback, H. Asplund, and J. Berg, “MIMO channel characteristics in a small macrocell measured at 5.25 GHz and 200 MHz bandwidth,” in Proc. VTC-Fall, vol. 1, Sept. 2005, pp. 372-376.

52. J. F. Vallenzuela-Valdés, M.A. García-Fernández, A.M. Martínez-González, and D. A. Sánchez-Hernández, “The Influence of Efficiency on Receive Diversity and MIMO Capacity for TRayleigh-Fading Channels,” IEEE Transactions on Antennas and Propagation, vol. 56, No. 5, pp 1444-1450, May 2008.

53. T. Zwick, C. Fisher, and W. Wiesbeck, “A stochastic Multipath Channel Model Including Path Directions for Indoor Environments,” IEEE J. Select. Areas in Commun., vol. 20, No. 6, pp. 1178-1192, August 2002.

54. M. Riback, H. Asplund, J. Medbo, and J-E. Berg, “Statistical analysis of measured radio channels for future generation mobile communication systems,” in Proc. VTC-Spring Conf., vol. 1, June 2005, pp. 68-72.

55. L. Schumacher, K. I. Pedersen, and P.E. Mogensen, “From antenna spacings to theoretical capacities – guidelines for simulating MIMO systems,” in Proc. PIMRC Conf., vol. 2, Sept. 2002, pp. 587-592.

56. P. Soma, D.S. Baum, V. Erceg, R. Krishnamurthy, and A.J. Paulraj, “ Analysis and modeling of Multiple Input Multiple Output (MIMO) radio channel based on outdoor measurements conducted at 2.5 GHz for fixed BWA applications,” in Proc. IEEE ICC Conf., New York, April 2002, pp 272-276.

57. C. N. Chuah, D. N. Tse, J. M. Kahn, R. A. Valenzuela, “Capacity scaling in MIMO wireless systems under correlated fading”, IEEE Trans. Information Theory, vol. 48, pp 637-650, 2002.

58. K. Yu and B. Ottersten, Models for MIMO Propagation Channels, A Review”, Wiley J. Wireless Communications and Mobile Computing, special issue on Smart antenna and MIMO systems, Oct. 2002.

59. M. Steinbauer, A. F. Molisch, and E Boneck, “The Double-Directional Radio Channel,” IEEE Antennas Propagat. Mag., vol. 43, No. 4 pp 51-63, Aug. 2001.

60. A. F. Molisch, “A Generic Model for MIMO Wireless Propagation Channels in Macro- and Microcells,” IEEE Trans. On Signal Processing, Vol. 52, No. 1, pp. 61-71, Jan. 2004.

61. A. M. Sayeed, “Deconstructing multiantenna fading channels”, IEEE Trans. Signal Proc. Vol. 50, No. 10, pp 2563-2579, Oct. 2002.

62. P. Almers, F. Tufvesson, and A.F. Molisch, “Keyhole Effect in MIMO Wireless Channels: Measurements and Theory;” IEEE Trans. On Commun., Vol. 5, No. 12, pp 3596-3604, Dec. 2006.

63. N. Blaunstein, M. Toeltsch, C. G. Christodoulou, J. Laurila, E. Tsalolihin, E. Bonek, P. Vainikainen, N. Tsouri, K. Kalliola, and H. Laitinen, “Azimuth, Elevation, and Time-Delay Distributions in Wireless Communication Channels,” IEEE Antennas and Propagat. Magazine, Vol. 48, No.1, pp 160-167, Feb. 2006.

64. A. G. Burr, “ Capacity Bounds and Estimates for the Finite Scatterers MIMO Wireless Channel,” IEEE Journal On Selected Areas in Commun., Vol. 21, No. 5, pp 812-818, June 2003.

65. M. R. Arias, and B. Mandersson, “Clusters PDF in Angle and Time Domain for Geometrically Based Channel Model,” Proc. of International Symposium on Intelligent Signal Processing and Communication Systems (ISPACS 2004), Seoul, Korea, Dec. 2004, pp 433-438.

66. M. R. Arias, “Derivación Analítica del Tiempo de Llegada en Modelos de Canal Basados en Geometría para Sistemas Inalámbricos”. Directory of Open Access Journals. “Revista Científica de la Universidad Nacional de Ingeniería: Nexo Vol. 20, No. 2, pp. 69-77, Nov. 2007.

67. A. Doufexi, S. Armour, M. Butler, A. Nix, D. Bull and J. McGeehan, “A comparison of the HIPERLAN/2 and IEEE 802.11a wireless LAN standards,” IEEE Commun. Mag., pp. 172-180, May 2002.

68. Y. Z. Mohasseb, and M. P. Fitz, “A 3-D Spatio-Temporal Simulation Model for Wireless Channels,” IEEE Journal On Select. Areas in Commun., Vol. 20, No. 6, pp 1193-1203, August 2002.

69. B. H. Fleury, “First- and Second-Order Characterization of Direction Dispersion and Space Selectivity in the Radio Channel,” IEEE Trans. On Information Theory, Vol. 46, No. 6, pp 2027-2044, Sept. 2000.

70. D. Gesbert, H. Boelcskei, D. A. Gore, and A. Paulraj, “Outdoor MIMO Wireless Channels: Models and Performance Prediction,” IEEE Trans. On Commun., Vol. 50, No. 12, pp 1926-1934, Dec. 2002.

71. K. Kalliola, K. Sulonen, H. Laitinen, O. Kivekaes, J. Krogerus, and P. Vainikainen, ”Angular Power Distribution and Mean Effective Gain of Mobile Antenna in Different Propagation Environments,” IEEE Trans. On Vehicular Techn., Vol. 51, No. 5, pp 823-837, Sept. 2002.

72. R. Kattenbach, “Statistical Modeling of Small-Scale Fading in Directional Radio Channels,” IEEE Journal On Selected Areas in Commun., Vol. 20, No. 3, pp 584-592, April 2002.

73. J. Laurila, K. Kalliola, M. Toeltsch, K. Hugl, P. Vainikainen, and E. Bonek, ”Wide-Band 3-D Characterization of Mobile Radio Channels in Urban Environment,” IEEE Trans. On Antennas and Propagat., Vol. 50, No. 2, pp 233-243, Feb. 2002.

74. S. L. Loyka, and A. Kouki, “On MIMO Channel Capacity, Correlations, and Keyholes: Analysis of Degenerated Channels,” IEEE Trans. On Commun., Vol. 50, No. 12, pp 1886-1888, Dec. 2002.

75. H. Oezcelik, and C. Oestges, “Some Remarkable Properties of Diagonally Correlated MIMO Channels,” IEEE Trans. On Vehicular and Techn., Vol. 54, No. 6, pp 2143-2145, Nov. 2005.

76. C. Oestges, B. Clerckx, D. Vanhoenacker-Janvier, and A. J. Paulraj, “Impact of Fading Correlations on MIMO Communication Systems in Geometry-Based Statistical Channel Models,” IEEE Trans. On Wireless Commun., Vol. 4, No. 3, pp 1112-1120, May 2005.

77. V. Erceg, P. Soma, D. S. Baum, and S. Catreux, “Multiple-Input Multiple-Output Fixed Wireless Radio Channel Measurements and Modeling Using Dual-Polarized Antennas at 2.5 GHz,” IEEE Trans. On Wireless Commun., Vol. 3, No. 6, pp 2288-2298, Nov. 2004.

78. M. A. Jensen, and J. W. Wallace, “A Review of Antennas and Propagation for MIMO Wireless Communications,” IEEE Trans. On Antennas and Propagat., Vol. 52, No. 11, pp 2810-2824, Nov. 2004.

79. V. Erceg, H. Sampath, and S. Catreux-Erceg, “Dual-Polarization Versus Single-Polarization MIMO Channel Measurement Results and Modeling,” IEEE Trans. On Wireless Commun., Vol. 5, No. 1, pp 28-33, Jan. 2006.

80. W. Weichselberger, M. Herdin, H. Oezcelik, and E. Bonek, “A Stochastic MIMO Channel Model with Joint Correlation of Both Link Ends,” IEEE Trans. On Wireless Commun., Vol. 5, No. 1, pp 90-100, Jan. 2006.

81. M. Kang, and M. Alouini, “Capacity of MIMO Rician Channels,” IEEE Trans. On Wireless Commun., Vol. 5, No.1, pp 112-122, Jan. 2006.

82. J. W. Wallace, and M. A. Jensen, “Modeling the Indoor MIMO Wireless Channel,” IEEE Trans. On Antennas and Propagat., Vol. 50, No. 5, May 2002.

83. R. S. Blum, and J. H. Winters, “On MIMO with Antenna Selection,” IEEE Communications Letters, Vol. 6, No. 8, pp 322-324, August 2002.

84. S. S. Mahmoud, Z. M. Hussain, and P. O’Shea, “A Space-Time Model for Mobile Radio Channel with Hyperbolically Distributed Scatterers,” IEEE Antennas and Wireless Propagat. Letters, Vol. 1, pp 211-214, Dec. 2002.

85. M. Chryssomallis, “Smart Antennas,” IEEE Antennas and Propagat. Magazine, Vol. 42, No.3, pp 129-136, June 2000.

86. M. Chryssomallis, “Simulation of Mobiles Fading Channels,” IEEE Antennas and Propagat. Magazine, Vol. 44, No.6, pp 172-183, Dec. 2002.

87. M. R. Arias and B. Mandersson, “A Generalized Angle Domain Clusters PDF and Its Application in Geometrically Based Channel Models”, Proceedings of International Conference on Information, Communications and Signal Processing (ICICS 2005), Bangkok, Thailand, Dec. 2005, pp 1339-1343.

88. M. R. Arias and B. Mandersson, “Time Domain Cluster PDF and Its Application in Geometry-Based Statistical Channel Models”, Proceedings of The 18th Annual IEEE International Symposium on Personal, Indoor and Mobile Radio Communications (PIMRC 2007), , Athens, Greece, Sept. 2007, pp 1-5.

89. A. Goldsmith, S. A. Jafar, N. Jindal, and S. Vishwanath, “Capacity Limits of MIMO Channels,” IEEE Journal On Selected Areas in Commun., Vol. 21, No. 5, pp 684-702, June 2003.

90. H. Xu, D. Chizhik, H. Huang, and R. Valenzuela, “A Generalized Space-Time Multiple-Input Multiple-Output (MIMO) Channel Model,” IEEE Trans. On Wireless Communications, Vol. 3, No. 3, pp 966-975, May 2004.

91. A. F. Molisch, M. Z. Win, Y. S. Choi, and J. H. Winters, “Capacity of MIMO Systems with Antenna Selection,” IEEE Trans. On Wireless Communications, Vol. 4, No. 4, pp 1759-1772, July 2005.

92. K. Kalliola, H. Laitinen, P. Vainikainen, M. Toeltsch, J. Laurila, and E. Bonek, ”3-D Double-Directional Radio Channel Characterization for Urban Macrocellular Applications,” IEEE Trans. On Antennas and Propagat., Vol. 51, No. 11, pp 3122-3133, Nov. 2003.

93. K. Yu, Q. Li, and M. Ho, “Measurement Investigation of Tap and Cluster Angular Spreads at 5.2 GHz,” IEEE Transactions on Antennas and Propagation, vol. 53, No. 7, pp 2156-2160, July 2005.

94. V. Kontorovich, S. Primak, A. Alcocer-Ochoa, and R. Parra-Michel, ”MIMO Channel Ortogonalisations Applying Universal Eigenbasis,” IET Transactions on Signal Processing, vol. 2 No. 2, pp 87-96, June, 2008.

95. M. K. Awad, and K. T. Wong, “An Integrated Overview of the Open Literature’s Empirical Data on the Indoor Radiowave Channel’s Delay Properties,” IEEE Transactions on Antennas and Propagation, vol. 56, No. 5, pp 1451-1468, May 2008.

96. N. Blaunstein, M. Toeltsch, J. Laurila, E. Bonek, D. Katz, P. Vainikainen, N. Tsouri, K. Kalliola, and H. Laitinen, “Signal Power Distribution in the Azimuth, Elevation and Time Delay Domains in Urban Environments for Various Elevations of Base Station Antenna,” IEEE Transactions on Antenna and Propagation, vol. 54, No. 10, pp 2902-2916, October 2006.

97. N. Blaunstein, R. Giladi, and M. Levin, “Characteristics’ Prediction in Urban and Suburban Environment,” IEEE Trans. On Vehicular Techn., Vol. 47, No. 1, pp 823-837, Feb. 2008.

98. J. Li, J. Conan, and S. Pierre, “Mobile Terminal Location for MIMO Communication Systems,” IEEE Transactions on Antenna and Propagation, vol. 55, No. 8, pp 2417-2420, Aug. 2007.

Appendix A

The Tables with channel coefficients (tap delays and corresponding powers) are details as following.

Table A.1 Model A (Optional Model).

	Tap index	**1**
	Excess delay [ns]	**0**
	Power [dB]	0
AoA	**AoA [°]**	45
AS (Rx)	**AS [°]**	40
AoD	**AoD [°]**	45
AS (Tx)	**AS [°]**	40

Table A.2 Model B.

	Tap index	**1**	**2**	**3**	**4**	**5**	**6**	**7**	**8**	**9**
	Excess delay [ns]	**0**	**10**	**20**	**30**	**40**	**50**	**60**	**70**	**80**
Cluster 1	**Power [dB]**	0	-5.4	-10.8	-16.2	-21.7				
AoA	**AoA [°]**	4.3	4.3	4.3	4.3	4.3				
AS (Rx)	**AS [°]**	14.4	14.4	14.4	14.4	14.4				
AoD	**AoD [°]**	225.1	225.1	225.1	225.1	225.1				
AS (Tx)	**AS [°]**	14.4	14.4	14.4	14.4	14.4				
Cluster 2	**Power [dB]**			-3.2	-6.3	-9.4	-12.5	-15.6	-18.7	-21.8
AoA	**AoA [°]**			118.4	118.4	118.4	118.4	118.4	118.4	118.4
AS	**AS [°]**			25.2	25.2	25.2	25.2	25.2	25.2	25.2
AoD	**AoD [°]**			106.5	106.5	106.5	106.5	106.5	106.5	106.5
AS	**AS [°]**			25.4	25.4	25.4	25.4	25.4	25.4	25.4

Table A.3 Model C.

14	**200**						-20.2	332.3	22.4	56.4	22.5
13	**170**						-18.0	332.3	22.4	56.4	22.5
12	**140**						-15.8	332.3	22.4	56.4	22.5
11	**110**						-13.7	332.3	22.4	56.4	22.5
10	**90**	-19.5	290.3	24.6	13.5	24.7	-11.5	332.3	22.4	56.4	22.5
9	**80**	-17.3	290.3	24.6	13.5	24.7	-9.3	332.3	22.4	56.4	22.5
8	**70**	-15.2	290.3	24.6	13.5	24.7	-7.2	332.3	22.4	56.4	22.5
7	**60**	-13.0	290.3	24.6	13.5	24.7	-5.0	332.3	22.4	56.4	22.5
6	**50**	-10.8	290.3	24.6	13.5	24.7					
5	**40**	-8.6	290.3	24.6	13.5	24.7					
4	**30**	-6.5	290.3	24.6	13.5	24.7					
3	**20**	-4.3	290.3	24.6	13.5	24.7					
2	**10**	-2.1	290.3	24.6	13.5	24.7					
1	**0**	0	290.3	24.6	13.5	24.7					
Tap index	**Excess delay [ns]**	**Power [dB]**	**AoA [°]**	**AS [°]**	**AoD [°]**	**AS [°]**	**Power [dB]**	**AoA [°]**	**AS [°]**	**AoD [°]**	**AS [°]**
		Cluster 1	AoA	AS (Rx)	AoD	AS (Tx)	Cluster 2	AoA	AS	AoD	AS

Table A.4 Model D.

18	**390**										
17	**340**						-25.5	320.2	31.4	49.3	32.1
16	**290**	-23.2	158.9	27.7	332.1	27.4	-21.9	320.2	31.4	49.3	32.1
15	**240**	-19.3	158.9	27.7	332.1	27.4	-17.4	320.2	31.4	49.3	32.1
14	**200**	-16.3	158.9	27.7	332.1	27.4	-14.7	320.2	31.4	49.3	32.1
13	**170**	-13.7	158.9	27.7	332.1	27.4	-12.1	320.2	31.4	49.3	32.1
12	**140**	-11.1	158.9	27.7	332.1	27.4	-9.5	320.2	31.4	49.3	32.1
11	**110**	-9.0	158.9	27.7	332.1	27.4	-6.6	320.2	31.4	49.3	32.1
10	**90**	-7.8	158.9	27.7	332.1	27.4					
9	**80**	-6.9	158.9	27.7	332.1	27.4					
8	**70**	-6.1	158.9	27.7	332.1	27.4					
7	**60**	-5.2	158.9	27.7	332.1	27.4					
6	**50**	-4.3	158.9	27.7	332.1	27.4					
5	**40**	-3.5	158.9	27.7	332.1	27.4					
4	**30**	-2.6	158.9	27.7	332.1	27.4					
3	**20**	-1.7	158.9	27.7	332.1	27.4					
2	**10**	-0.9	158.9	27.7	332.1	27.4					
1	**0**	0	158.9	27.7	332.1	27.4					
Tap index	**Excess delay [ns]**	**Power [dB]**	**AoA [°]**	**AS [°]**	**AoD [°]**	**AS [°]**	**Power [dB]**	**AoA [°]**	**AS [°]**	**AoD [°]**	**AS [°]**
		Cluster 1	AoA	AS (receiver)	AoD	AS (transmitter)	Cluster 2	AoA	AS	AoD	AS

-26.7	276.1	37.4	275.9	36.8
-25.2	276.1	37.4	275.9	36.8
-23.2	276.1	37.4	275.9	36.8
-18.8	276.1	37.4	275.9	36.8
Power [dB]	**AoA [°]**	**AS [°]**	**AoD [°]**	**AS [°]**
Cluster 3	AoA	AS	AoD	AS

Table A.5 Model E (part 1).

18	**730**										
17	**640**										
16	**560**						-22.4	251.8	41.6	293.1	42.5
15	**490**	-22.9	163.7	35.8	105.6	36.1	-19.9	251.8	41.6	293.1	42.5
14	**430**	-20.5	163.7	35.8	105.6	36.1	-18.7	251.8	41.6	293.1	42.5
13	**380**	-18.3	163.7	35.8	105.6	36.1	-14.7	251.8	41.6	293.1	42.5
12	**330**	-16.1	163.7	35.8	105.6	36.1	-14.3	251.8	41.6	293.1	42.5
11	**280**	-13.9	163.7	35.8	105.6	36.1	-10.3	251.8	41.6	293.1	42.5
10	**230**	-11.7	163.7	35.8	105.6	36.1	-9.9	251.8	41.6	293.1	42.5
9	**180**	-9.8	163.7	35.8	105.6	36.1	-7.1	251.8	41.6	293.1	42.5
8	**140**	-8.2	163.7	35.8	105.6	36.1	-5.8	251.8	41.6	293.1	42.5
7	**110**	-6.9	163.7	35.8	105.6	36.1	-4.5	251.8	41.6	293.1	42.5
6	**80**	-5.6	163.7	35.8	105.6	36.1	-3.2	251.8	41.6	293.1	42.5
5	**50**	-4.5	163.7	35.8	105.6	36.1	-1.8	251.8	41.6	293.1	42.5
4	**30**	-3.9	163.7	35.8	105.6	36.1					
3	**20**	-3.5	163.7	35.8	105.6	36.1					
2	**10**	-3.0	163.7	35.8	105.6	36.1					
1	**0**	-2.6	163.7	35.8	105.6	36.1					
Tap index	**Excess delay [ns]**	**Power [dB]**	**AoA [°]**	**AS [°]**	**AoD [°]**	**AS [°]**	**Power [dB]**	**AoA [°]**	**AS [°]**	**AoD [°]**	**AS [°]**
		Cluster 1	AoA	AS (receive)	AoD	AS (transmit)	Cluster 2	AoA	AS	AoD	AS

Table A.5 Model E (part 2).

												-24.6	182.0	40.3	275.7	38.7			
												-20.7	182.0	40.3	275.7	38.7			
												-20.5	182.0	40.3	275.7	38.7			
-22.8	80.0	37.4	61.9	38.0								-20.6	182.0	40.3	275.7	38.7			
-18.1	80.0	37.4	61.9	38.0															
-18.6	80.0	37.4	61.9	38.0															
-13.8	80.0	37.4	61.9	38.0															
-14.2	80.0	37.4	61.9	38.0															
-9.6	80.0	37.4	61.9	38.0															
-7.9	80.0	37.4	61.9	38.0															
Cluster 3	**Power [dB]**											Cluster 4	**Power [dB]**						
AoA	**AoA [°]**											AoA	**AoA [°]**						
AS	**AS [°]**											AS	**AS [°]**						
AoD	**AoD [°]**											AoD	**AoD [°]**						
AS	**AS [°]**											AS	**AS [°]**						

Table A.6 Model F (part 1).

18	**1050**										
17	**880**										
16	**730**						-19.9	180.4	55.0	183.7	55.2
15	**600**	-19.9	315.1	48.0	56.2	41.6	-15.7	180.4	55.0	183.7	55.2
14	**490**	-16.7	315.1	48.0	56.2	41.6	-13.8	180.4	55.0	183.7	55.2
13	**400**	-14.3	315.1	48.0	56.2	41.6	-10.4	180.4	55.0	183.7	55.2
12	**330**	-12.5	315.1	48.0	56.2	41.6	-10.3	180.4	55.0	183.7	55.2
11	**280**	-11.0	315.1	48.0	56.2	41.6	-7.0	180.4	55.0	183.7	55.2
10	**230**	-9.5	315.1	48.0	56.2	41.6	-7.4	180.4	55.0	183.7	55.2
9	**180**	-8.2	315.1	48.0	56.2	41.6	-5.3	180.4	55.0	183.7	55.2
8	**140**	-7.1	315.1	48.0	56.2	41.6	-4.4	180.4	55.0	183.7	55.2
7	**110**	-6.2	315.1	48.0	56.2	41.6	-3.5	180.4	55.0	183.7	55.2
6	**80**	-5.3	315.1	48.0	56.2	41.6	-2.8	180.4	55.0	183.7	55.2
5	**50**	-4.6	315.1	48.0	56.2	41.6	-1.8	180.4	55.0	183.7	55.2
4	**30**	-4.2	315.1	48.0	56.2	41.6					
3	**20**	-3.9	315.1	48.0	56.2	41.6					
2	**10**	-3.6	315.1	48.0	56.2	41.6					
1	**0**	-3.3	315.1	48.0	56.2	41.6					
Tap index	**Excess delay [ns]**	**Power [dB]**	**AoA [°]**	**AS [°]**	**AoD [°]**	**AS [°]**	**Power [dB]**	**AoA [°]**	**AS [°]**	**AoD [°]**	**AS [°]**
		Cluster 1	AoA	AS (receive)	AoD	AS (transmit)	Cluster 2	AoA	AS	AoD	AS

-18.5	74.7	42.0	153.0	47.4
-12.7	74.7	42.0	153.0	47.4
-14.1	74.7	42.0	153.0	47.4
-9.6	74.7	42.0	153.0	47.4
-10.4	74.7	42.0	153.0	47.4
-6.7	74.7	42.0	153.0	47.4
-5.7	74.7	42.0	153.0	47.4
Power [dB]	**AoA [°]**	**AS [°]**	**AoD [°]**	**AS [°]**
Cluster 3	AoA	AS	AoD	AS

Table A.6 Model F (part 2).

Cluster 4	AoA	AS	AoD	AS	Cluster 5	AoA	AS	AoD	AS	Cluster 6	AoA
Power [dB]	**AoA [°]**	**AS [°]**	**AoD [°]**	**AS [°]**	**Power [dB]**	**AoA [°]**	**AS [°]**	**AoD [°]**	**AS [°]**	**Power [dB]**	**AoA [°]**
-8.8	251.5	28.6	112.5	27.2							
-13.3	251.5	28.6	112.5	27.2							
-18.7	251.5	28.6	112.5	27.2	-12.9	68.5	30.7	291.0	33.0		
					-14.2	68.5	30.7	291.0	33.0		
										-16.3	246.2
										-21.2	246.2

38.2	62.3	38.0
38.2	62.3	38.0
AS [°]	**AoD [°]**	**AS [°]**
AS	AoD	AS